Two-Dimensional Massive Parallel Dispenser for Microarray Printing

Development of a multi-channel, modular and scalable, piezoelectric printing device loaded from standard well plates using polymer substrate.

Dissertation
submitted to the Faculty of Sciences of the University of Neuchâtel to obtain the degree of Doctor of Science

by

Andreas Kuoni

Institute of Microtechnology
University of Neuchâtel
Rue Jaquet-Droz 1
CH-2007Neuchâtel
Switzerland

IMPRIMATUR POUR LA THESE

Two-Dimensional Massive Parallel Dispenser for Microarray Printing

M. Andreas KUONI

UNIVERSITE DE NEUCHATEL

FACULTE DES SCIENCES

La Faculté des sciences de l'Université de Neuchâtel, sur le rapport des membres du jury

MM. N. de Rooij (directeur de thèse), U. Staufer, M. Boillat (Neuchâtel) et H. Keppner (Le Locle)

autorise l'impression de la présente thèse.

Neuchâtel, le 22 janvier 2004

La doyenne:

Martine Rahier

MACHE NUR DAS UNMÖGLICHE

Andreas Kuoni, 2004

ABSTRACT

Microarrays of bioactive substances are becoming more and more important for medical diagnostics and drug research. The ability to carry out assays in parallel in a microarray format is required for high-throughput screening (HTS). This thesis presents a new type of dispenser that dispenses 384 droplets of a volume of 65 pL in parallel in a 16x24 array format onto a substrate (biochip) at a spacing of 500 µm. The dispenser is continuously loaded from a standard 384 µ-titer plate with a well spacing of 4.5 mm during dispensing.

A novel technology for a micro-fabricated 2-dimensional dispenser has been developed. One-dimensional dispenser arrays are constructed by lamination of structured flexible polymer sheets and the desired two-dimensional array is obtained by stacking the required number of dispenser rows. Microlithographic technique followed by reactive ion etching or Laser ablation is used for precise structuring of the fluidic channels and dispenser nozzles. Printing is activated by piezoelectric actuators integrated onto the polymer sheets. The flexible construction allows a format transfer from a standard 384-well plate to the final two-dimensional array printing at a pitch of 0.5 mm.

PREFACE

The goal of the presented work is to evaluate and demonstrate the feasibility of using micromachined elements in an integrated miniaturized 2-dimensional multi-channel for liquid aspiration and dispense. The developed dispenser is integrated as sub-system in automated equipment for pharmaceutical and biotechnology industries for "printing" arrays of bio-active molecules on various types of substrates (biochips) for medical diagnostics and drug screening. While miniaturization of the components is the key for the success of the project, the emphasis, however, is put on the manufacturability of the integrated "printing head" and the reliability of its operation.

This thesis is presented in two major parts. In the first part, the 384-channel dispenser is presented as a global system and it is shown how the task has been solved including the characterization of the 384-channel dispenser and conclusion. Most of the technology steps and intermediate prototypes and their characterization are published in articles and proceedings. These are part of the thesis and marked as Ref. 1, 2, 3, 4 and 5, see appendix, where they are added in their full length. As a short introduction, the titles of the Ref. 1-5 are listed below. Other references are mentioned with the name of the first author and the year of publishing e.g., [Lankard, 1992].

Ref. 1

A high insulating thin film ZnO piezoelectric actuator on a Polyimide substrate.

Ref. 2

Polyimide Membrane with ZnO Piezoelectric Thin Film Pressure Transducers as a Differential Pressure Liquid Flow Sensor.

Ref. 3

Two-Dimensional Parallel Dispenser for Micro-array Printing.

Ref. 4

A Modular High Density Multi-channel Dispenser for Micro-array Printing.

Ref. 5

A Highly Parallel Piezoelectric Printing Device for Micro-Array Technology.

TABLE OF CONTENTS

1 INTRODUCTION

1.1 General introduction

The motivation of this thesis is the development of a 2-dimensional multi-channel dispenser. The main goal is to increase the parallel dispensing capabilities compared with existing dispensers. For high throughput applications the droplet volume should be kept as small as possible because sample preparation is tedious and expensive. The main application of the developed dispenser is printing of microarrays applied for research in the field of life sciences. First, in this chapter, a short introduction of microarray technology is given below followed by the state-of-the-art printing technology and, finally, the concept of the dispenser.

1.2 Microarray technology

It is widely believed that thousands of genes and their products in a given living organism function in a complicated and orchestrated way create the mystery of life. However, traditional methods in molecular biology generally work on a “one gene in one experiment” basis, which means that the throughput is very limited and the whole picture of gene function is hard to obtain. In the past several years, DNA microarray has attracted tremendous interests among biologists. This technology promises to monitor the whole genome on a single chip so that researchers can have a better picture of the interactions among thousands of genes simultaneously. Terminologies that have been used in the literature to describe this technology include, but are not limited to biochip, DNA-chip, DNA-microarray and gene array, [Ramsay, 1998].

DNA-microarrays are fabricated by high-speed robotics, generally on glass but sometimes on nylon substrates, for which probes with known identity are used to determine complementary binding, thus allowing massively parallel gene expression and gene discovery studies. An experiment with a single DNA chip can provide researchers parallel gene expressions - a dramatic increase in throughput. Many fields, including drug discovery, toxicological research, disease diagnosis and gene discovery benefits from the use of DNA-microarray technology. There are several steps in the design and implementation of a DNA-microarray experiment as shown in table 1.1: First a probe with a know identity (cDNA, chromosome, etc) are prepared in standard well plates. These samples are loaded into a dispenser and are then spotted onto a DNA-microarray by pipetting, by contact or non-contact printing such as piezoelectric dispensing. The DNA microarray is then covered with a target. The target, of an unknown identity, is tagged with a fluorescent label. In the hybridization step, the probe can bind with the labeled target when they are of complimentary nature. After hybridization step, a wash cycle is performed to remove excess target material from the microarray surface. The information of the reaction can be read optically using a scanner by measuring the fluorescence activity of hybridized probes. The last step is the data mining from the scanner image.

1) **Probe** cDNA with known identity	2) **Chip** Fabrication, dispensing, pipetting, lithography	3) **Target** Fluorescently labelled sample, unknown identity	4) **Assay** Hybridization and washing	5) **Readout** Fluorescence with scanners	6) **Informatics** data mining, visualization

Table 1.1: Design of a DNA-microarray experiment, modified from www.gene-chips.com

Microarray technology allows an unprecedented view of biological systems by allowing genomics to be examined on DNA-microarray. What used to require several weeks per gene with traditional assays using nylon membranes and radioactivity can now be performed in less than a day for 10'000 genes. The pillars of the microarray industry are similar to those that have served as the foundation for the computer chip industry: parallelism, miniaturization and automation of sequence information for microarray manufacture and analysis. Much has been published regarding the power of microarray technology for use in genomics (functionality of genes) and proteomic (functionality of protein) applications. What was not clear to the life science industry in 1995, when Marc Schena wrote the first paper demonstrating the usefulness of microarray technology, is clear now… microarray technology is here to stay, [Schena, 1995].

1.3 Microarray life cycle

A microarray life cycle can be divided into five subjects as shown in figure 1.1. The cycle starts with a biological question focusing of the study. Next is the sample preparation, samples are usually prepared in 384-well plate and small droplets are then spotted onto a microarray. The microarray reaction is done by hybridization. A scanner detects optically the results of the hybridization. The image of the scanner is then analysed and data mining is carried out by informatics.

Microarray analysis has made biological interrogation technique more important than ever. Because of the enormous power of microarray assays as data generating devices, a single set of microarray experiments often generates an amount of data that requires several months to analyze. It is important to emphasize that

microarray analysis is fundamentally different from traditional assays that employ gels and nylon membranes. In traditional assays, the ratio of analysis time to experimental time is small, and in microarray assays this ratio is enormous. It is therefore suggested that a biological or technical question precede the other four basic step of the life cycle (sample preparation, microarray reaction, microarray detection, data analysis) of every microarray experiment, figure 1.1. If the experimentalist adheres to this basic methodological principle, the microarray data glut is more easily managed.

Microarray experimentation should begin with a question, but need not begin with a hypothesis. The distinction seems subtle, but again the difference is actually substantial. Starting with a question means that the focus, scope, and intent of a study has been formulated prior to undertaking an experiment. Starting with a hypothesis means that the study has been undertaken with an a priori understanding of what the outcome is likely to be. Because microarray analysis allows a totally unprecedented look at biological systems it is often impossible to formulate a hypothesis a priori because so little quantitative information is available about biological systems at the genomic level.

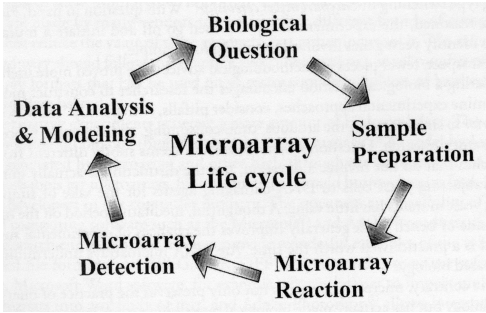

Figure 1.1: Schematic of the microarray assay life cycle with the five main steps. Every microarray experiment should begin with a biological question or query and proceed stepwise. Successive rounds of experimentation provide an increasingly view of biological function, [Source: Schena, 2000].

1.4 Methodology

The methodology describes the most important criteria, which a printing technology has to fulfill for a successful microarray printing. The eight points, listed below, cover mostly the requirements of the end user. The end user is the person who operates the spotting device. These points have been taken into account during the development of the concept for the present device.

1. Print uniform spots measured in micron

   One of the largest benefits of microarray technology is using very small amounts of precious sample to generate tremendous amounts of valuable data. By definition, a microarray contains array elements that are microscopic.
2. Print individual spots in regular array patterns

   Samples must be printed to order and kept in order. A spotting technology that does not put samples in ordered rows and columns is useless, since it would be impossible to track results.
3. Easy to implement

   For a microarray technology to be used, it must be integrated in a traditional research setting with a minimal amount of additional training. The technologies that are easily implemented will be widely used. Widely used technologies allow laboratories all over the world to share methods, which will ultimate lead to standards. Microarray technology has no official governing body, therefore the most widely used methods and technologies become *de facto* standards.
4. Cost effective/affordable

   The limited budgets of research institutions require a technology to be cost effective and affordable. A technology must be durable, easy to maintain, and

scalable. Most labs start out at low-density 1-d microarrayers, and build up to high-density 2-d microarrayers. Therefore, having a sample delivery technology that is scalable increases its cost effectiveness and utility.

5. Print without damaging the sample

   Not every sample is going to survive being shot out of a piezoelectric device, stamped out by a pin, or heated by a thermal printer. Some contact printing technologies have been documented to damage glass and nylon based surfaces.

6. Easy to fix and maintain

   All laboratory equipment requires some maintenance. Typically the more sophisticated the technology, the more difficult it is to maintain and repair. Microarray printing techniques with high-level performance, easy maintenance and repair, with minimal effort and training are best.

7. Compatible with a variety of scientific applications

   Microarray technology has its roots in DNA research, but it is not limited to genomics. A variety sample types are being printed in the fields of proteomics. The disciplines taking advantage of microarray technology are endless.

8. Print multiple samples, multiple times on multiple substrates with one efficient loading of sample

   Sample preparation is tedious, expensive and primarily done in 384 well formats, which makes the handling of samples very important. Loss of sample at any step of microarray manufacturing, storage and processing should be minimized as much as possible. Printing multiple times from one loading of sample is critical for high-throughput. The best technologies make the most spots, over the highest number of substrates, from the lowest single sample volume.

1.5 Printing technology "State-of-the-art"

Microarray manufacturing technologies can be divided into two basic groups, contact and non-contact printing. Contact printing technologies for manufacturing microarrays currently include solid pins, split pins, quills and tweezers, capillary tubes. Non-contact printing technologies include solenoid, thermal and piezo devices and more recently electrostatical devices.

1.5.1 Contact printing

Contact printing is still widely used for microprinting. Contact printing involves direct contact between the pin and the solid surface. The printing can be done parallel from 4 up to 384 pins at a spacing of 4.5 or 9 mm. The 4.5 mm spacing allows loading the pins from a 384-well plate. Once the pins are loaded 200 to 400 spots can be printed per load. Spot sizes of 75 to 360 µm are possible depending of the pin dimensions. The spotted volume is about 0.5 nL to 3 nL. Different pins are shown in figure 1.2.

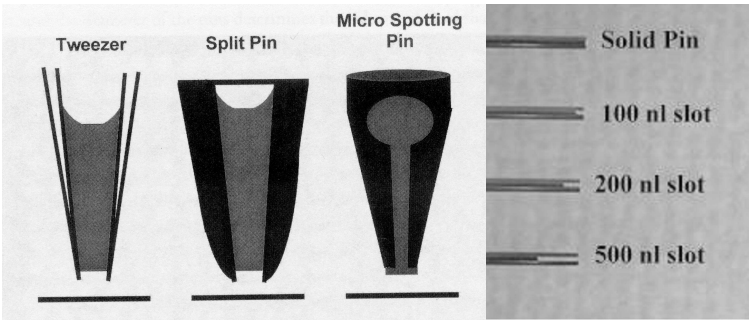

Figure 1.2: Schematic drawings of the pin for a contact printing dispenser, [Source: Schena, 2000].

Contact printing has a major drawback, that it can be applied only to solid surfaces. More and more other substrates such as Nylon, plastics, etc. are used for microarray technology. It is also reported that the pins damage the glass substrate and that the pins wear out. Contact printing is very sensitivity to different surfaces properties. To overcome these drawbacks non-contact printing is the technology of choice.

1.5.2 Non-contact printing

Solenoid

Solenoid dispensing technique combines a pressure source with a microsolenoid valve to provide quantitative dispensing in the low nanoliter range up to microliter range. One system, commercialized by Seyonic, has a MEMS fabricated flow sensor integrated for high precision aspirating and dispensing volume control, shown schematically in figure 1.3. The dispenser fills the sample from a well plate by aspirating and dispenses contactless droplets to a substrate. The heart of the system is the self-diagnosing microflowmeter feedback controlled liquid handling system applied to each channel. Real time monitoring of the performance and make on the fly adjustments to compensate for variations like temperature, viscosity, that would degrade the low volume performance of other approaches.

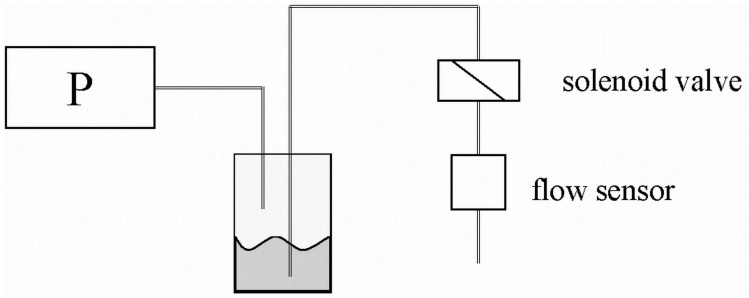

Figure 1.3: Schematic drawing of a solenoid valve dispenser including a flow sensor for realtime volume measurements.

Solenoid dispensing technique is widely used for well-plate based applications where a large dynamic range of dispensing liquid is required. A 1-dimensional array dispensing different volume from 25 µL down to 25 nL is shown in figure 1.4. All solenoid printing technique has the limiting factor of a minimal spotting volume of some nanoliters, which makes it less suitable for microarray printing. To overcome this limit a thermal or piezoelectric actuation is required.

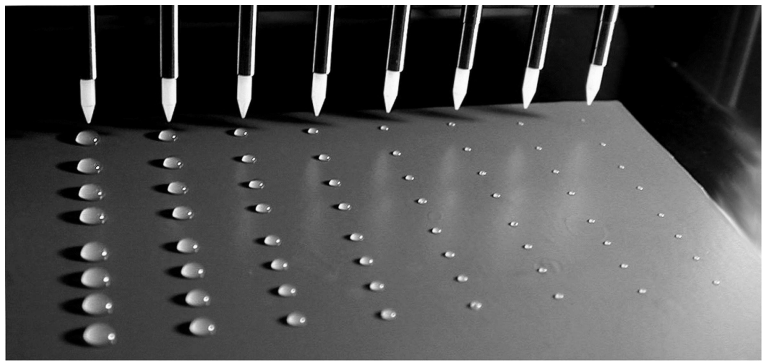

Figure 1.4: Dynamic dispensing range of Solenoid valve dispenser. The liquid volume changes from 5 µL down to 25 nL controlled by a flowsensor. The spacing of the

channel is 9 mm. The system is commercially available from Seyonic SA, Neuchâtel, [www.seyonic.com].

Thermal and piezo devices

Dispensing of droplets in the picoliter range is today well known from ink-jet printers used in many households. There are two major technologies available namely thermal and piezoelectric mechanism.

Thermal

Thermal printers use heat as part of the delivery mechanism. The sample is repeatedly heated to create bubbles, which ejects drops of sample from the nozzles to the substrate. A team of Japanese researchers, led by Nobuko Yamamoto, adapted a Canon brand bubble-jet printing head for printing spots of DNA onto glass slides to create microarrays. However, to date there is no product available to researchers using this method. A few of the technical hurdles this group had to overcome were the temperature of 200℃ and the shearing stress given by the droplets velocity of 10 m/s on the DNA sample. Other hurdles are, first, how to efficiently pick-up samples from micro plates and, second, how to change samples in the thermal reservoir while avoiding cross contamination, [Okamoto, 2000].

Piezoelectric

A piezoelectric printing mechanism uses a dielectric crystal closely apposed to a fluid reservoir. Ink-jet printers from Epson are based on this technology. The fast response of the crystal permits fast dispensing rates, in the range of several thousands of droplets per second. A piezoelectric dispenser with a glass capillary was developed by Microdrop GmbH, Germany and is shown in figure 1.5. By applying a voltage to the piezo, the capillary is squeezed and a stroke volume of some hundreds of picoliter is created. The stroke

volume generates a pressure wave, which accelerates the liquid and, finally, a droplet is ejected through a narrow nozzle. The dispenser, shown in figure 1.5, has a nozzle diameter of 75 µm resulting in droplet volume of 350 pL. The outer dimension of 4.5 mm does not allow building a high-density array. To date, piezoelectric dispensing technology has been shown making small numbers of gene expression microarrays, but development into a commercially available dispensing system has been slow, [Schena, 2000].

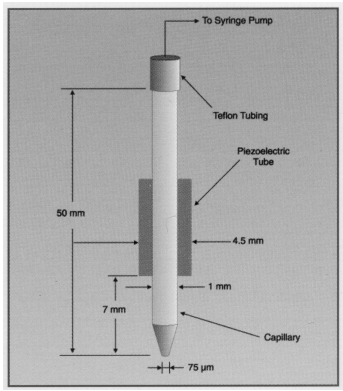

Figure 1.5: Schematic view of piezoelectric dispenser with a glass capillary. This dispenser dispenses 350 pL out of 75 µm nozzle. [source: www.microdrop.de].

Another approach of piezoelectric dispenser has been developed by GeSiM, Grosserkmannsdorf, Germany. The channel and membrane is dry etched into a Silicon wafer. The channels are sealed with a glass wafer, which is anodic bonded to the silicon wafer. A piezoelectric actuator is glued onto the Silicon membrane. The nozzle is fabricated by dicing with a diamond saw following a polishing step. A fabricated device is shown in figure 1.6. Droplets of 0.5 - 2 nL, depending on the geometry, are ejected at a driving voltage of about 60 volt and repetition rate of up to 1 KHz.

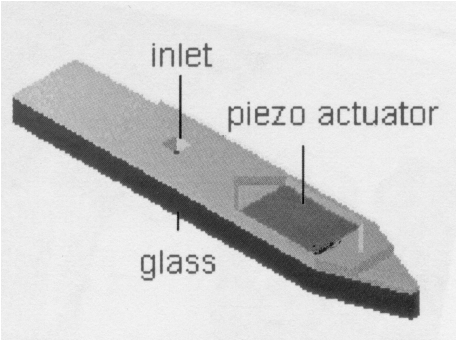

Figure 1.6: Schematic view of the micropipettes, [source: www.gesim.de].

The width of the GeSiM micropipettes is about 3 mm and does not allow building a high-density array. The nozzle rim of the pipettes is of different materials (Glass-Silicon), which results in different contact angles between liquid and nozzle rim. It is not straightforward to control the jet directionality for a stable spotting.

PicoJet, Hillsboro, OR, USA, developed a printhead based on piezoelectric bending mode technology, as shown in figure 1.7. They introduced a device made of stainless steel laminated sheets. The stainless steel is photochemically patterned. Droplets of a volume of 50-70 pL are dispensed up to a frequency of 18 KHz.

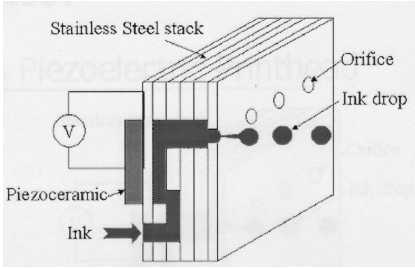

Figure 1.7: Schematic view of laminated stainless steel sheets forming a printhead, [source: www.picojet.com].

By bonding the stainless steel laminates using a low cost proprietary metal-to-metal bonding process, all adhesives are removed from the fluid path giving the dispenser the robust all metal construction necessary to jet a wide range of fluid on porous and non-porous surfaces. However, the filling of the complex fluidic path through the different layers is not straightforward and air bubbles may be easily trapped in corners and dead volumes. Another limitation of such a device made as a solid block is that it cannot be built as 2-dimensional.

A piezoelectric Silicon dispenser was developed by Thomas Laurell, [Laurell, 1999]. This dispenser is filled by a flowthrough channel and a schematic view is shown in figure 1.8. The dispenser is mainly made out of Silicon wafers. The main processes are wet etching and fusion bonding. The dispenser is limited to one nozzle, which makes it less suitable for high-throughput microarray printing. Droplets of 50 pL are ejected at 500 Hz for an excitation of 50 volt. The droplet velocity is around 3 m/s.

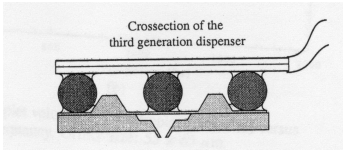

Figure 1.8: Schematic view of the flow–through microdispenser, [Source: Laurell, 1999].

An application that is investigated aims at interfacing microseparation systems such as nano liquid chromatography or capillary electrophoresis. The dispenser acts as a picoliter fractionating unit and dispenses separated fractions onto high density MALDI-TOF MS (matrix assisted laser desorption ionisation - time of flight mass spectrometry) target plates.

A shear mode piezoelectric dispenser has been developed by MicroFab, Plano, TX, USA, and is shown in figure 1.9. This print head is fabricated from PZT (Lead Zirconate Titanate). The channels are machined by diamond saw dicing. The device is assembled by gluing. The nozzle surface is a polyimide sheet bonded to the end of the PZT channels. The nozzles are fabricated by laser ablation, [Wallace, 1998]. Droplets of 120 pL are ejected at a velocity of 2.5 m/s at a peak-to-peak driving voltage of 30 volt.

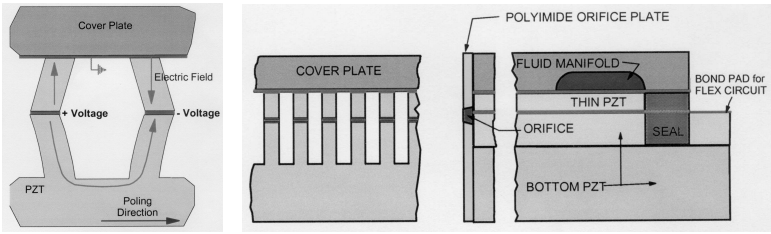

Figure 1.9: Printhead fabrication process: cover and orifice plate attachment and channel sealing, [Source: Wallace, 1998].

A critical point of this device is that the dispensing liquid is in contact with the PZT material. If PZT material is exposed to liquids such as water the piezoelectric activity will be reduced as function of the time.

Another point is that the liquid is also in contact with adhesive used for the lamination of the two PZT plates.

PicoliterInc, Mountain View, CA, USA, developed a new system, which precisely transfers low nanoliter quantities of liquid between microwell plates, figure 1.10. Droplets are ejected from a source well plate to a receiving plate by acoustic droplet ejection (ADE) technique. A piezoelectric transducer generates the acoustic energy.

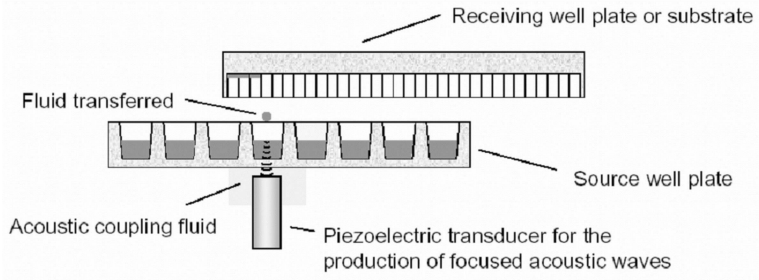

Figure 1.10: Schematic view of acoustics droplet ejection (ADE), [Source: www.picoliterinc.com].

Acoustic drop ejection (ADE) is used to eject protein and DNA solutions, suspension of mammalian cells, and immiscible and miscible solutions containing multiple layers. Interactions of chemicals with different surfaces can be altered by the use of multilayer or immiscible solutions, [Mutz, 2002].

A unique combination of piezo technology and microfluidic cartridge is being implemented by IMTEK, Freiburg, Germany. Schematic view is shown in figure 1.11. The printhead consists of 96 microfluidic channels. Each channel feeds one of the 96 nozzles by capillary forces in an 8x12 pattern. The nozzles are set at 500 µm spacing

and the sample is pushed out of each nozzle by a pneumatic pump activated by a piezo actuator. All 96 samples are delivered simultaneously in nanoliter volume. What the company considers a distinct advantage is likely considered a disadvantage by most of the microarray community. The channels on the printhead are loaded at the top of the printhead with a manual pipette. Since just about every biological sample that is prepared for microarray spotting is done in standard microtiter plates, the extra pipetting step required to operate the device is cumbersome.

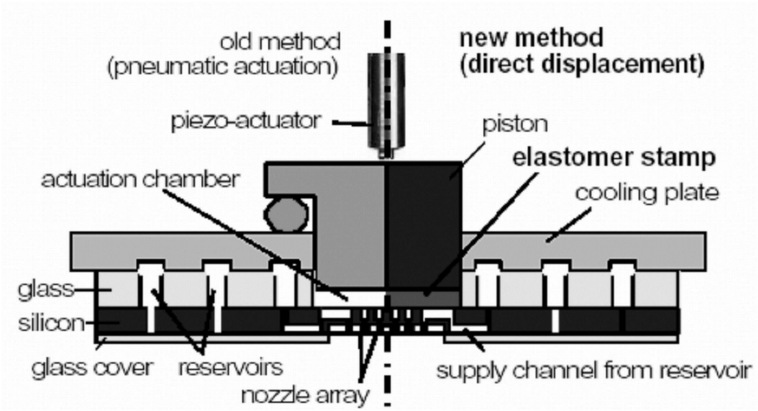

Figure 1.11: Schematic view of the TopSpot print head, [Source: de Heij, 2003].

Electrostatical

The first commercially available electrostatically actuated print head was developed by Kamisuki, [Kamisuki, 1998]. The electrostatic actuator comprises a silicon pressure plate and a corresponding transparent ITO electrode, which is parallel to the pressure plate, as shown in figure 1.12. They are assembled to keep the air gap between electrodes within 0.2 ± 0.015 µm. The driving voltage is 38

volt and the frequency goes up to 3 KHz. The droplet has a size of 160 pL at a relatively high velocity of 8 m/s.

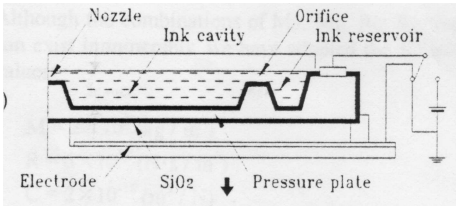

Figure 1.12: Schematic view of an electrostatically actuated print head, [source: Kamisuki, 1998].

The advantage of this device is the low power consumption of a calculated average power of about 150 µW per channel.

Conclusion

This overview is not necessarily exhaustive, but represents the variety of liquid handling technologies available today to the microarray community. There are many more other suppliers of printing tools, which are not listed here. All, but the Imtek device, lack highly parallel printing capabilities with spot spacing at 500 µm or smaller. Today, microarray technologies require high-throughput, which can actually only be reached by massive parallel dispensing at a spot spacing of 500 µm or smaller and by fulfilling most of the 8 rules mentioned earlier.

1.6 Concept

Based on the analysis of the pro and cons of the existing devices, as exposed in the precedent section, the concept of the new microarray printing device has been investigated and is the subject of the discussion below.

The state-of-the-art dispensers are all based on solid materials such as glass, Silicon and Stainless steel. To build 2-dimensional nozzle array in a microarray format is a difficult challenge. It was envisioned to overcome this challenge by using flexible material. The flexibility of the material allows building in modular way 2-dimensional printing arrays.

The concept is based on the following conditions. First the dispenser spots 384 droplets in parallel in a 16x24 array format at pitch of 500 µm. Second, the dispenser is loaded from the industry standard 384 microtiter plate at 4.5 mm spacing. The droplet volume has been set to 65 pL which corresponds to a droplet diameter of about 50 µm. The device must be later scalable up to a 32x48 array format (1536 nozzles). This device would then be loaded from a 1536-well plate. Finally, the device should be used without any complex robotics and should be easy to use.

The bloc diagram depicted in figure 1.13, shows the principle of the dispenser. Starting at the bottom, a 384-well plate acts as reservoir for 384 different samples for the dispenser channels. The samples can be prepared in 384-well plates as usually done today. The 384-well plates are a standard in most laboratories and automation is based on this format.

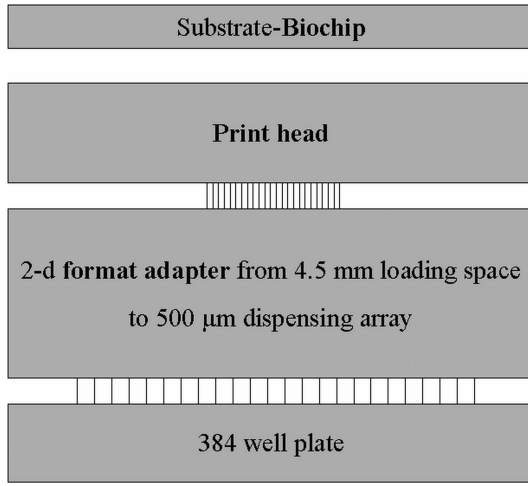

Figure 1.13: Bloc diagram of a 384-channel dispenser including a 384-well plate as reservoir.

From the well plate a format adapter is used to reduce the spatial spacing of 4.5 mm to 500 µm. The spatial reduction must be done in x- and y-direction. The simplest solution is to use flexible materials such as polymer. A polymer technology based on polyimide sheets featuring micro-machined and sealed µ-channels has been developed during this work. The flexibility of the sheets allows building a 2-d format adapter with 4.5 mm loading space and 500 µm dispensing spacing.

For non-contact dispensing, a print head is required. The selected dispensing mechanism relies on piezoelectric actuator made of thin-film piezo material or bulk PZT ceramics (Lead Zirconate Titanate). The print head should be integrated in one piece in the format adapter. Its integration into a polyimide sheet makes the fluidic channel smooth and without discontinuities or fluidic interconnections involving different material, thus eliminating sites at which air bubble

could be trapped. Air bubbles would be detrimental to the device performances as in most microfluidic devices.

The substrate (microarray, biochip) is placed over the print head at a distance of 0.25 to 1 mm. The droplet diameter is 50 µm, given by the nozzle size, and corresponds to a nominal volume of 65 pL. The droplet velocity can be controlled by the actuation voltage in the range of 1 to 4 m/s. The upward shooting has no influence on the drop formation because the effect of gravity can be neglected compared to that of the kinetic energy. For instance, the kinetic energy is about 50 to 100 times higher than the potential energy at a droplet speed of 2.5 m/s. The upward shooting avoids complex robotics for positioning and displacing, the system becomes easy to handle and can be displaced manually.

For microarray spotting it is a crucial requirement that no splashing of the droplet when arriving on the substrate occurs. Splashing can only occur when the surface energy of the free droplet is smaller than the kinetic energy. Using the formula in table 1.2, the surface energy is 0.57 nJ and the kinetic energy 0.20 nJ for a 65 pL water droplet at 2.5 m/s. The relation E_{kin}/E_{sur} is then 0.36, meaning that no splashing can happen because the droplet velocity is too small. Splashing may occur for values of $E_{kin}/E_{sur} \geq 1$, which would require a droplet velocity of $v \geq 4.2$ m/s. Therefore the droplet velocity has been specified to be 2.5 m/s.

$$E_{sur} = \sigma \cdot A, \quad A = 4 \cdot \pi \cdot r^2$$

$$E_{sur} = (4 \cdot \pi \cdot \sigma) \cdot r^2$$

$$E_{kin} = \frac{1}{2} \cdot m \cdot v^2, \quad V = \frac{4}{3} \cdot \pi \cdot r^3$$

$$E_{kin} = (\frac{2}{3} \cdot \pi \cdot \rho) \cdot r^3 \cdot v^2$$

$$\frac{E_{kin}}{E_{sur}} = \frac{1}{6} \cdot \frac{\rho}{\sigma} \cdot r \cdot v^2$$

Legend:

E_{sur}	surface energy [J]
σ	surface tension of the liquid [N/m]
A	surface of a droplet [m²]
r	radius of the droplet [m]
E_{kin}	kinetic energy [J]
m	weight [kg]
v	velocity of the droplet [m/s]
ρ	density of the liquid [kg/m³]
V	volume of a droplet [m³]

Table 1.2: Formules for the calculation of the surface and the kinetic energy for micro-droplets. For values of $E_{kin}/E_{sur} < 1$ no splashing occurs.

The major advantage of the proposed concept is the flexibility of the µ-channel. A cross section of a polyimide sheet is shown in figure 1.14. The thickness of the polyimide sheet is only 150 µm, being flexible enough to assemble an array. By integrating piezoelectric actuators and electrical contacts onto the sheets, a total thickness of less than 500 µm can be achieved. Thus allowing a spot 2-dimensional pitch of 500 µm. The single sheets are precisely held in place. All sheets are mechanically aligned by pin/bores and tightly held together. This allows exchanging every single sheet by a technician if a failure occurs.

The filling of the device with the samples stored in a 384-well plate, is done using a small backpressure of some tens of mbar. The liquid is pushed into the channels and flows up passing the restriction and stops at the nozzle by the surface tension effect. All channels are filled simultaneously. Once the channels are filled no backpressure needs to be applied to operate the device.

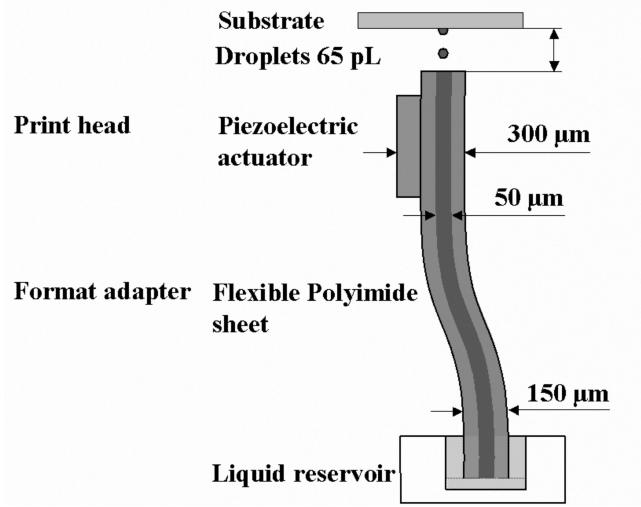

Figure 1.14: Cross section of a polyimide sheet showing a single channel. The liquid reservoir corresponds to the well of 384-microtiter plate.

A schematic 3-dimensional view of 384-channel dispenser is presented in figure 1.15. Each sheet contains 24 µ-channels, 24 actuators and 24 nozzles. To form a complete array, 16 of these independent sheets are assembled together. The device is scalable first by building only a one-dimensional array. A single sheet can carry 24 channels at 4.5 mm spacing, 48 channels at 2.25 mm spacing or any other customized sizes. Later, single sheets can be added to build a 2-dimensional array up to 16 or 32 sheets. The modularity allows building any shape for a maximum sheet size up to 150*150 mm².

For high-throughput screening (HTS) it is crucial that the device dead volume is kept as small as possible, since the preparation and the sample itself can be very expensive. One single channel of the 384-channel dispenser has an internal volume of only about 2 µL. Having the channel filled once, thousands of 65 pL droplets can be dispensed at a frequency of up to 1 KHz.

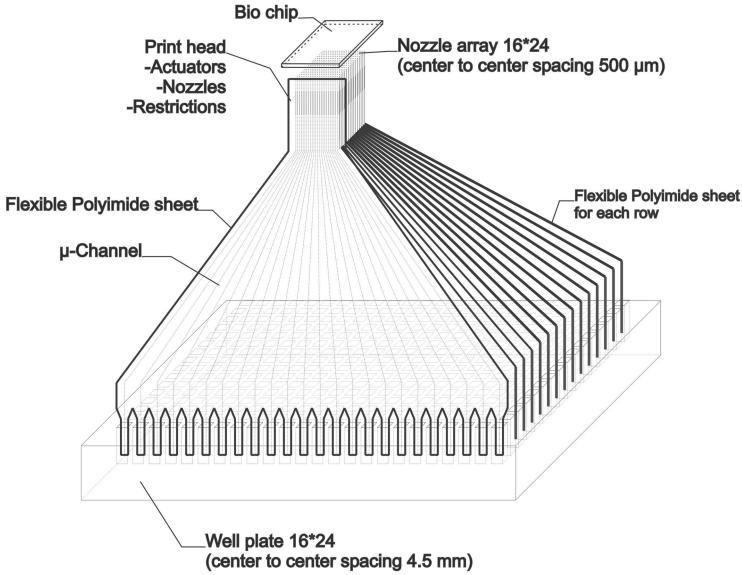

Figure 1.15: 3-dimensional concept of a 384-channel dispenser. This concept is realized and characterized within this work.

Now that the overall concept of the new device is in place, the technological steps that need to be investigated or developed for its fabrication are exposed in the form of a roadmap. This roadmap has been generated early in the project as a way to navigate through technological details and associated risks, while keeping the visibility of the overall goal in mind.

The different technological steps, as depicted in figure 1.16, consist of independent sub-processes investigated individually to measure the manufacturability of the device and the performances that could be expected form the completed device.
After having solved point 1,2 and 3 in the roadmap the highest risk was point 6. Because we were aware of the challenge in point 6, two other less risky solutions in point 5 and 7 have been added. With this

palette the risk could be clearly reduced and a successful outcome has been achieved.

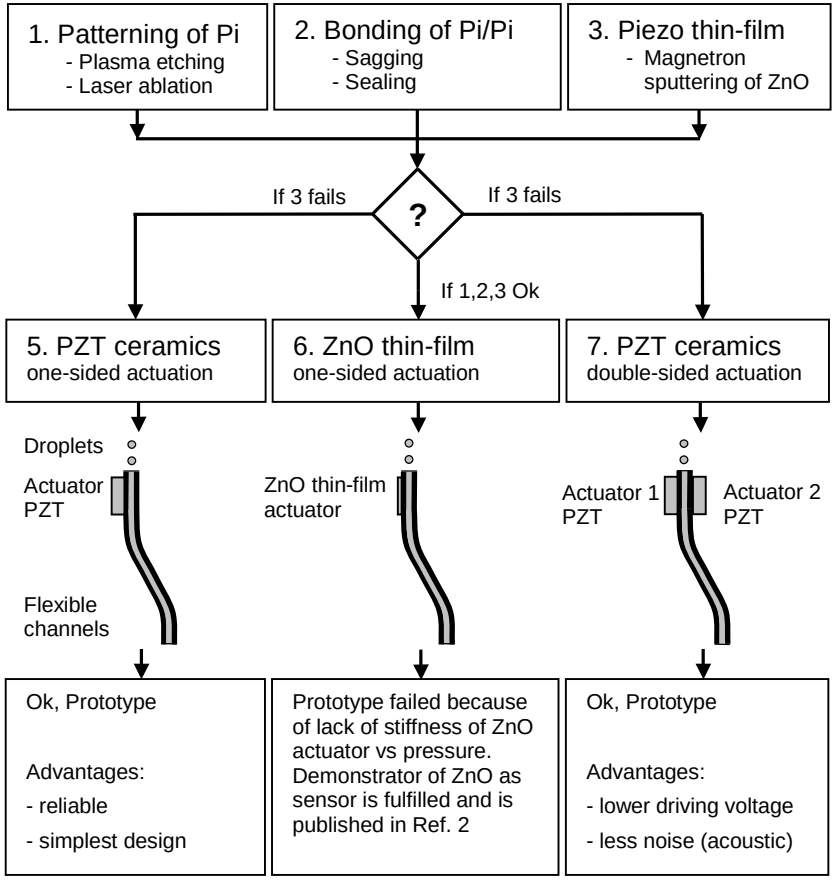

Figure 1.16: Roadmap of the developing steps for the fabrication of the 384-channel dispenser. The different steps are explained in the following chapters.

Starting from the top left of the roadmap, point 1, different patterning technologies of polyimide were investigated. The best and fastest solution is laser ablation. Next, bonding of polyimide sheets was developed. Void free bonding is achieved for a sheet size 150*150 mm² or 6 by 6 inch square. In point 3, the sputter deposition of piezo thin-film directly onto polyimide membrane was developed. Zinc oxide (ZnO) was chosen because it can be deposited at a temperature below 120 ℃. ZnO sputtered films were characterized as actuators, Ref. 1, and as sensors, Ref. 2.

After developing points 1, 2 and 3 of the roadmap, three different prototypes have been fabricated in parallel. ZnO thin-film actuators would have the major advantage of complete integration onto polyimide sheets. However, ZnO thin-film failed as actuator because of lack of stiffness against pressure as will be shown later. The two other prototypes, one-sided and double-sided PZT actuators, work well and both types have been characterized for dispensing different liquids and for different driving signals. The 384-channel dispenser is built from 16 sheets using the straightforward design with one-sided PZT actuation.

Compared to "traditional" ink-jet print heads, the system that is proposed in this work differs in three major aspects: First, the nozzle array extends in two directions instead of only one for ink-jet printers. The nozzle spacing of 500 µm corresponds to approx. 50 dpi density and the 384-nozzle array is 8x12 mm². Second, each nozzle is fed by its own individual reservoir and holds 384 different biological active samples. Third, the printing system is filled from a standard 384-(16x24)-well plate format with an outer dimension of 85x130 mm.

2 PIEZOELECTRIC ACTUATORS

2.1 Introduction

The heart of the dispenser is the printhead where piezoelectric actuators are integrated. The non-contact dispensing of small droplets (picoliter) requires a fast contraction of the channel. This contraction has to take place within about 5-20 µs for successfully ejecting droplets. Piezoelectric actuators are able to generate such fast contractions. Moreover, piezoelectric actuators can be integrated into polyimide membranes. The challenge of using piezoelectric actuators is the limited space given by the 2-dimensional nozzle spacing of 500 µm. Finite element modeling (FEM) was used to analyze different layouts and to optimize the performance of the actuators. As actuation material thin-film, bulk ceramic and polymer piezoelectric material were analyzed.

2.2 Piezoelectric material

As shown on the roadmap in the introductory chapter, two different approaches were developed for equipping the dispenser with piezoelectric actuators. First, thin-film piezoelectric material was deposited directly onto the polyimide membrane. This has the advantage that the piezoelectric layer and its electrodes are fully integrated. It was also expected that a thin-film layer would require a much lower driving voltage than thick ceramic actuators. Moreover, the nozzle spacing of 500 µm in two directions could be reduced to 250 µm for one of them. For the piezoelectric thin-film actuation

layer, Zinc oxide (ZnO, wurtzite structure) had been chosen because it can be deposited with no external heating by sputtering it onto the polyimide membrane. ZnO does not require a subsequent electric-thermal poling as would PZT (Lead Zirconate Titanate), or PVDF (Polyvinylidenefluoride) because of its self-poling capability, [Zeng, 1998]. Another advantage is that no seed layer, as for instance for AlN (Aluminumnitrate), is necessary, [Dubois, 1999]. This is an important aspect as a seed layer must usually be deposited at temperatures higher than the glass transition temperature Tg of polyimide. The relative high surface roughness of a bonded polyimide membrane compared to polished silicon has a minor influence on the piezoelectric efficiency when using ZnO. On the other hand, ZnO thin-films usually exhibit a low resistivity, preventing low frequency operation. As a way to increase the resistance, a PECVD (plasma-enhanced chemical vapor deposition) co-deposition of two amorphous SiO_2 (Silicon dioxide) insulation layers was selected. This allows increasing the film resistance as reported in Ref. 1 and Ref. 2. Second, PZT ceramic material was chosen as actuator. PZT plate actuators are commercially available in different thicknesses. The plate can be diced to custom-sized shapes by means of a diamond-blade saw in-house. The actuators were glued onto thin-film metal-electrodes. The advantages of the PZT plate actuators are their stability and reliability. Their drawback is that more handling is required during the fabrication process.

2.3 The piezoelectric constitutive equation

Piezoelectricity is the property of some materials to develop electric charge on their surface when mechanical stress is exerted on them. An applied electric field, on the other hand, produces a linear proportional strain in these materials. The electrical response to the mechanical stimulation is the so-called direct piezoelectric effect (e.g. used in sensors) and the mechanical response to the electrical

stimulation is called the converse piezoelectric effect (e.g. used in actuators). The piezoelectric constitutive equations are defined by four different forms and are shown in table 2.1, [Ikeda, 1990].

Strain-Charge or d-form	Stress-Charge or e-form
$S = s_E \cdot T + d \cdot E$ $D = d \cdot T + \varepsilon_T \cdot E$	$T = c_E \cdot S - e \cdot E$ $D = e \cdot S + \varepsilon_S \cdot E$
Strain-Voltage or g-form	**Stress-Voltage or h-form**
$S = s_D \cdot T + g \cdot D$ $E = -g \cdot T + \varepsilon_T^{-1} \cdot D$	$T = c_D \cdot S + h \cdot D$ $E = -h \cdot S + \varepsilon_S^{-1} \cdot D$

Table 2.1: Piezoelectric constitutive equations.

UNITS AND DESCRIPTION OF SYMBOLS

S = strain [m/m]
T = stress [N/m² or Pa]
E = electric field [V/m]
D = electric displacement [C/m²]
ε_T = dielectric constant, free [-]
ε_S = dielectric constant, clamped [-]
d = piezoelectric tensor, strain/field at const. Stress [C/N or m/V]
g = piezoelectric tensor, electric field/stress at const. Stress [Vm/N]
e = piezoelectric tensor, stress/electric field at const. strain [C/m²]
h = piezoelectric tensor, electric field/strain at const. charge [V/m]
s_E = elastic compliance at constant electric field [m²/N]
s_D = elastic compliance at constant charge density [m²/N]
c_E, c_D = elastic stiffness [N/m²]

Between the different piezoelectric constants transformations are possible. Often, manufacturers only give one set of piezoelectric coefficients instead of all four. Using a FEM program requires a certain set of piezoelectric constants, usually the d or e-form. The FEM program ANSYS 7.1 only works with the e-form and CFDRC 2002 can select between e- and d-form. The most important transformations for converting piezoelectric constitutive data from one form into another one are shown in table 2.2.

d-form to e-form $e = d \cdot s_E^{-1}$	d-form to g-form $g = \varepsilon_T^{-1} \cdot d$
e-form to h-form $h = \varepsilon_S^{-1} \cdot e$	g-form to h-form $h = g \cdot s_D^{-1}$

Table 2.2: Transformations of piezoelectric constants.

A complete set of piezoelectric constants for different PZT composites are given by Morgan, [Morgan, 1999].

2.4 Principle - models and boundary condition

For successful droplet ejection, the actuator must generate a stroke volume by deforming the channel. This stroke volume must be about

twice the volume of the ejected droplet and is around 130 pL in our case. Meaning that one part (65 pL) of the volume is ejected through the nozzle while the other is flowing backward through the fluidic restriction into the supply channel. A fluidic restriction reduces the backward flow and therefore, the driving voltage. The restriction is placed at one end of the piezoelectric actuator and at the other end of the actuator is the nozzle. The droplet is only ejected when the actuator creates a sufficient large stroke volume. The stroke volume generates a pressure wave in the channel, which accelerates the liquid column and a droplet is forced out of the nozzle. The break-off of the droplet is complete in about 65 µs after having applied the driving signal. The driving signal for the actuator is applied during 5 to 20 µs depending on the driving voltage. The channel inside can be deformed in shear, compression or bending mode depending on the assembling of the actuators. The bending mode has been chosen for the actuation as shown in figure 2.1. This mode allows enlarging the relative small strain generated by the piezoelectric actuator (10^{-5}-10^{-4}) by bending a membrane.

Three different layouts shown in figure 2.1 were investigated: First, a ZnO thin-film actuator, deposited onto the polyimide membrane, second, a PZT ceramic plate, and third, a design with two PZT actuators. In the later case, the actuators are assembled opposite of the actuators and are actuated simultaneously. This actuation is called double-sided actuation and the others are called one-sided actuation. The one-sided actuation has a stiffener plate opposite of the actuator. This stiffener plate increases the stability of the flexible dispenser sheets in the zone where the print head is and is also indicated in figure 2.1.

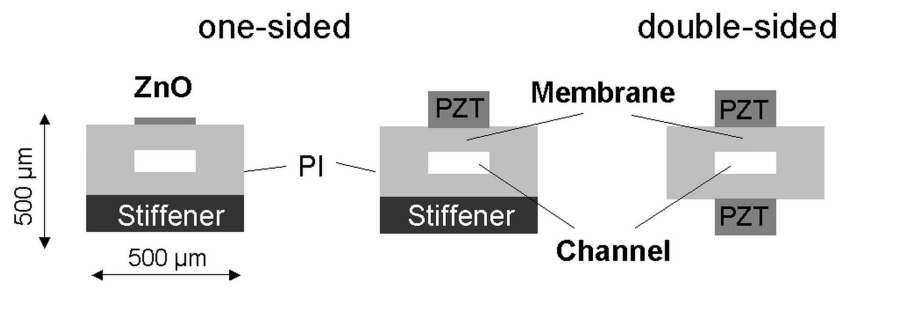

Figure 2.1: Different model with thin-film actuator (ZnO) and ceramic actuator (PZT) on polyimide (PI) membrane including the channel.

For the simulation of the actuator a simplification was done. In reality, a piezoelectric actuator is built as sandwich with a piezoelectric active layer in the middle and electrodes on both sides. Instead of simulating the piezoelectric active part and the electrodes (passive part) as different elements, it was decided to model the entire thickness as one active layer. This method counts on one side the mechanical stiffness of the electrodes and on the other side the electric field in the active layer is reduced, because of the electrical potential is applied across the entire thickness. The error with this method is around 5-10 % compared to a simulation with an active layer and electrodes. The major advantage is that, the numbers of the elements can be reduced for a given aspect ratio for the element size, which results in a shorter calculation time.

2.5 Finite element modeling (FEM)

For solving the piezoelectric equation, finite element modeling program ANSYS was used. The FEM allows modeling the deformation of piezoelectric actuator assembled to a membrane. The

membrane displacement was modeled with and without a static channel pressure. The results were displacement (stroke volume) and mechanical stress for applied voltage and pressure. The goal of the FEM simulation was to optimize the size of the actuator (length and thickness) and the thickness of the membrane in relation to the driving voltage and membrane displacement under pressure. The modeling was done for three different layouts as shown in the roadmap and in figure 2.1: First, ZnO thin-film actuators, then PZT one-sided actuation and finally, PZT double-sided actuation. In the following paragraphs, these three models will be analyzed and compared with measurements made on prototypes. The employed piezo-electric constants and material properties for ZnO thin-film and PZT ceramic material, grade PZT-5H, are listed in table 2.3.

		ZnO	**PZT**
ε	[-]	9.8	830
$\mathbf{d_{31}}$	[pC/N]	-4	-171
$\mathbf{d_{33}}$	[pC/N]	12	374
$\mathbf{e_{31}}$	[C/m²]	-0.3	-14.3
$\mathbf{e_{33}}$	[C/m²]	1	27.8
E	[GPa]	94	66

Table 2.3: Overview of some typical material properties for ZnO thin-film and PZT-5H.

The modeling can be done for a 2-dimensional and/or 3-dimensional model. A 3-d model increases enormously the computing time and if possible the model should be reduced to a 2-d model, which is possible in our cases. Most of the design parameters are given because of the 2-d nozzle spacing of 500 µm only. Two parameters can be optimized: The thicknesses of the actuator and of the membrane.

2.5.1 ZnO thin-film actuator

ZnO thin-film was analyzed for different membrane thickness and actuator thickness against pressure. In figure 2.2, a 1.5 µm thin ZnO actuator with membrane thicknesses of 13, 25 and 50 µm respectively were simulated. The channel pressure was changed from zero to 600 mbar at a constant driving signal of 100 volt. At no pressure, a displacement larger than 130 nm is shown for a 13 µm membrane. The pressure dependence of 730 nm/bar is high and the displacement is already reduced to zero at a pressure of about 200 mbar.

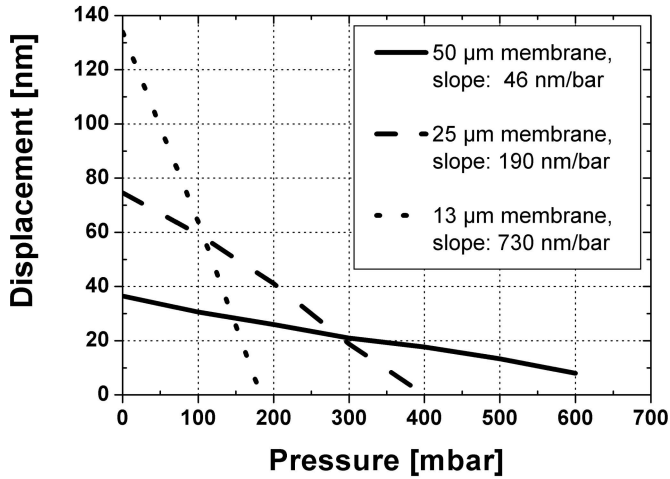

Figure 2.2: Displacement against pressure for ZnO actuation at different membrane thicknesses and for a driving voltage of 100 volt.

By increasing the membrane thickness, a higher stability can be reached on the expense of the membrane displacement. The membrane thickness was set to 25 µm as a compromise between stability and displacement. Next, in figure 2.3, the thickness of the

ZnO actuator was parameterized as function of the channel pressure. A 5 µm thick ZnO would further increase the stability. However, such a layer could not be deposited successfully onto polyimide substrates because of a too high internal stress in the piezoelectric layer. Again, as a compromise, prototypes with a 1.5 µm thin ZnO layer on a 25 µm thick membrane were fabricated and characterized.

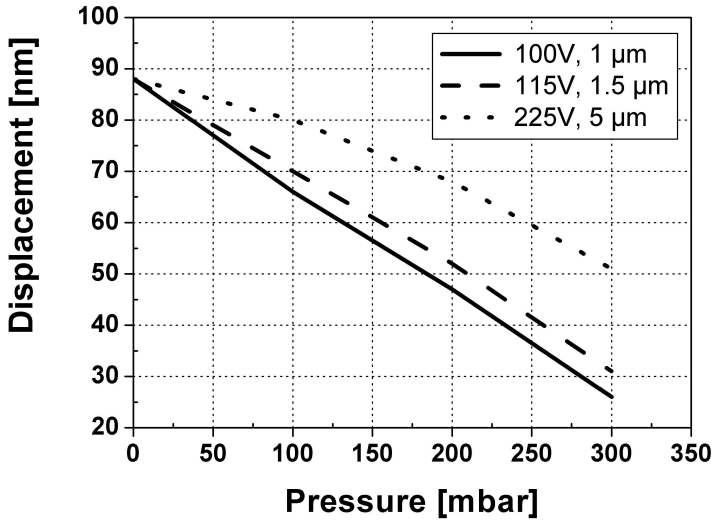

Figure 2.3: Displacement of a ZnO actuated membrane against pressure for a 25 µm polyimide membrane. The ZnO thickness was parameterized from 1 to 5 µm. The driving voltage was set for identical displacement at zero pressure.

In figure 2.4, the FEM model of a ZnO-actuated dispenser with four channels is shown. The model is to scale with a channel spacing of 500 µm. The displacement is enlarged by a factor 300 for demonstrating the deformation. For the simulation, four channels were chosen to allow observing crosstalk between the channels. No

crosstalk has been observed. The deformed shape of the polyimide channel is shown in figure 2.4. Next to the membrane deformation, the actuators bend also the entire substrate. The substrate bending is 40 nm, indicated as u_{sup}=-40 nm. This deformation creates acoustic vibrations. Prototypes indeed showed acoustical noise because of this substrate bending!

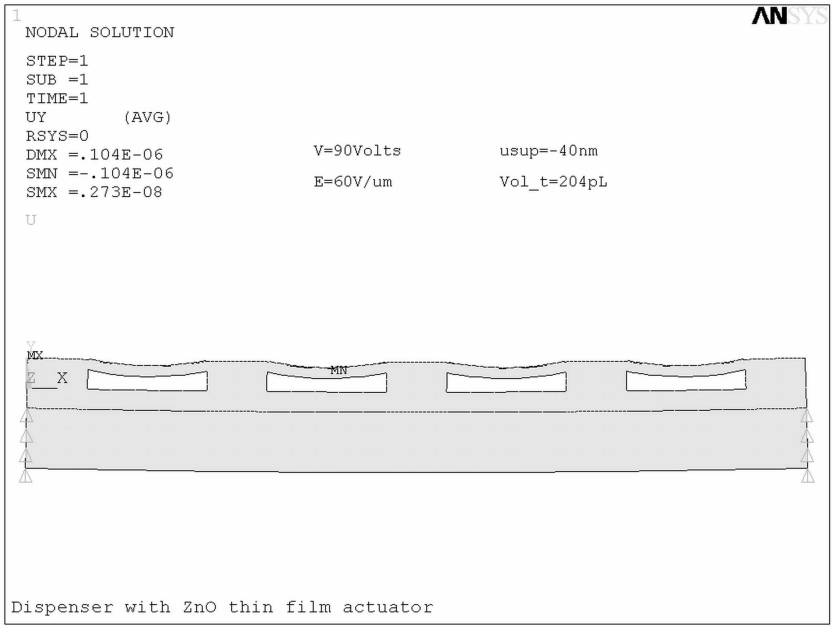

Figure 2.4: FEM model with ZnO actuators. A stroke volume of Vol_t=204 pL was calculated for a driving voltage of 90 volt and at zero pressure.

The stroke volume was calculated by integrating the channel deformation multiplied by the channel length between the nozzle and restriction, and was found to be 204 pL, Ref. 4. This stroke volume as such would be high enough but as shown in figure 2.2 and 2.3 there is also a high pressure dependency to be considered. The lack of stiffness against pressure reduces the amplitude during

dispensing and no droplet could be ejected. The dispensing with a prototype was not successful. To overcome this difficulty, PZT actuators were chosen and will be analyzed in the next paragraph.

2.5.2 PZT Ceramic actuator

Dispenser sheets were fabricated with one-sided and double-sided PZT ceramic actuators. The actuators were assembled on polyimide membranes by gluing. Both layouts, see figure 2.1, were modeled with ANSYS 7.1. The size of commercially available PZT plates was also taken into considerations.

One-sided actuation

The behavior of PZT ceramics actuator was modeled for a one-sided actuation. The thickness of the actuator and membrane were parameterized for the simulation. A 100 µm thick PZT actuator at 100 volt shows a displacement of 34 nm for a membrane thickness of 50 µm and a slightly smaller displacement of 31 nm for a membrane thickness of 25 µm, as shown in figure 2.5. An FEM model of four channels is shown in figure 2.6. The pressure dependency of the displacement by using PZT ceramics is small (2 nm/bar, figure 2.5) and not significant up to 2-3 bar. In figure 2.5 on the left side, the displacement as function of the PZT thickness has been simulated. High displacement could be reached with thin PZT plates with a thickness of 25 or 50 µm because the mechanical stiffness of the actuator plate is reduced and closer to the stiffness of the membrane. For instance, a 50 µm thick PZT plate would decrease the driving voltage significantly by about a factor of 3 compared to a 130 µm PZT plate. However, such thin PZT plates are not easy to handle and they are not commercially available as standard products.

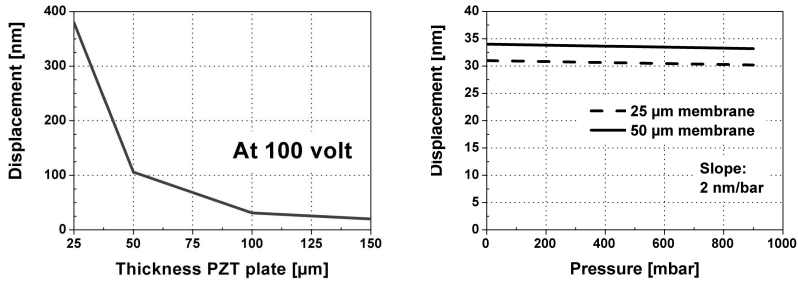

Figure 2.5: Left, displacement versus PZT plate thickness at 100 volt for 25 µm thick polyimide membrane. Right, pressure dependency of 100 µm thick PZT plate at 100 volt.

A one-sided actuated four-channel model is shown in figure 2.6 with an actuator thickness of 130 µm. At this point, the commercially available PZT actuators have been taken into consideration. Dispensers were built according to the simulation result, shown in figure 2.6. The figure 2,6 shows the deformed shape at a driving voltage of 138 volt. This driving voltage corresponds to the used in prototype, which has dispensed droplets at a velocity of 1.8 m/s.

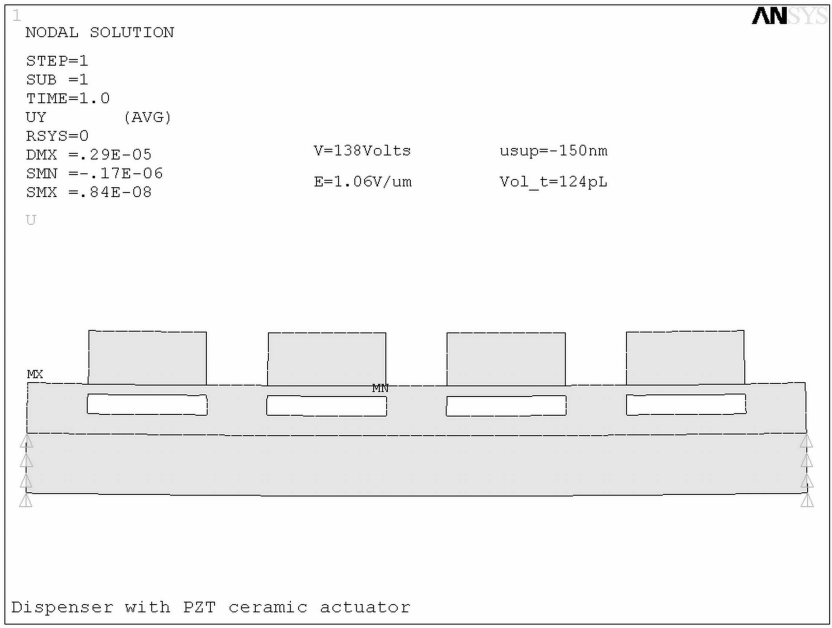

Figure 2.6: FEM model with 130 µm PZT plate actuator. The channel size is 300 µm times 50 µm. The stroke volume is vol_t=124 pL for 138 volt. Prototypes built to this model showed successful dispensing at 138 volt.

Two deformations are visible in figure 2.6. First, there is the deformation of the channel. By integrating the channel deformation the stroke value can be calculated as before. The integrated stroke volume is 124 pL for a driving voltage of 138 volt. This stroke volume is required for dispensing droplets at a velocity of 1.8 m/s. Second, the entire stiffener plate is bent at about 140 nm indicated as u_sup in figure 2.6. This bending occurs because the relative high thickness of the actuator (130 µm) compared to the thickness of the membrane (50 µm). The bending of the stiffener plate results in acoustic noise, which may be uncomfortable for the operator, when high dispensing frequencies are used. The bending can be compensated using a double-sided actuation as shown in the next paragraph.

Double-sided actuation

The motivation of using double-sided actuation is to reduce the driving voltage, to reduce the substrate bending and therefore, reducing the acoustic noise during dispensing. The deformed model is shown in figure 2.7. The driving voltages were compared for identical stroke volumes (129 pL) for one-sided and double-sided actuation. The simulation showed that the driving voltage is reduced by about 20 % from 138 volt to 110 volt. This result was experimentally confirmed at a constant droplet velocity of 1.8 m/s. For one-sided actuation, the substrate bending is about 150 nm over 4 channels. This deformation is now reduced to 0 nm for double-sided actuation as shown in figure 3.6 (u_{sup}=0 nm). The acoustic noise was clearly reduced in the experiment.

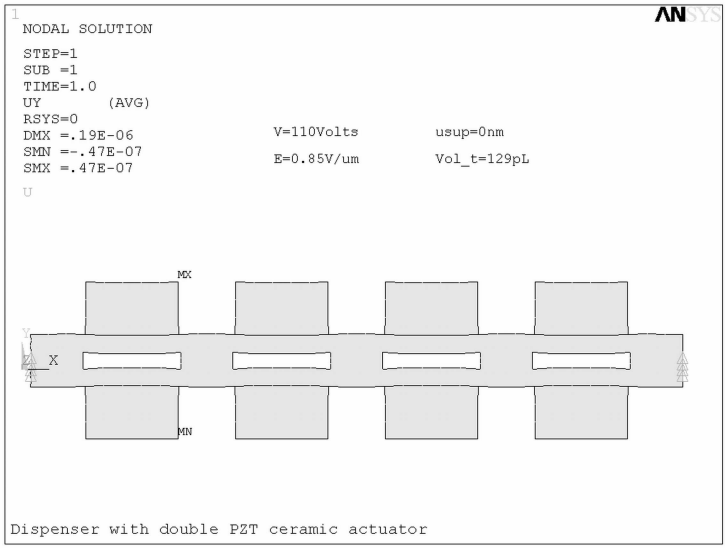

Figure 2.7: Deformed shape of a double-sided actuated PZT plate. A stroke volume of 129 pL is achieved at 110 volt. A prototype was built and showed successful dispensing at 110 volt.

At the prototype level, no in the drop formation was observed for both one-sided and double-sided actuation at 138 volt and 110 volt respectively. The fabrication and assembling is not more complicated but more fabrication steps are required for a double-sided actuation 24-channel dispenser sheet. The measured total thickness of a such a dispenser sheet is about 475 µm.

2.5.3 Alternative piezoelectric actuator

Thin-film and ceramics PZT material were used for fabricating prototypes. We also investigated an alternative piezoelectric material based on polymer. A commercially available polymer with piezoelectric activity is PVDF (Polyvinylidenefluoride). Sheets in different sizes and thicknesses from 9 to 40 µm are commercially available. The PVDF actuator has been only modeled. The modeling showed that the low Young's modulus of 2 GPa and the low piezoelectric coefficient of e_{31} = -0.016 C/m² are far too small for using PVDF as an actuator. In general, PVDF is mostly used for sensors.

2.6 Summary with experimental results

In table 2.4, the modeled values are compared with measurements performed on different prototypes. The column "voltage" contains the driving signal, which must be applied to the prototype for dispensing droplets. These voltages also correspond with the stroboscopic image of drop formation shown in figure 2.8. The stroboscopic images were taken at a delay time of 60 µs. The stroke volume was calculated from the difference of the initial channel volume and the contracted channel volume for the given voltage in table 2.4. The ZnO actuator created a calculated stroke volume of 204 pL at zero pressure and at a maximum voltage of 90 volt. The calculated stroke

volume should be sufficient for droplet dispensing. However, no droplets were ejected for ZnO actuated dispenser as shown in figure 2.8. The pressure during dispensing reduced the stroke volume to about 60 pL, as estimated from figure 2.8. The ZnO actuator pushed the meniscus of about 30 pL at the nozzle side that means that also about 30 pL flowed through the supply channel which resulted in a stroke volume of about 60 pL. To bring a ZnO actuator dispenser to success, the stroke volume should at least be doubled. That means the driving voltage would need to increase from 90 volt to 180 volt, which is far above the measured breakdown voltage of 90 volt.

Actuation mode	Mat.	Actuator Thick. [µm]	Mem. Thick. [µm]	Voltage Prototype [V]	Simulated Volume [pL]	Droplets of 65 pL
One-sided	**ZnO**	**1.5**	**25**	**max 90*** **	**(204)**	**No**
One-sided	**PZT**	**130**	**25**	**138****	**124**	**Yes**
One-sided	**PZT**	**130**	**50**	**132****	**124**	**Yes**
Double-sided	**PZT**	**130**	**50**	**110****	**129**	**Yes**
One-sided	*PZT*	*50*	*25*	*38*	*125*	*N.A.*
Double-sided	*PZT*	*50*	*50*	*26*	*124*	*N.A.*
Extracted					*90-120**	

** published in Ref. 4, ** measured and used for modeling,*
**** breakdown voltage of ZnO thin-film actuator*

Table 2.4: Simulation results verified by dispensing with prototypes. The simulated stroke volume is based on a 20 mm long actuation chamber. There is no prototype available for the values in italic because 50 µm thin bulk PZT actuators with the required specification were not commercially available.

Again, the calculated stroke volume for PZT actuators was around 125 pL, meaning that, about half of the stroke volume was flowing forward to the nozzle and was ejected (65 pL) and the other half was

flowing backward through the supply channel into the reservoir. The relation of forward to backward flow depends on the fluidic resistance of the channel and nozzle, which is discussed later. The simulated stroke volumes are in agreement with those observed in prototypes using PZT ceramics actuators.

Figure 2.8: Stroboscopic image of droplet and meniscus position at driving voltage given in table 2.4. ZnO was not able to push the droplet completely out of the nozzle because the pressure becomes important at that moment. Successful dispensing is achieved with PZT ceramic actuators.

PZT actuators with a thickness of 130 µm worked well for one-sided and double-sided actuation. We conclude that if 50 µm thin PZT plates were commercially available the driving voltage could be reduced by about 100 volt. Experimental results of the measurements of membrane displacement and extraction of the stroke volume have been published in Ref. 4.

2.7 Conclusion

ZnO thin-film actuators have the unique possibility of full integration onto the polyimide membrane. No assembling or gluing process is required. However, as demonstrated, ZnO lacks of stiffness for microfluidic applications where pressure becomes important. A complete characterization of ZnO thin-film was published in Ref. 1 and Ref. 2.

PZT ceramic actuators fulfill all required specifications and successful dispensing was proven. PZT actuators are commercially available and show a high stability. PZT plates are customized diced and assembled by gluing onto the polyimide membrane.

3 CFD MODELING

3.1 Introduction

The goal is to simulate the formation of a drop for different channel geometries of a one-channel dispenser. The piezoelectric actuator and the membrane were added to the model, which allows simulating the drop formation as function of the driving voltage. For solving this task, a computational fluid dynamics (CFD) algorithm was used in combination with finite element modeling (FEM) for the actuator-membrane displacement. As simulation tool CFD-ACE(U) was chosen, [CFDRC, 2002]. CFD-ACE(U) has the excellent capability of multi-physics solving which is required for the given task. The dispenser was first been simulated as 2-dimensional axisymmetric model. Within a short calculation time, this model delivered the results of the effect of a fluidic restriction. The more complex 3-dimensional model was used for evaluating membrane displacement, drop formation, pressure and velocity profile. The simulation results are compared with measurements.

3.2 Modeling

For modeling a one-channel dispenser different modules of the CFD-ACE(U) tool must be chosen. The flow, free surface volume of fluids (VOF), stress and electric module have been selected and are described below.

The flow module is the heart of the CFD-ACE(U) solver, and is used for most simulations. Activation of the flow module initiates the solution of the velocity-field, by solving for the x, y and z-momentum

equations and the pressure-field by solving the pressure correction equation. The flow module is based on the Navier–Stokes equation, the primary equation of computational fluid dynamics. This equation relates pressure and external forces acting on a fluid to the response of the fluid flow. The motion of a non-turbulent, incompressible, Newtonian fluid is governed by the Navier-Stokes equation given below:

$$\vec{a} = \frac{\partial \vec{u}}{\partial t} + (\vec{u} \cdot \nabla)\vec{u} = -\frac{1}{\rho}\nabla p + \nu \nabla^2 \vec{u} + \frac{1}{\rho}\vec{F}.$$

f_n = acceleration force [m/s^2]
dV = infinitesimal volume part [m^3]
υ = kinematic viscosity [m^2/s]
ρ = density [kg/m^3]
u = velocity vector [m/s]
v = component of velocity vector [m/s]
t = time [s]
p = pressure [N/m^2]
∇ = gradient operator = $(\delta/\delta x, \cdot \delta/\delta y, \cdot \delta/\delta z)$

The left side of the equation describes the transient and convection term and the right side the forces acting on the fluid. The convection term, also called convective acceleration arises when the fluid flows through regions of spatially varying velocity, as in a nozzle or diffuser. Flows, which are nominally “steady” may have large accelerations due to this convective term. The term ∇p describes the pressure force density $f_p = dF_p/dV = -\nabla p$ created by a pressure gradient. The term $\nu\nabla^2 u$ describes the viscosity loss in the fluidic, where $f_n = dF_n/dV = \nu\delta^2 u/\delta x^2$. The last term describes any other acceleration forces acting on the fluidic such as gravity, turbulence, etc. In microfluidic devices the gravity is negligible. For compressible fluids the term $1/3 \cdot \upsilon(\nabla(\nabla \cdot u))$ is added to the right side, [White, 1999].

This capability is often used in conjunction with more of the other modules to provide a multi-physic based solution to an engineering task such as coupling of finite-element modeling, etc.

The free surface volume of fluids (VOF) capability in CFD-ACE(U) allows the simulation of a mixture of two immiscible fluids such as water/air, including the effects of surface tensions. Several methods have been previously used to approximate free boundaries in finite difference numerical simulations. A simple but powerful method is based on the concept of fractional volume of fluid (VOF). This method is known to be flexible and efficient for complicated free boundary configurations, [Bogy, 1984], [Dijksman, 1984], [Eggers, 1995], [Hirt, 1981], [Papageorgiou, 1995], [Wilkes, 1999], [Yeh, 2001]. However, the VOF calculations lack the resolution needed to capture the details of satellite droplets, [Notz, 2001].

The stress module adds a finite element structural analysis capability to CFD-ACE(U). The structural model may be coupled with other modules for multidisciplinary analysis. Two-way coupling mode represents an implicit coupling between the stress module and the other modules. Pressure, temperature, etc. are sent to the stress module, where deformation and stresses are calculated. Then these results are sent back to the other modules where the solution is recalculated on the new deformed geometry. Iterations are performed until convergence is obtained.

The electric module solves the governing equations for electrostatics, electrical conduction including DC and AC conduction, and piezoelectricity. It can be chosen between the d- and e-form of the constitutive piezoelectric equations.

The drop formation is analyzed as a function of time. For a transient simulation in combination with VOF, the automatic time step option is

used to ensure that the free surface crosses less than a cell during that time step.

3.3 2-d Model

The goal of the 2-d simulation was to evaluate the driving voltage for droplet ejection as function of the ratio of the restriction size r to the nozzle size R. The driving voltage was for a droplet velocity of 2.7 m/s for the simulation and also for experimental measurements. For the 2-d axisymmetric model the parameters are shown in figure 3.1. To reduce the number of grid elements, hence computing time, the supply channel and reservoir were not included in the model. Moreover, a reference pressure of 980 mbar was set to the environment, meaning that p=0 mbar is equal to the reference pressure of 980 mbar. For the simulation a voltage-time function similar to the driving voltage of the prototype was applied.

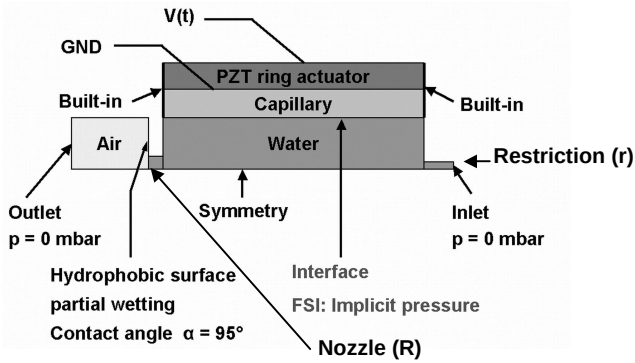

Figure 3.1: Boundary conditions of the 2-d axisymmetric model including piezoelectric actuation. For the simulation a voltage time function similar to the driving voltage of the prototype was applied.

A two-fluid model is used for the calculation of the drop formation: The primary fluid was air and the secondary fluid was water. This option allowed also calculating a filling process of the microfluidic devices. For all the simulations, the values of table 3.1 were used for the properties of the fluids.

		Primary fluid	**Secondary fluid**
Medium	**---**	**Air**	**Water**
Density ρ	Kg/m^3	1.16	1000
Viscosity ν	m^2/s	$1.59*10^{-5}$	10^{-6}
Surface tension σ	mN/m	---	72.5

Table 3.1: Properties of fluid used in CFD simulations.

Different channel geometries

Again, the goal of the simulation was to calculate the variation of driving voltage for a constant droplet velocity, while changing the restriction size (r) for a constant nozzle size (R).

If the fluidic resistance of the restriction is much larger than the fluidic resistance of the nozzle, the fluid will mostly flow out through the nozzle. As relatively little is flowing in the restrictor, the damping of the compression phase is poor. As the filling phase requires fluid to flow through the restrictor to fill the chamber, the damping is higher and causes a long wait for filling.

If the fluid resistance of restrictor is much lower than the one of the nozzle, the fluid mostly flows out of the restrictor during the compression phase. The energy required to eject a droplet is expected to increase. The major fluid flow in the compression phase is expected to be between the actuator and the restriction. This flow is not well damped and the frequency response will be decreased.

The conclusion of the above discussion is that the fluidic resistance of restriction and nozzle should be about the same. To the considerations above, the pressure drop at the nozzle rim, created by the surface tension effect of small droplets, should be added. Thus, the restriction should be slightly smaller than the nozzle for an equal pressure drop on the nozzle and the restriction.

In figure 3.2, the results of a simulation and experimental measurements are shown and compared. The driving voltage corresponds to a droplet velocity of 2.7 m/s. It has been normalized, such that the minimal driving voltage is 1. The normalizing factor for the experimental curve is 89.8 volt. The normalization allows comparing the 2-d simulation results with experimental measurements. The x-axis describes the ratio of the restriction size r to the nozzle size R. For the prototype, r corresponds to the restriction width and R to the nozzle width. The graph in figure 3.2 can be divided in three different zones $r/R>1$, $0.4<r/R<1$ and $r/R<0.4$.

For the zone of $r/R>1$ the effect of the fluidic resistance of the supply channel becomes dominate over the fluidic resistance of the restriction. In the CFD simulation the supply channel was omitted which explains the higher normalized driving voltage compared with measurements.

In the zone of $0.4<r/R<1$, simulations and measurements show similar linear behavior as function of the driving voltage. This allows concluding that the supply channel resistance has a minor influence as observed for different prototypes with a channel length of 2 cm and 10 cm. This is an important result because the supply channels of a 24-channel dispenser sheet have a length difference from the outer to inner channel of 10 %. The difference of channel length will

not influence the driving voltage when a restriction is used.

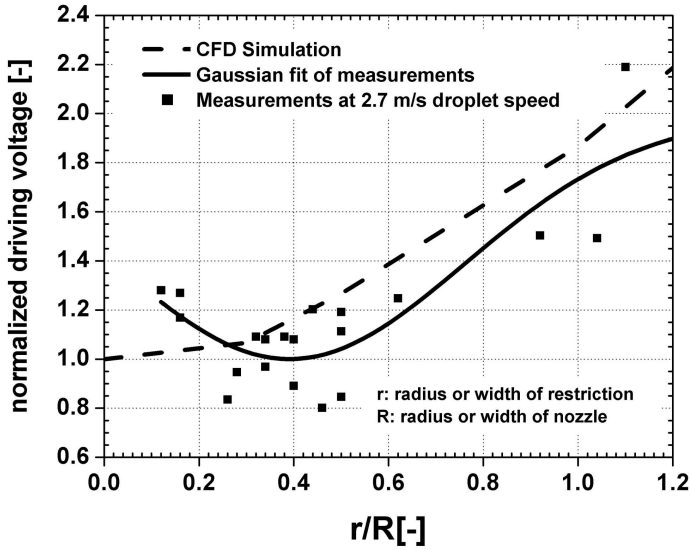

Figure 3.2: CFD simulation and measurements vs. relation of restriction size to nozzle size (r/R). The driving voltage corresponds to a droplet velocity of 2.7 m/s for the simulation and measurements. For comparison the driving voltage has been normalized so that the minimal driving voltage is 1 for simulation and measurements at a droplet velocity of 2.7 m/s.

In the left zone of figure 3.2, r/R<0.4, the experimental driving voltage increases compared to the CFD simulation. The fluidic resistance of the restriction is high and the refilling of the chamber is slow. The chamber may even temporarily starve of liquid, which explains the higher driving voltage. In the CFD simulation, the refilling of the chamber was not simulated.

A prototype, without a restriction, was analyzed. From extrapolated measurements we obtain a driving voltage of 260 volt, or a normalized driving voltage of 2.9 respectively. These results are published in Ref. 5. In other words, I found that the driving voltage was about three times higher without a restriction ($r/R \approx 6$), than with a restriction ration of r/R=0.4.

In conclusion, a restriction lowers the driving voltage considerably. The relation r/R should be within $0.4<r/R<1$. Considering the initial channel filling and the manufacturing of narrow µ-channels it is recommended to set the relation r/R to 0.7, which results in a restriction width of 35 µm at a nozzle size of 50 µm. The dispensing is in that case independent of the supply-channel length. This independence was observed between the first 4-channel dispenser prototype with a channel length of 2 cm and the full size device with a channel length of 10 cm: Both designs showed the same driving voltage as published in Ref. 3 and Ref. 5.

3.4 3-d Model

A 3-dimensional model was generated. The goal within this CFD simulation was to analyze the membrane displacement, velocity and pressure profile as a function of time. A 3-dimensional model may require a computing time of several days. For that reason the length of the chamber where the piezo actuator is fixed was reduced by a factor 40 from 20 mm to 0.5 mm. The other dimensions corresponded to those of the prototype. By scaling the length of the chamber only the stroke volume is affected and is reduced linearly. The surface to volume ratio of the nozzle and restriction does not change and so the fluidic behavior is unchanged. The model is shown in figure 3.3. The restriction size for this model is 35 µm with a 50 µm nozzle.

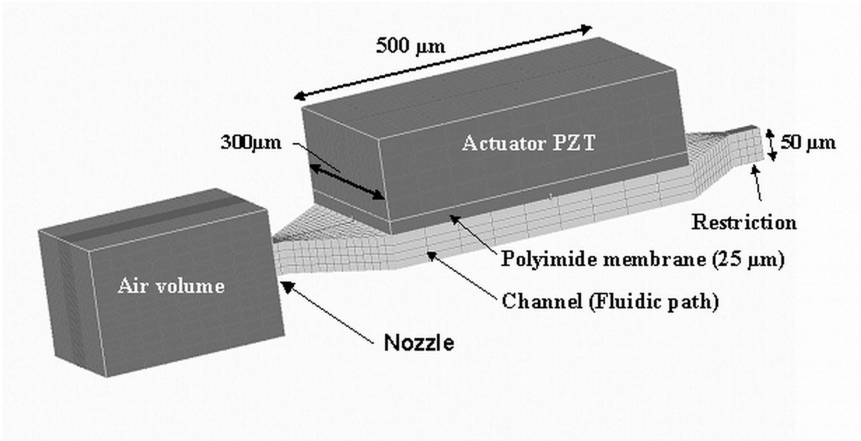

Figure 3.3: 3-dimensional CFD simulation model of one dispensing channel, including piezoelectric actuator and membrane. The chamber length is reduced from 20 mm (prototype) to 0.5 mm for saving computing time.

The calculated model is presented in figure 3.4, where drop formation is shown. The droplet is completely separated from the nozzle at a time of about 25 µs. It was not possible to simulate satellite droplets, which nonetheless may occur at too high driving voltage as observed with the prototype. The used VOF algorithm is not able to calculate satellite droplets, [Notz, 2001].

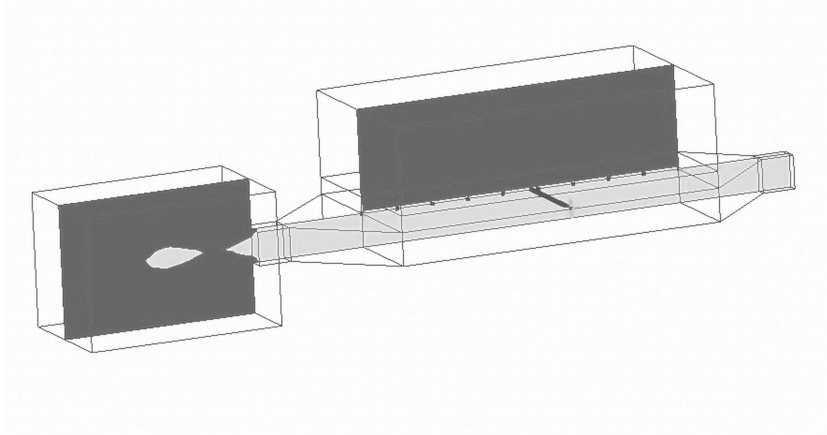

Figure 3.4: 3-d CFD simulation of drop formation at optimized driving voltage at a delay time of 32 µs. Light gray surface corresponds to the dispensing liquid, here water. For visualization only a cut along the center-axe of the dispenser is shown.

The membrane center displacement was analyzed during drop formation. The simulated membrane center displacement was plotted versus time and is shown in figure 3.5. The maximum center membrane displacement is 800 nm for a droplet ejection at 2.7 m/s. The maximum membrane displacement is reached 6 µs after pulse applies, given by the shape of the driving signal. By keeping the stroke volume constant, the simulated center membrane displacement was then rescaled to the prototype size. The scaling factor is 1/40 and results in membrane center displacement of 20 nm for a chamber length of 20 mm. This simulation result is also confirmed by measurements published in Ref. 4. A maximum center displacement of 15-20 nm was measured during dispensing.

Interesting is also the moment of necking and break-off. Necking starts when the pressure changes sign and gets a negative value. The pressure is proportional to the acceleration of the membrane displacement, in other words the pressure is proportional to the second derivative of displacement (d^2y/dt^2). This is observed at t=11

µs. By increasing the pulse width, the point (d^2y/dt^2) is placed more to the right and the necking starts later. With this method the droplet volume can be increased within the range of some tens of picoliter as published in Ref. 3. The break-off process is about finished when the membrane reaches the initial position.

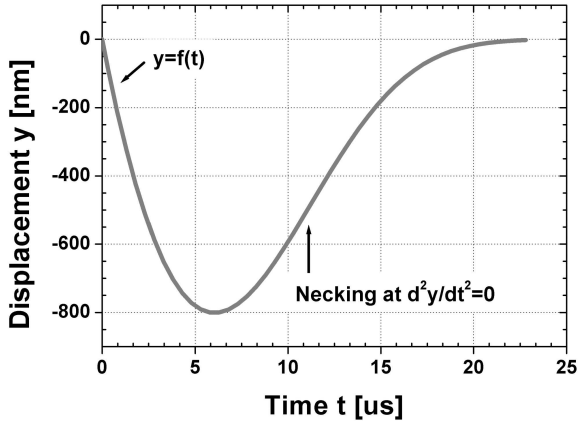

Figure 3.5: Membrane center displacement versus time.

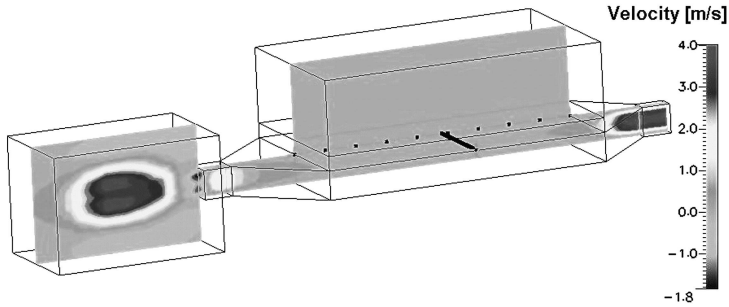

Figure 3.6: Velocity profile at the moment of droplet break-off.

The velocity profile of the liquid was analyzed. The droplet velocity after break-off as shown in figure 3.6 is 2.7 m/s. At the same time step the velocity at the restriction is slightly higher at about 4 m/s because of the smaller cross section of the restriction compared to the nozzle. There is a negative velocity of 1.8 m/s observed at the nozzle, given by the break-off effect. The droplet velocity measured with stroboscopic illumination varied from 1.5 to 3 m/s depending on the driving voltage. The droplet velocity is proportional to the driving voltage, Ref. 5.

The pressure profile as function of time was not possible to analyze within the CFD-ACE(U) Version 2002. The pressure should be proportional to the acceleration of the membrane displacement, in other words, the pressure is proportional to the second derivate of displacement. CFD simulation results show an oscillation with a time period of 5 µs. The oscillation was also observed in the 2-d model. This oscillation cannot be explained physically and may be instability of the software. In co-operation with CFDRC it was found that the pressure oscillation is an effect of the coupling between mechanical and fluidic because of the transient boundary condition.

To get an idea about the pressure in the pump chamber during dispensing, a pure static analysis can be done. Supposing that one half of the liquid is flowing through the nozzle and forms a 65 pL droplet and the other half (also 65 pL) is flowing backward through the restriction, Ref. 3. The pressure pulse is applied for 25 µs, meaning pulse width including rise time but without fall time. The static flow rate is then Q=V/t=65pL/25µs=2.6µL/s. The fluidic resistance of the restriction (rectangular channel) was calculated and is R=336mbar*s/µL. The pressure drop is the product of $\Delta p=Q*R=2.6\mu L/s*336mbar*s/\mu L=874$ mbar. This calculation does not include any acceleration forces acting on the liquid. The pressure of about 874 mbar is high, but as demonstrated with FEM simulation,

the displacement of PZT actuation stays almost constant because of the low pressure dependency of 2 nm/bar.

The CFD simulations were made for incompressible flow. This is valid for a velocity much smaller than the speed of sound in the liquid (v_{sound}=1483m/s at 20℃ compared to v_{liquid}=4 m/s). Nevertheless, without compressibility, the propagation of a pressure wave in a transient simulation cannot be seen. The compressibility could be added by writing a user subroutine describing the liquid density as function of pressure.

In general, CFD simulation was demonstrated for dispensing. The excellence in multi-physics allowed building an entire dispenser including piezoelectric actuation. The restriction size could be optimized within a 2-d model. A 2-d model takes a computing time of some hours. The computing time for a 3-d model is about a day and allows calculating the required membrane center displacement and velocity. The CFD code must be improved for the transient calculation of the pressure field.

3.5 Conclusion

We demonstrated the feasibility of multi-physics modeling. During the development of the prototypes we proved the effect of the restriction by simulation and the size of the restriction was determined. This result reduced the number of prototypes, which was the main goal of a CFD simulation. Furthermore, the interaction between different elements has been better understood through CFD simulation. At an industrial level, CFD simulations become more and more integrated in the development of prototypes.

4 BASE MATERIAL AND FABRICATION

4.1 Introduction

The dispenser, as presented in the concept, is built from flexible sheets. The flexible sheets contain sealed µ-channels, which reduce the spatial spacing from 4.5 mm to 0.5 mm. The final thickness of the sheets is less than 0.5 mm. This allows stacking of individual sheets to build a 2-dimensional dispenser with a nozzle spacing of 0.5 mm. This chapter discusses the choice of base material and describes the key fabrication processes.

Base material selection criteria:
Potential base materials of different polymers have been confronted to a set of criteria which need to be simultaneously fulfilled in order to meet both manufacturability and application requirements of the dispensers.

Out of the different polymers, a commercially available heat sealable polyimide sheet has been chosen as base material. This material can be processed by standard Micro-Electro Mechanical Systems (MEMS) technology. Polyimide sheets have good chemical resistance and the mechanical properties such as Young modulus and ultimate tensile strength are higher compared to other plastics such as Polyethylentherephthalat (PET) or Polycarbonat (PC).

4.2 Base material selection criteria

Flexibility

The µ-channels must be mechanically flexible in order to build a 2-dimensional dispenser. It is preferred that the printhead and format adapter are made out of one piece to minimize the internal volume of the dispenser and to avoid any changes of surface properties such as contact angle along the fluidic path. This would complicate the filling and air bubbles could be trapped in the channel.

Patterning

Channels with a high aspect ratio have to be patterned into the polymer. The minimal feature size is about 20 µm in width and 50 µm in depth. To reach a tight dimension control, the substrate should be patternable by anisotropic plasma etching or by laser ablation.

Packaging

The µ-channels must be tightly sealed without any adhesives. A polymer direct bonding process is required. The thermal bonding can be carried out at a temperature around the glass transition temperature Tg. The bond must withstand a channel backpressure of up to 1-3 bar. The high backpressure is useful for cleaning the µ-channels by flushing a cleaning solution through the channels and for a fast drying of the channels.

Thermal and mechanical stability

In order to electrically connect the actuators, thin film electrodes needs to be deposited onto the sealed channels. The thin films may be patterned by wet etching, for instance. Onto thin-film electrodes, piezoelectric actuators are integrated by sputtering or gluing,

reaching process temperatures in the order of 80-100℃. Mechanically, the squeezing of the membrane by the piezoelectric actuator creates compressive and tensile stresses. Therefore, the material should behave linearly for stress versus strain up to at least 20 MPa, as calculated using finite element modeling (FEM).

Chemical and biological compatibility

When exposed to commonly used solvents, polymer material can be subject to swelling or leaching. Fluid permeating into the material can cause swelling. Leaching is another reaction caused by fluid transfer. The fluid that had previously permeated into the device material can move back into the biological liquid and carry material particulates suspended within. These effects need to be avoided by choosing an adequate material.

Conclusion

All the criteria above are fulfilled for heat sealable polyimide sheets. However other polymers, such as Polyethylentherephthalat (PET) or Polycarbonat (PC), could be also considered as base material. Though, these materials have a much lower chemical and thermal resistance than polyimide. Polyimide sheets are well known in the biological world as inert base material and therefore well accepted.

4.2.1 Surface properties and liquid-solid interaction

While it is desirable that the nozzle outside surface of the dispenser be hydrophobic allowing stable and straight droplet ejection, the inner surface of the channels should preferably be hydrophilic for self-filling by capillary forces.

An important part of a droplet dispenser is the surface properties of the nozzle outer surface, because it strongly affects the dispenser performance. A hydrophobic nozzle outer surface without any further coatings is required for stable dispensing and straight droplet trajectory. A hydrophobic outer surface avoids wetting of nozzle surface during dispensing and controls the position of the meniscus of liquid column from droplet to droplet, resulting in a high stability of the dispenser performance.

A drawback of using polymer as substrate for micro fluidic devices is the hydrophobicity inside the channels. The channel stays hydrophobic even after patterning which does not allow the self-filling of the µ-channel by means of a capillary force. The capillary force is driven by the surface free energy. A consequence is the contact angle α at liquid-gas-solid interface. If $\alpha > 90$ deg no wetting of the surface occurs (hydrophobic), and if $\alpha < 90$ deg the liquid is wetting the surface (hydrophilic) and the µ-channel starts filling by capillary force. The contact angle α for sealed polyimide channels have been measured and is 95 deg for water-air-polyimide interface. [Frohn, 2002]

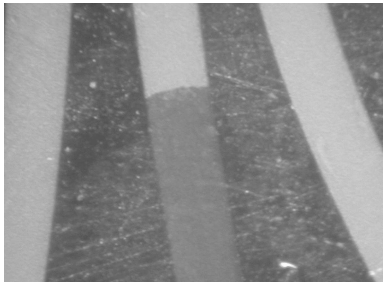

Figure 4.1: Water plug in a sealed polyimide channel. The contact angle to the sidewall is 95 degrees.

The not self-filling of the device has been solved by applying a backpressure onto the well plate. At a pressure of about 20 mbar,

the channels fill simultaneously. The liquid is then stopped by surface tension effect at the nozzle. This method requires a print device, which is tightly held onto the well plate for filling.

4.2.2 Material availability and key characteristics

Polyimide is available in different forms starting from photosensitized liquid used for spin coating, over heat sealable sheets up to non-bondable inert polyimide sheets. The main characteristic value of polyimide is the glass transition temperature Tg, which ranges from 80℃ up to 550℃. The glass transition temperature is important for two reasons. First, it is the temperature at which the Young modulus usually drops significantly. Second, thermoplastic films start flowing at Tg, which can lead to line deformation if external stress is applied. Many polyimides do not exhibit marked glass transition and, hence their determination is not possible by calorimetry. However, measurements of the linear CTE (coefficient of thermal expansion) by thermal mechanical analysis (TMA) usually allow determination of the Tg because the CTE increases markedly above this temperature.

Heat sealable polyimide materials have been developed in the last few years mainly for flex print circuits (FPC). The development of heat-sealable polyimide films results of demands from the field of electrical and electronics industries. So far, a popular structure of copper clad lamination used for FPC is a three-layer type consisting of a polyimide film, a copper foil and an acrylic adhesive. However, there are some drawbacks pointed out for FPC; heat-resistance of FPC decreases more than the polyimide film because of adhesives, and the thickness of the FPC substrate is also restricted to the need of thickness due to that of the bonding layer. For these reasons heat sealable polyimide sheets have been developed in recent years.

4.2.3 Different polyimides

The range of polyimide available for electronics applications is staggering. In addition, the development of new material is continuing. It would exceed the scope of this work to discuss all these polyimides in detail. Fortunately, the bulk of applications involves only two polyimides, PMDA-ODA (pyromellitic dianhydride-oxydianiline diamine) and BPDA-PDA (biphenyltetracarboxylic dianhydride-paraphenylene diamine). The exact chemical structure of heat sealable polyimides are not known to the author. However these materials are based on the base material Kapton HN, with former trade name H, and Upilex S. For that reason, the chemical structures of monomeric units for the two classical polyimides Kapton HN and Upilex S are shown in figure 4.2, [Ghosh, 1996].

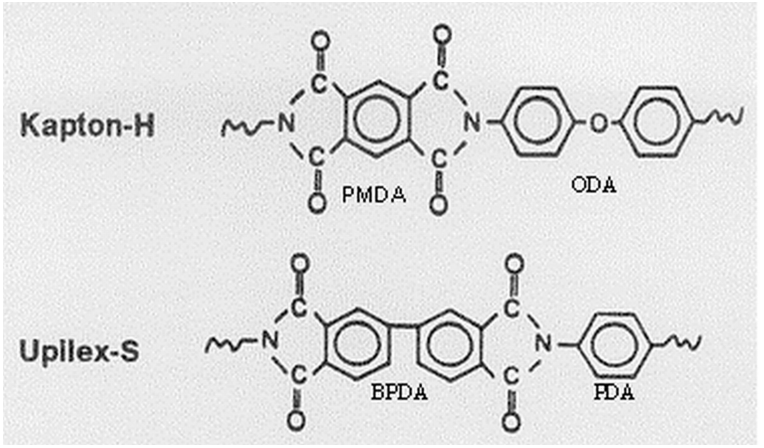

Figure 4.2: Chemical structure of the monomeric units for Kapton HN (former trade name is H) and Upilex S, [Source: Ghosh, 1996].

The polyimide based on PMDA-ODA has the longest history among all commercial polyimides utilized in electrical and electronics

applications and is widely used even today. It was first commercialized by DuPont under the trade name “Kapton” in form of sheets or Vespel in form of molds. The typical material properties are listed in table 4.1.

Trade Name		**Kapton**		**Upilex**	
Chemical Structure		PMDA-ODA		BPDA-PDA	
Type		KJ	HN	VT	S
Heat Sealability		Yes	No	Yes	No
Mechanical Properties	Units				
Stress at 5% Elongation	MPa	N.A.	90	180	260
Ultimate Tensile Strength	MPa	138	231	320	530
Elongation	%	150	72	54	42
Tensile Modulus	GPa	2.8	2.5	6.8	9.3
Thermal Properties					
Glass Transition Temperature	℃	220	360	300	500
Thermal Coefficient of Linear Expansion	ppm/℃	60	20	18	12
Laminating Properties					
Temperature	℃	220		290	
Pressure	Kg/cm²	14-30		50-100	
Time	min.	10-30		30-60	

Table 4.1: Typical properties of Kapton and Upilex polyimide sheets.
Sources: [www.Dupont.com] and [www.ube.com]

To overcome some of the shortcomings of PMDA-ODA, in particular the relatively high CTE (coefficient of thermal expansion), BPDA-PDA polyimides were introduced. Similar to PMDA-OPA polyimide, BPDA-PDA is available in the form of sheets under the trade name Upilex. Another advantages of BPDA-PDA are that it exhibits lower water uptake (1.5 wt %) and lower swelling in hot NMP than PMDA-ODA. Furthermore, the Young modulus is about a factor 2-3 higher, which is favorable for PZT piezoelectric actuation. The higher Young

modulus reduces the required driving voltage of about 10-20 % for dispensing, which has been simulated with finite element modeling.
The dispensers are actuated piezoelectric using PZT piezoelectric ceramic actuators, which are glued onto polyimide membrane. By applying the driving signal, the actuator induces a mechanical stress into the polyimide membrane and therefore the membrane bends towards the channel. The deformations are only a few tens of nanometers but stress is about up to 20 MPa. The strain is in the order of 0.1-0.2 %. These results have been simulated with finite element modeling (FEM). The stress-strain behaviors of two types of polyimide have been plotted in figure 4.3. Both polyimide types show a linear region of stress-strain relation. The maximum stress in the linear region for Upilex VT is 150 MPa and for Kapton H only 70 MPa.

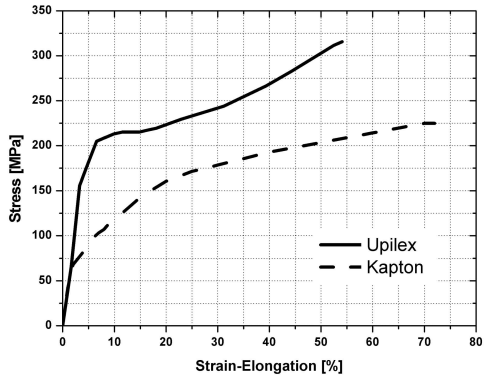

Figure 4.3: Stress-strain curves for Upilex VT and Kapton HN,
Sources: [www.Dupont.com] and [www.ube.com].

Stresses of 10-20 MPa and strains in the order of 0.1-0.2 % are well in the linear region of the stress-strain curve of polyimide. There is no risk of plastic deformation of the polyimide membrane during dispensing. Working in the linear region of the stress-strain curve increases the lifetime of the membrane.

4.3 Fabrication

4.3.1 Patterning

Polyimide can be patterned by two main methods: plasma etching and laser ablation. Both methods have been used for the fabrication of dispenser sheets.

Plasma etching

The major structural components of plasma processing systems are a vacuum chamber, pumping systems, a gas introduction, and an excitation source. The excitation source is an electric power supply usually rf (radio frequency). Processing gas selection is determined by the material to be removed. For etching processes, gases are selected such that their dissociative products react with surfaces to weaken chemical bonds in the material being removed to form volatile products that can desorb from the surface. A mixture of CF_4/O_2 (tetrafluoromethane) or SF_6/O_2 is usually used as etch gas. A pure oxygen plasma has a very low etch rate for polyimide sheets. For etching patterns into polyimide sheets, a masking material must be resistant to etching in the plasma or thick enough to survive until the polyimide etching is completed. Nonerodible mask materials include spin-on-glass, metals like chromium, copper being the most common. Isotropic processes result in undercutting of etch masks and an inability to pattern features with a high aspect ratio. The ability to plasma etch features with a minimum of lateral undercutting of mask materials is the major driving force behind an anisotropic plasma process. The results of an anisotropic plasma etching of polyimide sheet is shown in figure 4.4. We used an evaporated copper metal as masking layer. The copper was patterned by a

lithography following copper etch in a mixture of water and Sodium peroxodisulfate $Na_2S_2O_8$ at a temperature of 42℃.

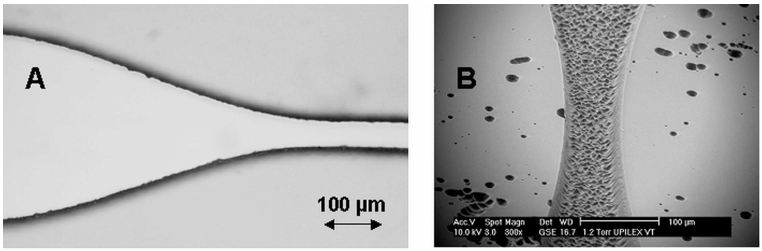

Figure 4.4: Anisotropic plasma etching of polyimide sheet. Picture A shows a complete through etch of a 50 µm thick sheet. Picture B shows a 30 µm deep etch into polyimide. The etched surface shows a high roughness Ra and is about 1-2 µm.

The etching gas used for anisotropic etching is a mixture of SF_6/O_2.The etch rate is about 50 µm/hr. The mask undercutting has been reduced to 10 µm for a minimal structure size of 30 µm in width and 50 µm in depth. An example anisotropic plasma etching of polyimide sheet is shown in figure 4.4. A high roughness Ra of about 1-2 µm was measured on the etched surface. For that reason the polyimide has been etched completely trough and is then sealed from both sides by two virgin polyimide sheets to avoid the high channel roughness given by the plasma etching.

Laser micromachining

Another process for polyimide patterning is laser ablation. The essential features of the interaction of a laser pulse with a target are illustrated in figure 4.5. Unless the target is completely transparent at the laser wavelength, incident radiation will be absorbed within some finite volume of the material. A small fraction of the laser light is reflected from the surface. Most of the absorbed energy is converted

into heat, which diffuses out of the absorbing region into the surrounding bulk material. The relative rates of these two processes, laser absorption and thermal diffusion determine the build-up of energy within the irradiated target. If energy concentration becomes large enough, the absorbing material will decompose into volatile fragments ejected into the ambient environment. Precise laser ablation of the polymer occurs when the absorbed energy density becomes so high that the decomposition/ejection event occurs virtually instantaneously compared with the timescale for thermal diffusion, [Lankard, 1992], [Srinivasan, 1989].

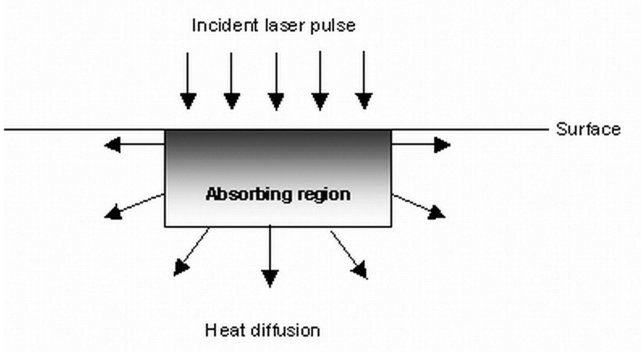

Figure 4.5: Fundamental laser/surface interaction, which is central to the polyimide ablation process. An incident laser pulse is absorbed in a surface layer of the polymer. After absorption, the energy originally contained in the pulse can diffuse as heat into the surrounding bulk. When the energy is delivered quickly (pulses in ns) and a laser wavelength chosen at which the target is highly absorbing, the laser energy can be initially confined to a small region. This will cause explosive vaporization of that thin layer before appreciable heat diffusion occurs.

The earliest pulsed UV lasers for ablation experiments were generally excimer lasers. The common lasers used in commercial applications are listed in table 2.2. These devices typically produce pulse widths of 10-30 ns and contain a few millijoules of energy. Thus while the energy per pulse is quite modest, the peak power is

on the range of 10^7 W. Kilohertz repetition rates can be used to achieve relatively high average power.

Excimer lasers have excellent ablation capabilities, but they are not without practical drawbacks. Among their less desirable characteristics are a fairly large physical size and a need for pressurized halogen gases. These limitations have prompted development of alternative pulsed ultraviolet sources such as solid-state lasers, which are compact and simple to operate. Currently, the most advanced scheme involves the Nd:YAG laser. This solid-state laser produces energetic (up to one joule) nanosecond pulses at a wavelength of 1064 nm. When this intense IR radiation has passed optically nonlinear crystals, ultraviolet pulses at 3 wavelengths are derived: 355 nm, 266 nm and 213 nm. An overwiew of ablation rate per pulse is shown in table 4.2.

Name	Gas Mixture	Wavelength [nm]	Ablation rate per pulse (µm)
ArF	**Argon/Fluorine**	193	0.2*
KrF	**Krypton/Fluorine**	248	0.5*
XeCl	**Xenon/Chlorine**	308	1*
Nd:YAG	**Solid state**	355	5**

*at a laser pulse fluence of 3 J/cm² for PMDA-ODA, ** for BPDA-PDA

Table 4.2: Overview of laser ablation rate for polyimide substrate, [extracted from Gosh, 1996].

For writing a layout onto a substrate there are two different methods: Mask writing and direct writing. Mask writing is mostly used together with excimer lasers. A metal mask in the optical path is illuminated uniformly and then the image is usually reduced by a factor 10 to focus the energy onto the substrate. Disadvantages of this method are that only a small image of some millimeters can be written at once and the table with the substrate has to be displaced for writing larger images. The reduction of the image is necessary for having

enough energy to ablate polymers. Samples of laser cutting by direct (A) and mask writing (B and C) are shown in figure 4.6.

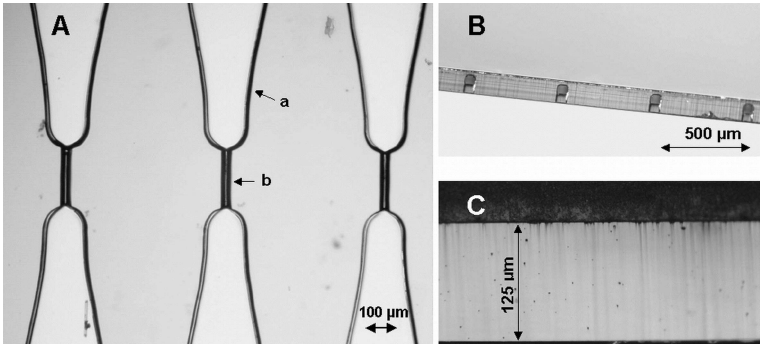

Figure 4.6: Samples of laser ablation for the fabrication of a dispenser sheet.

Photo A in figure 4.6 shows the layout of a direct writing on polyimide sheets with a Nd:YAG laser (355 nm) at 40 kHz repetition. The sheet is cut through for line “a” and line “b” is 30 µm deep ablated into the material. Photos B and C were ablated with an excimer laser at a wave length of 193 nm. B shows the outer surface of four nozzles of a dispenser sheet. The cutting quality of a laminated polyimide structure of 2 sheets at 50 µm and one sheet of 25 µm (total 125 µm) is shown in photo C.

The direct writing is mostly used together with Nd:YAG. The laser beam is steered by optical mirrors in the optical path. A control unit allows scanning an entire surface with the laser beam within a short time. This method is very fast and accurate. The laser beam can be driven from an AUTOCAD or equivalent designing source file. A sample of Laser direct writing is shown in figure 4.7. The sheet has a

cutting size of 11*12.6 cm², which corresponds to a 24-channel dispenser sheet. The cutting time is about 15 minutes at a repetition rate of 40 KHz. The sheet is cut completely through.

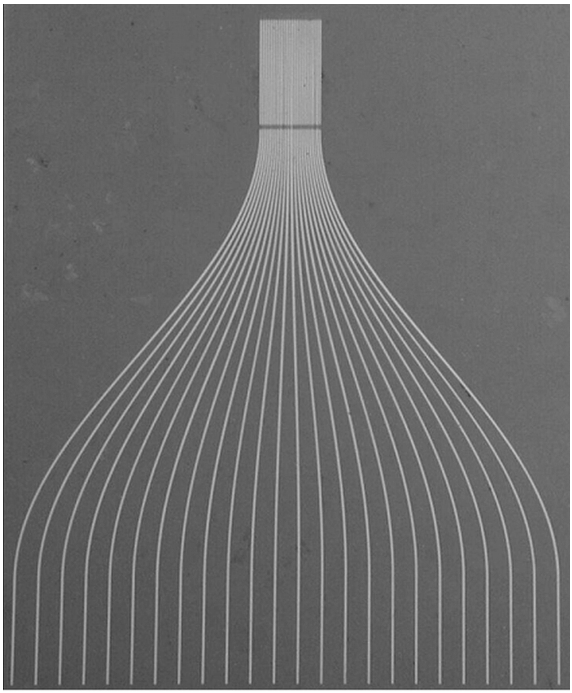

Figure 4.7: Laser ablation with Nd:YAG (355 nm) for the fabrication of a 24-channel dispenser sheet with a cutting size of 11*12.6 cm². The sheet is cut completely through. The cutting time is about 15 minutes at a pulse rate of 40 KHz.

Conclusion

Two different fabrication methods have been developed for the patterning of the polyimide sheets. Plasma etching allows etching the channel in parallel. The designed layout is transferred onto the masking layer by lithography. A major drawback of plasma etching are that several process steps are required: metallization,

lithography, mask opening, plasma etching, metal etching. At each fabrication step error may occur, which reduces the yield of a 24-channel sheet enormously.

On the other side, laser direct writing of the polyimde sheets requires only one process. For a 24-channel layout (6-inch square), it takes about 15 minutes writing time when using a Nd:YAG laser at wavelength of 355 nm and a repetition rate of 40 kHz. A high throughput in the fabrication is achieved with laser direct writing. Also the yield is very high because of only a process step.

4.3.2 Bonding

The key process of the fabrication of the dispenser sheets is the polymer direct bonding. Heat sealable polyimide sheets are today commercially available. The direct bonding allows sealing the channel without adhesive. Other methods of polyimide bonding can be found in, [Brown, 1988], [Oh, 1990], [Selby,2001].

Process

Bonding of the polyimide sheets is carried out on a commercially available press equipped with custom-made heating chucks. The chucks have a size of 150x150 mm² (about 6-inch square). The polyimide sheets are then clamped between the two chucks and are heated up to about the glass transition temperature of the polyimide. The clamped sandwich is heated for about 20 to 60 minutes. This set-up can also be used for hot embossing, for instance.

Result

A cross-section of bonded structure is shown in figure 4.8. The image in figure 4.8 corresponds to the inlet of one channel out of a 24-channel dispenser sheet. The cross-section has been cut by laser ablation. The channel itself was also cut with the Nd:YAG laser. Important for the dispenser is that the channel does not shown sagging. The sagging over 300 µm wide channels was measured with a profilo-meter. The sagging is less than 1 µm for the entire channel lengths of 24-channel dispenser sheet.

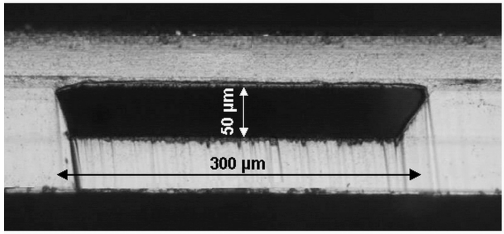

Figure 4.8: A bonded µ-channel with a height of 50 µm and a width of 300 µm. This channel has been fabricated with a Nd:YAG (355 nm) for cutting the channel and also for cutting the bonded sheets.

The bonded channels withstand a channel pressure of 3 bar without any damage. No delaminating has been observed. A pressure of 3 bar is required for a fast cleaning process of the dispenser. It is believed that the device could be used more than once. After dispensing of some thousands of droplets, the dispenser is placed onto a well plate filled with a cleaning solution. By applying a backpressure up to 3 bar the cleaning solution is flushed through the channels and out of the nozzle, where the cleaning solution is collected by an absorbing tissue. The internal volume per channel of a full size dispenser is only 2 µL and a well of 384-plate has a volume of 100-120 µL. After the cleaning solution is flushed through the channels, nitrogen from the pressure source dries the µ-

channels. The cleaning procedure takes some time, but once the channels are dried, the device can be refilled from another well plate.

4.4 Conclusion

The developed polyimide technology fulfills all requirements, which were defined at the beginning. Different patterning methods have been evaluated. By considering the fabrication yield and also the economy of the fabrication process, it is obvious that laser direct writing ablation with Nd:YAG (355 nm) is the method of choice. The lamination bonding is advanced to a level of void-free bonding surface for 6-inch square sheets. Polyimide has been chosen because of high mechanical and chemical stability. The fabrication of the dispenser sheets without actuation requires only three process steps: ablation of channels, lamination and ablation of outer surface shape. A high yield is reached for these process steps, which results in lower fabrication cost and time.

5 384-CHANNEL DISPENSER

5.1 Introduction

After the design, choice of materials and the development of the fabrication processes described in previous chapters, this one deals with the characterization of the dispenser devices.

First in this chapter is the description of the experiment set-up that allows performing simple basic tasks like to load a sample fluid into the device, shoot droplets and make accurate measurements of key parameters, such as droplet size and speed.

In a second section, the influence of the different driving signal parameters are analyzed and optimized for satellite-free dispensing. With the resonant frequency measurement, the shape of the driving signal can be defined.

In a third section, the sample liquid properties will be studied and the effects of key physical parameters will be discussed. This will lead to understanding the device capabilities and limitations related to the fluid properties.

The fourth section deals with the observation of droplet generation for simultaneously actuation of all 24 channels at once. The performances of droplet ejection for both a single channel and a 24-channel dispenser sheet are described and discussed.

Finally, the assembly and performances of a 384-channel dispenser will be presented and discussed in the fifth section.

5.2 Experiment Set-up

For the characterization of the dispenser a laboratory set-up has been built as depicted in figure 5.1. The drop ejection is analyzed by video observation under stroboscopic illumination. A microscope is installed horizontally at the height of the nozzle to observe the drop formation. Opposite of the microscope a red light emitting diode (LED) for the stroboscopic illumination is positioned. The driving signal for the LED is a square wave with an amplitude of 5 volt and pulse length of 2 µs. During a 2 µs pulse the droplet moves typically only about 4 µm at a velocity of 2 m/s, which still results in a sharp image. The LED-driving signal is synchronized with the driving signal of the actuator with a variable delay time from zero to 500 µs. On top of the microscope a black and white charge-coupled device (CCD) camera with video output is installed. The video is recorded onto a Mini DV cassette for further treatment. The rotation of the microscope and CCD camera allows observing the dispensing onto a transparent substrate (biochip) from the backside. The pressure source is used for filling the device from a 384 well plate. The electric signal is generated by a pulse generator and amplified with a high speed and high voltage amplifier. The driving and LED signal is observed with an oscilloscope.

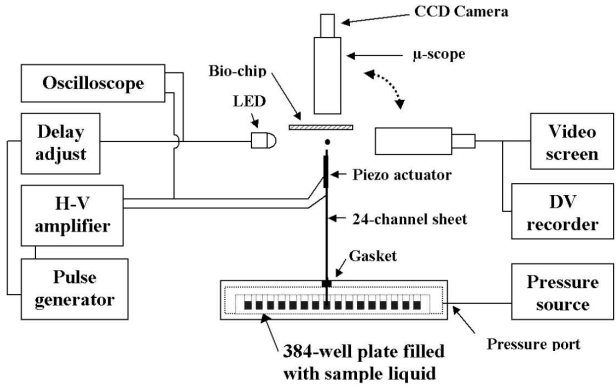

Figure 5.1: Diagram of the experimental set-up

5.3 Driving signal

In this section we analyze different driving signals. First, the influence of the driving signal shape (rise and fall time) is investigated. Second, the change in pulse width of the driving signal is characterized by measuring the change in droplet volume. Next, the dispensing performance is analyzed by changing the shape of the amplitudes. Finally, the capacity and resonant frequency of the assembled actuator has been measured and the current is calculated.

Signal shape

The shape of the driving signal has been optimized for suppressing any secondary small drops to the main droplet, called satellite droplets. Ink-jet based dispensers often show these small secondary droplets. Satellite droplets are undesirable because of cross contamination between spotting sites. We found experimentally an optimized driving signal with a rise and fall time of 5 µs. No satellite droplets were observed at these times. For short rise time (<1 µs) satellite droplets may occur because of resonance effect of the piezoelectric actuator. Measurements are published in Ref. 4.

Pulse width

The stability of multi-channel parallel dispensing was also investigated for different pulse width. A square-shaped pulse with a rise and fall time of 5 µs at 150 volt was applied to the piezoelectric actuators at different pulse widths. For pulse widths from 20 to 70 µs, droplets are ejected as shown in Figure 5.2.

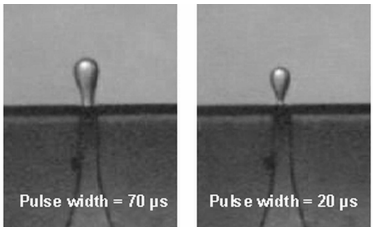

Figure 5.2: Drop formation for different pulse widths. Volume changes can be seen in the left image, droplet of 87 pL, and the right image, droplet of 65 pL. These pictures were taken under stroboscopic illumination at a delay time of 60 µs.

The droplet volume has been calculated by measuring the size of the droplet for a pulse width of 70 µs and 20 µs. The droplet volume is 87 pL for 70 µs and is 65 pL for a pulse width of 20 µs. The volume change between two pulse widths of 20 and 70 µs is about 30 %. This effect is demonstrated in Ref. 3. At a larger pulse width, the actuator creates a larger stroke volume, which explains the volume change. Furthermore, it was observed experimentally that identical dispensing in droplet volume is achieved for different pulse widths, when adapting the driving voltage. We conclude that dispensing is non-sensitive to small signal changes. This allows driving all 384 actuators by one power supply.

Shape of amplitudes

A method to reduce the absolute driving amplitude was investigated. Piezoelectric PZT actuators can be actuated up to an electric DC field of 1 V/µm parallel to the polarization. It is also allowed applying electric fields against the polarization. This field must be limited to about 0.3 V/µm at DC, otherwise, depolarization of the piezoelectric activity may occur. A driving signal with a negative part, figure 5.3 right, has been compared experimentally to a classical driving signal, figure 5.6 left, for identical droplet velocity. The two shapes of amplitude shown in figure 5.6 are compared for identical droplet velocity at 2.7 m/s. Both pulse lengths t_1 and t_2 has to be the same

(t_1=t_2). The pulse duration of the negative part t_3 must be longer than t_2 (t_3>t_2). The negative voltage increases the chamber volume and if the pulse is too short no filling can take place and no effect is observed. Epson uses this method for their ink-jet print heads for controlling the ink volume. Considering the amplitudes, A_2 must be the same value as A_1 for identical dispensing (A_2=A_3+A_4). That means the positive amplitude has only a value of A_3, which is reduced by the value of A_4. The risk of PZT depolarization of the PZT limits the amplitude A_4.

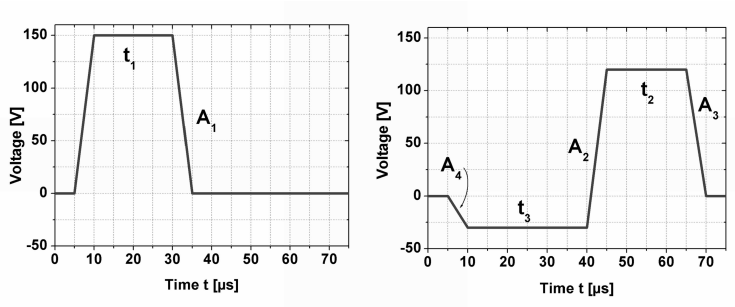

Figure 5.3: Both driving signals produce exact the same dispensing in term of droplet speed and drop formation (satellite-free) when A_1=A_2, t_1=t_2 and t_3>t_2. The depolarization of the PZT limits the amplitude A_4.

The drawback of this method is the more complex driving electronic. The advantage is the lower absolute driving voltage, which may simplify the driving electronic. For the further characterization of the dispenser sheets a classical driving signal (figure 5.3, right) was used.

Capacitance, current and resonant frequency

The PZT actuator behaves electronically as a capacitance. This capacitance must be charged within 5 µs for an optimized

dispensing. The current I(t) can be described by the differential equation:

$$I(t)=C\cdot dU/dt.$$

The term dU/dt corresponds to the slope of the voltage curve and C is the capacitance of the assembled actuator. The capacitance C has been measured as a function of frequency (ω) by a Gain-Phase Analyzer and is 30 nF at 100 Hz for a 24-channel dispenser sheet. By using the differential equation $I(t)=C\cdot dU/dt$ the peak current I_{max} has been calculated. The peak current for a 24-channel dispenser sheet is $I_{max,24}$=0.9 A during the rise time of the signal. For the 384-channel dispenser the peak current $I_{max,384}$ increases, by multiply by the number of sheets, 16 in this case, to $I_{max,384}$=14.4 A at 150 volt. The high current is a consequence of the capacitance of PZT which can also be calculated by $C=\varepsilon_r\cdot\varepsilon_o\cdot A/d$, where A is the surface of the electrode, d the plate thickness and ε_r the relative dielectric constant. An overview of the results is shown in table 5.1.

	Voltage	**Peak current**	**Capacity at 100 Hz**	**Resonance**	
				unfilled	**filled**
	[V]	[A]	[nF]	[MHz]	[MHz]
One channel		0.04	1.25		
24-channel sheet	150*	0.9	30*	1.4*	0.82*
384-channel dispenser		14.4	480		

Table 5.1: Overview of the electrical characterization of the actuators. The values marked with (*) have been measured. The other values are extracted from these measurements.

The resonant frequency of the PZT actuator was determined by measuring the impedance as function of the frequency (ω) for an assembled 24-channel dispenser sheet. The measurement has been

done for unfilled channels and then the measurement was repeated with the same prototype, but this time, the channels are water-filled. In the filled condition the resonant frequency is about 40 % lower than in the unfilled condition. The resonant frequency is 1.4 MHz for unfilled channels and decreases to 0.82 MHz for water-filled channels because of adding the mass of the liquid in the channel.

The maximum rise time of the piezoelectric actuator is about a quarter of the time period at resonance and is in filled condition 0.3 µs. When applying a rise time close to 0.3 µs the actuator would work in resonance and dispensing stability would rely on the resonant frequency of each channel. Further, this resonant frequency would depend on fabrication tolerances. During dispensing, the actuator works below resonance because the rise time of the driving signal is set to 5 µs. The off-resonance mode increases the dispensing stability and also suppresses satellite droplets, as observed experimentally.

Conclusion

From the electrical characterization of the actuator we learnt that the actuators are working in an off-resonance mode. The off-resonance mode allows applying driving signal with different pulse widths and amplitudes. Moreover, in this mode, geometry changes between channels on a sheet, given by fabrication tolerances, has insignificant influence of the dispensing behaviour. This allows driving all 24 channels with a common driving signal and therefore also a 384-channel dispenser.

5.4 Effects of liquid properties

In applications, many different liquids need to be spotted onto substrates. For the dispensing, the viscosity, surface tension and density are main parameters. For spotting biological active liquids a

wide range of buffers (DMSO, phosphate buffer, butyl carbitol, etc.) is usually used for diluting the sample. A short description of the influence of the different liquid properties is given below. Moreover, the dimensionless Weber and Ohnesorge number are introduced. The Weber number describes the break-off conditions and the Ohnesorge the droplet size in relation to the nozzle size.

Viscosity effects

A higher viscosity requires higher amplitude of the pressure wave in the pump chamber. The amplitude of the pressure wave is proportional to the acceleration of the membrane displacement, in other words the pressure is proportional to the second derivative of displacement (d^2y/dt^2). The low-pressure dependence on the actuator membrane of only 2 nm/bar allows compensating the viscosity effect by increasing the driving voltage. At very high viscosity the filling of the channel becomes more critical than the dispensing part. Then, a larger cross section of the channels may be required according to the used fluid.

Surface tension effects

Surface tension has a minor effect on the required driving voltage. However, very low surface tension can result in a bigger likelihood of air ingestion through the nozzle, particularly at high drop velocities ($v>3$ m/s). The dispensing of liquids with different surface tensions can be done with the same driving signal and is demonstrated with a 24-channel dispenser sheet later.

Density effects

Variation of the density does not directly affect the performance of a drop formation, but usually indicates a variation of acoustic speed

and bulk modulus of the fluid; both of them may affect the optimum waveform (timing and amplitude).

Weber number (We)

The Weber number defines the minimal droplet velocity for break-off for different geometry sizes and different liquids. The Weber number is defined by:

$$We = \frac{\rho \cdot d \cdot v^2}{\sigma}$$

ρ = density [kg/m^3]
d = nozzle diameter [m]
σ = surface tension [N/m]
v = velocity [m/s]

The Weber number is proportional to the inertial force divided by the surface tension force and is used in breakage of liquid jet calculations in particular. Break-off occurs when Weber number is higher than 1. For the given prototype the theoretical minimal droplet velocity v is 1.2 m/s for water and 0.75 m/s for ethanol at We=1(break-off condition). For a droplet velocity of 2.5 m/s, the Weber number is high at We=4.3 for water and We=11.3 for ethanol. Clear break-off is certain in both cases as shown in figure 5.4. A similar investigation about drop break-off has been done by [Chen, 2002].

Ohnesorge number (Z)

Ohnesorge number describes the droplet size compared to the nozzle size. It is proportional to the viscous force divided by the square root of the surface tension force and is defined by:

$$Z = \frac{\mu}{\sqrt{\rho \cdot d \cdot \sigma}}$$

μ = dynamic viscosity [Pa·s]
ρ = density [kg/m^3]
d = nozzle diameter [m]
σ = surface tension [N/m]

At Ohnesorge number Z<<1 the droplet has the diameter of the nozzle. If Z ≈1, then smaller droplets than the nozzle size are possible because of viscous drag. In the cases of water and ethanol as dispensing liquids the Ohnesorge number Z is 0.02 for water and 0.04 for ethanol. At such small Ohnesorge numbers the droplet size corresponds to the nozzle size, which is experimentally confirmed. Only very viscous liquids such as glycerol in water reaches Ohnesorge numbers close to 1.

5.4.1 Dispensing of liquids with different properties

Two different liquids have been chosen for the characterization of the dispenser. First, water is used because of the high surface tension force of 72.8 mN/m. Second, ethanol is used because of the low surface tension of 22.3 mN/m and similar viscosity compared to water. The viscosity is similar and for water it is 1 cp and for ethanol it is 1.1 cp at 20℃.

For the characterization of the drop formation a video with stroboscopic illumination has been taken, as described before. The water dispensing is compared with ethanol dispensing. In the left image of figure 5.4 water droplets are dispensed and in the right

image ethanol droplets are dispensed. Both the droplet velocity and driving voltage are similar. In both cases satellite-free dispensing is achieved.

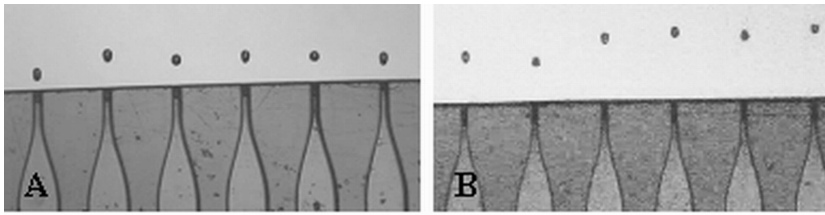

Figure 5.4: Comparison of droplet size for water dispensing A and ethanol dispensing B. No wetting of the outer surface is observed. In both cases satellite-free dispensing is achieved. The stroboscopic images A and B were taken at different delay times.

More important, during dispensing no air is sucked back into the channel through the nozzle. No air is sucked into the channel because the liquid stays attached to nozzle rim during dispensing. This is an advantage of polyimide as base material because of a clean nozzle outer surface cut of the polyimide by laser ablation. Important for dispensing at low surface tension is that no wetting of the outer surface occurs. If wetting of the nozzle outer surface occurs the dispenser would fail. We conclude that for ethanol dispensing, a reliable dispensing is achieved as for water.

Conclusion

Successful dispensing has been achieved with water and ethanol. ethanol has been chosen because of its low surface tension of about 22.3 mN/m compared to water with a surface tension of 72.8 mN/m. Considering the results of dispensing with these two liquids, we claim that the dispenser works with any intermediate value of surface tension.

5.4.2 Upward or downward dispensing

During spotting, the dispenser stays, for convenience, together with the well plate, thus the dispenser shoots upward, as shown in diagram 5.1 and figure 5.4. The upward shooting has no influence on the drop formation because the gravity can be disregarded compared to the kinetic energy. The kinetic energy is about 50 to 100 times higher than the gravity at a droplet speed of 2 m/s. The upward shooting avoids complex robotics for positioning and displacing. The system becomes easy to handle and can be displaced manually. If required the entire system could also be turned upside down and the dispenser would spot downward. The reservoir of the well plate would not leak out because of the surface tension effect in small containers.

5.5 Characterization of a single channel

The variation of the droplet volume for a single channel from droplet-to-droplet has been analyzed by measuring the evaporation time of a single droplet. Droplet-to-droplet dispensing is then important when thousands of identical slides will be spotted. The coefficient of variance (CV) has been calculated.

Experiment set-up

The set-up, as described in figure 5.1, has been used for the measurements. In this experiment, the evaporation time of droplet was measured by counting the numbers of frame from droplet arriving on a glass slide until the droplet is evaporated. The precision is defined by the time difference between two single frames and is 40 ms, given by the video register frequency of 25 Hz. The error of the method is around 5 % in time.

Coefficient of variance (CV)

The coefficient of variance (CV) is defined by the following equation

$$CV = \frac{\sigma}{avg} \cdot 100\% ,$$

where σ is the standard deviation and avg is the average value, Ref. 5.

Results

The dispensed droplet has a nominal volume of 65 pL, calculated from the droplet diameter. The variation of dispensed droplet volume of a single channel has been compared by, first, calculating the evaporation rate and then applying this to the droplet evaporation time. The average evaporation time for a single channel, measuring 30 successive droplets, is t=1.40 sec ± 0.12 sec resulting in a CV value of 8.6 %, Ref. 5.

Conclusion

The method of the measuring the evaporation time is a fast method for a first analysis. A CV value of 8.6 % per channel is slightly higher than the desired value of about 5 %. Again by refining the driving circuit, the CV value could be reduced down to 5 %.

5.6 Characterization of a 24-channel dispenser sheet

Characterizing the dispensers involves several types of measurements allowing to verify the range of usability of the device. The characterization of each single 24-channel dispenser sheet, 16

in total, defines then the performance of the entire 384-channel dispenser. In the following sub-chapters 24-channel dispenser sheets are thoroughly characterized.

5.6.1 Droplet volume and velocity

Drop size and drop velocity are measured in this section. Also drop formation, drop trajectory, the absence of satellite droplets and maximum shooting frequency are investigated.

Experiment

By using the set-up shown in figure 5.1 the droplet diameter and the velocity was measured. Dispensing liquid is water for this experiment. The 24-channel dispenser sheet used for characterization is shown in figure 5.5 including the 384-well plate, which acts as reservoir. The 24-channel dispenser sheet has been filled with the standard procedure by applying a backpressure of some tens of millibar to the µ-titer plate through the pressure port. The liquid is then forced into the channel and flows upward passing the restriction and stops at the nozzle by the surface tension effect of the liquid.

The drop shape from a stroboscopic image is shown in figure 5.6. This image corresponds to a single frame of a video. The dispensing frequency is 500 Hz, meaning that during one frame about 20 droplets are registered. The image, in figure 5.6, shows a super-positioning of 20 droplets. The droplet volume has been calculated by measuring the droplet diameter.

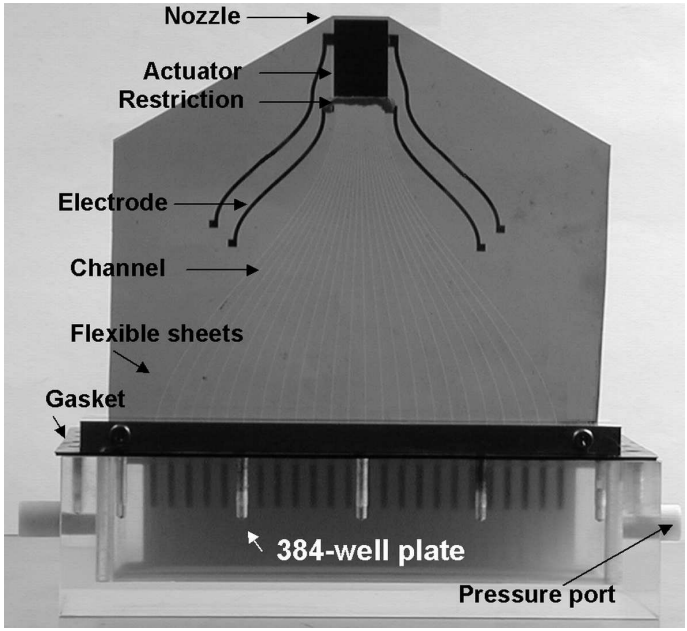

Figure 5.5: Front view of a 24-channel dispenser sheet. A 384-well plate acts as reservoir for the individual channels.

Results

The average measured droplet diameter over 24-channel is 50 µm, resulting in a calculated droplet volume of 65 pL nominal.

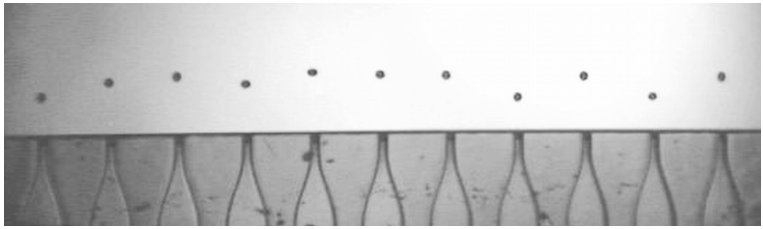

Figure 5.6: Stroboscopic observation of parallel drops of 12 channels out of 24. The nozzle spacing is 500 µm. The droplet diameter is 50 µm resulting in a droplet volume of 65 pL.

The sharpness of the image 5.6 indicates the high stability of drop formation. Moreover, the velocity is stable and no satellite droplets have been observed. The maximum dispensing frequency is about 2 kHz. The velocity has been calculated by measuring the travel distance for a stroboscopic time difference of 100 µs. The velocity is 1.78 m/s ± 0.2 m/s for a driving voltage of 140 volt for a 24-channel dispenser sheet.

An important advantage of the device is the hydrophobic nozzle outer surface. The hydrophobic nozzle outer surface avoids any wetting of the nozzle surface. When wetting of the nozzle outer surface would occur the droplet trajectory would be less precise as seen for hydrophilic outer surfaces such as glass or silicon. A hydrophilic surface must usually be covered with a hydrophobic layer. These layers are usually not stable while in contact with dispensing liquid and droplets will be deviated and misplaced or leaking of the nozzle occurs. These difficulties have been overcome by choosing polyimide as base material.

5.6.2 Statistics of droplet volume of different liquids by 1-d parallel spotting

In this subchapter we are analyzing repeatability from one channel to all 24 channels of dispenser sheet. It is important for the data mining by scanner or other instruments that the spot sizes on glass slide are regular over the entire array. Single droplets in parallel are dispensed onto a glass slide and then the spot size is measured and the coefficient of variance (CV) has been calculated.

Experiment set-up

For observing a single droplet a glass slide is placed on top of the nozzle at a distance of about 0.5 mm. A droplet is shoot upward to the bottom side of the glass slide. From the topside of the glass slide, the droplet is observed by a microscope. The dispenser is actuated with a single impulse. Each impulse ejects one droplet per channel. All 24 channels are actuated in parallel and with the same driving signal. A video registers the dispensing onto the glass slide. For the measuring the spot size, a single frame out of the video has been taken. Such a frame shows a single droplet per spot site as shown in figure 5.7.

Results

Images of single droplets, dispensed onto a glass slide, have been taken for water and ethanol. The images are shown in figure 5.7. Again each spot size has a single droplet. From the images in figure 5.7 the spot size has been measured and the average spot size and its coefficient of variance (CV) have been calculated.

In figure 5.7, ethanol and water droplets are parallel dispensed onto a glass slide. The ethanol droplets show a larger spot size compared to water because of the lower surface tension properties of the liquid. The low surface tension of ethanol allows spreading the liquid on a hydrophilic surface such as a clean glass slide. The droplets are spaced at 500 µm. The droplet volume for both liquids is the same as shown earlier in figure 5.4.

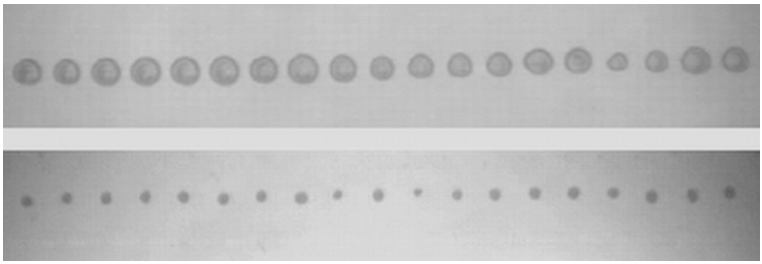

Figure 5.7: Top, parallel dispensing of one 65 pL ethanol droplet onto a clean glass slide. Bottom, dispensing of one 65 pL water droplet onto a clean glass slide using the same driving parameters as for ethanol. The droplet spacing is 500 µm.

The average spot size for ethanol is 340 µm with a CV of 9 %. The average spot size of water is 110 µm with a CV of 20 %. Water and ethanol have been dispensed with identical driving parameters. Both measurements have been done for 24 channels and for a common driving signal. The common driving signal means that all channels have been applied with an identical driving signal. This allows using only one power supply.

Conclusion

The advantage of the common driving signal method is that only one power supply is required even for a full 384-channel dispenser. The disadvantage of the “common driving signal” method is the relatively high CV of 20 % for water. The CV should be reduced to about 10 % for water dispensing. This is possible be further refining of the driving circuit.

5.6.3 Lifetime and Stability

The dispenser has been investigated for lifetime of the actuator and stability of dispensing. Two tests have been carried out. First, about

300'000 cycles have continuously been applied to the actuators. Second, a few droplets has been dispensed each day over three days.

The lifetime test for the actuator has been for the 24-channel dispenser sheets. The test method allows verifying if the actuators are well assembled, glued and piezoelectric active. The actuator has been tested with a driving voltage of 280 volt, a frequency of 500 Hz and during 10 min. During the test time of 10 min, 300'000 cycles have been applied to the actuators. No failure or voltage breakdown of the actuators has been observed.

The stability of the dispenser has been tested as a function of the time. The test method is to dispense a few droplets per day during three days as it may happen in research laboratories. The tests have been done for several 24-channel dispenser sheets. During the test days the dispensing was stable, meaning, that no adaptation of the driving signal was necessary. The same driving signal could be always applied. The dispensing was successful and no failure in form of missing droplets has been observed during the three-day test phase.

5.7 384-channel dispenser prototype

A complete 384-channel dispenser consists of the assembly of 16 individually fabricated 24-channel sheets.

5.7.1 Introduction

A 384-channel dispenser with 2-d nozzle pitch of 500 µm has been fabricated, assembled and characterized. The nozzle array has a 16x24 format given by a 384 µ-titer plate. The spotted array has a

size of 8x12 mm² carrying 384 individual spots with a nominal volume of 65 pL each. The spots are dispensed at once.

An innovative advantage of the presented device is the modular assembling of sixteen 24-channel dispenser sheets to build a 384-channel dispenser. Any other format would be also possible by staking any numbers of sheets. Another important advantage of the 384-channel dispenser is, that it can be directly interfaced to a 384-well plate for filling. Most of biological substances are prepared in standard 384 µ-titer plates.

5.7.2 Assembly

The flexibility of the laminated polyimide sheets allows building a 384-channel dispenser as shown in figure 5.8. 16 dispenser sheets are held mechanically together, by clamping in between two metal plates. The sheets are separated by spacers in order to respect the 500 µm spacing.

The 384-channel dispenser is placed over the µ-titer plate by mechanical alignment and is lowered to the well plate and the channels are immersed into the wells. A gasket seals the surroundings between casing and fluidic interface holder. Then, the dispenser is held tight to the casing for filling the dispenser by applying a backpressure through the pressure port, as shown in figure 5.8.

The substrate (biochip) is placed onto the metal plates for printing. The distance between the substrate and the nozzle was set to 500 µm. No critical alignment or displacement of the substrate (biochip) is required since the whole array is spotted at once.

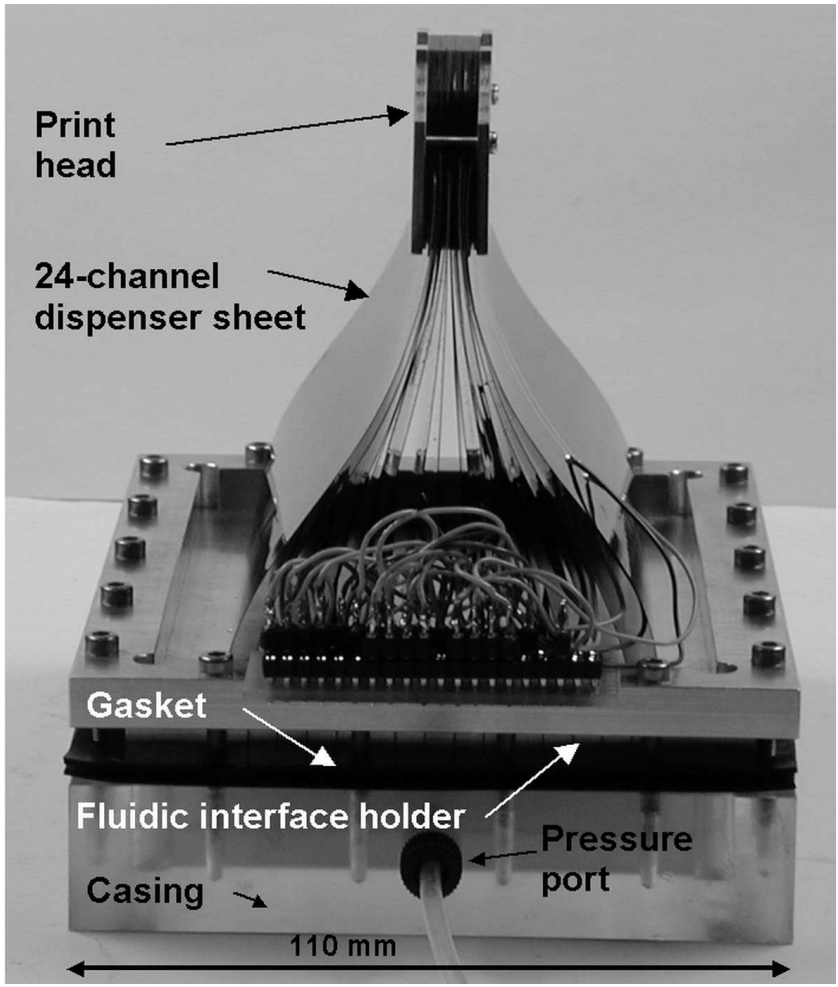

Figure 5.8: Side view of a 384-channel dispenser including 384-well plate in the casing, which functions as a reservoir, the electrical connections and, on the top, print head where the substrate is placed for parallel printing.

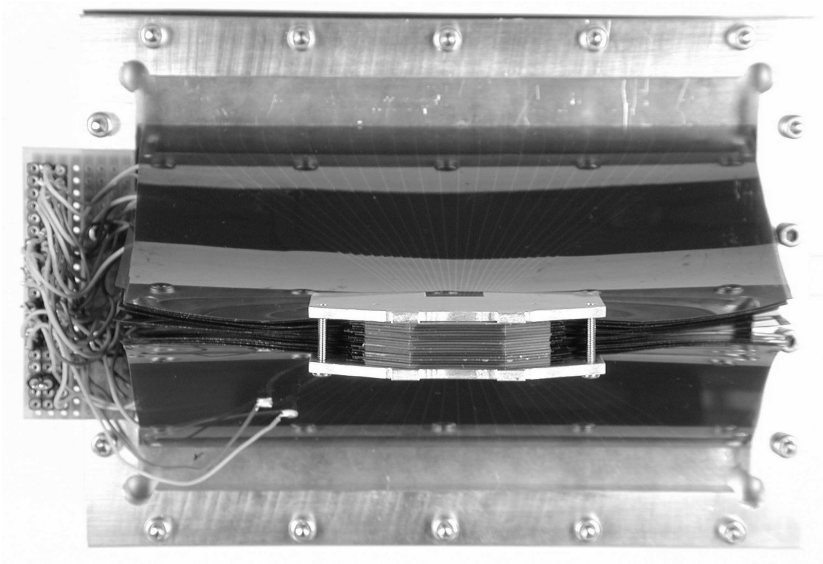

Figure 5.9: Top view of a 384-channel dispenser, showing the flexibility of the polyimide sheets and the nozzle array in a 16x24 format, where the substrate is placed for printing.

Figure 5.9 shows a top view of the 384-channel dispenser. A section of the assembled 16x24 nozzle array can be seen in figure 5.10. This assembling method has the very important advantage that each single sheet, if a failure occurs, can be replaced by a technician. No special skills are required for this procedure. This feature is highly required for HTS (high-throughput screening) applications.

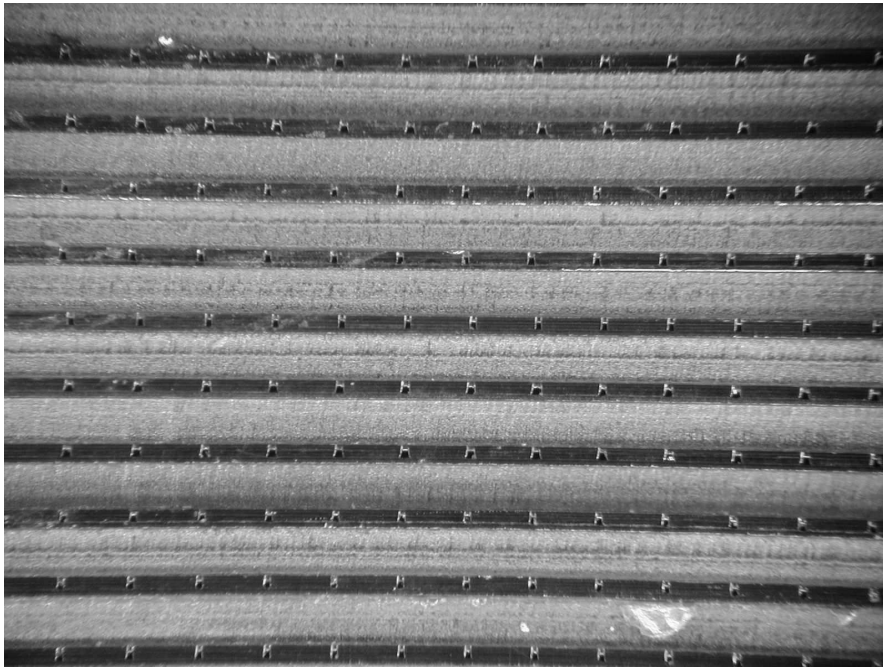

Figure 5.10: Close up of figure 5.9 top view, showing a section of the 16x24 nozzle array. The dark lines correspond to the polyimide sheets with nozzles and the white lines are spacers cut out of a Mylar sheet.

To complete the illustration of the prototype a bottom view of the fluidic interface holder is added in figure 5.11. The holder is made of aluminum beams and clamps 16 dispenser sheets together at a spacing of 4.5 mm. The sheets are also aligned by pins/bores. The polyimide sheet has a fingered shape and each finger fits into the well of a standard 384 µ-titer plate. A standard 384-well plate is shown in figure 5.12.

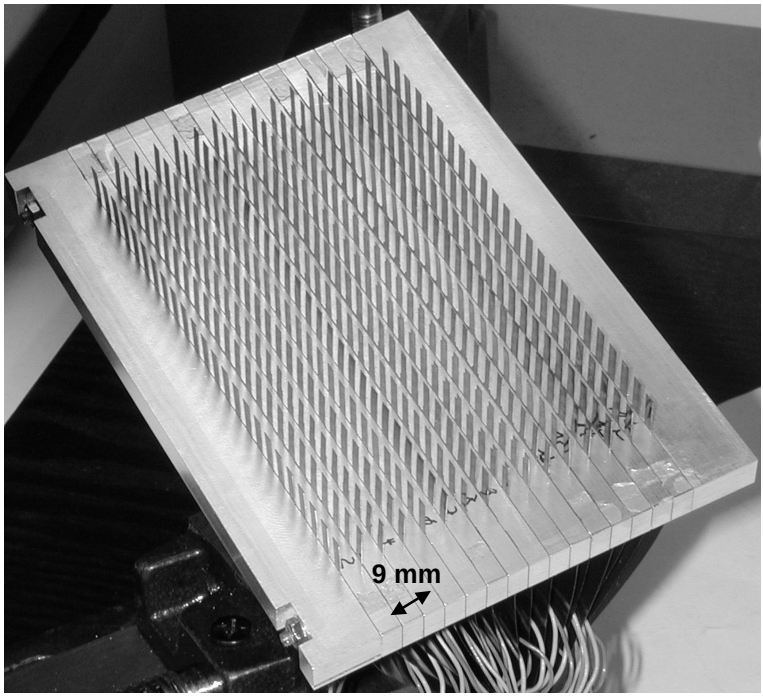

Figure 5.11: Bottom view of the 16x24 dispenser, showing the fluidic interface holder. Each channel is independent and spaced at 4.5 mm.

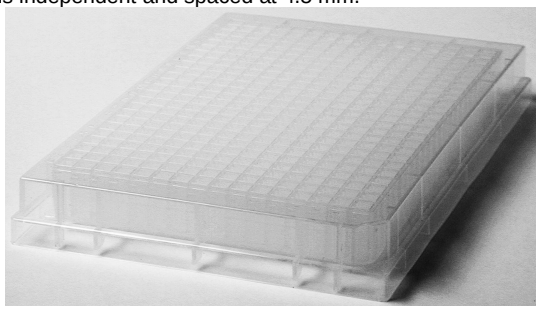

Figure 5.12: A standard 384-well plate used as reservoir for the dispenser. The volume per well is about 120 µL. The internal of the µ-channel is only about 2 µL and allows dispensing thousands of 65 pL droplets.

5.7.3 Sheet lengths

The assembling of 16 sheets requires that each pair of sheets has another length. The lengths of these sheets are cut by laser and the positioning is made by the same pins as for the print head alignment.

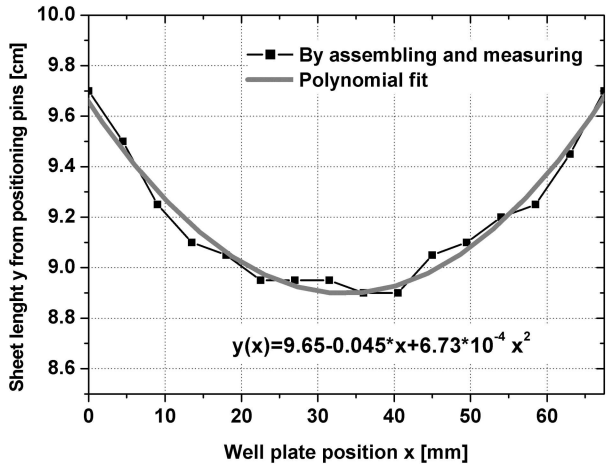

Figure 5.13: Each pair of sheets has a different length given by the geometric shape. The lengths of the sheets are adapted within the laser cutting process of the outer shape of the polyimide sheets.

This method allows a very precise cutting of the sheet lengths. As shown in figure 5.13, a length difference of 0.8 cm from the middle to the outer sheet has been measured, results in a variation length of less than 10 %. The dispensing is independent of the channel length as demonstrate with CFD simulation earlier in this work.

5.7.4 Parallel filling of 384-channel dispenser

For filling and dispensing, the fluidic interface holder is placed over the casing, where the well plate is placed and sealed with a gasket for pressurizing the wells and filling the channels simultaneously. Applying a backpressure of about 20 mbar, as for a 24-channel dispenser sheet, does the filling. No self-filling happens because of hydrophobic behavior polyimide surface (contact angle α=95 deg for water). The pressure forces the liquid into the channels. The liquid flows up passing through the restriction and stops at the nozzle by surface tension effect. Once filled no backpressure is required for water dispensing. While dispensing low surface tension liquids such as ethanol a backpressure of a few millibar increases the stability of droplet velocity. The internal volume of a channel is only about 2 µL. This allows dispensing thousands of droplets.

5.7.5 Characterization

In the microarray technology the spot misplacement are important parameters next to the volume and spot size. For a safe detection by scanners, the spots must be clearly separated so that no cross contamination occurs.

The 24-channel dispenser sheets have been completely characterized in the previous sub-chapters. These characterizations are still applicable for the 384-channel dispenser because the 24-channel dispenser sheets do not change the characteristics while assembled to a 384-channel dispenser.

The goal in this sub-chapter is to analyze the precision of the droplet placement onto the substrate (biochip).

Experiment

To characterize the spot misplacement of the 384-channel dispenser a dye methylene blue has been added to the water. The evaporation time of water droplets is about 1.4 sec. This short time does not allow analyzing the droplet misplacement in real time. By using a dye the spot misplacement can be measured once the liquid is spotted and dried. The droplets have been spotted onto bright white regular paper, for convenience. The distance between nozzle and substrate was set to 500 µm.

Results

A section of 2-d array parallel dispensing is shown in figure 5.14. The positions of the dispensed and dried droplets have been compared to a 500x500 µm² grid. This method does not only count the misdirection of the droplet trajectory but also the misalignment of the dispenser sheets itself. The deviation to the grid has been measured and the maximum deviation is reported below.

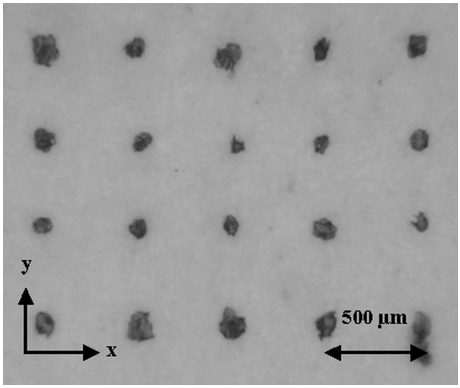

Figure 5.14: A section of a parallel spotted array. A mixture of water/methylene blue dye has been dispensed onto a bright white paper for characterization of spot misplacement.

The maximum misplacement of droplets is ± 29 µm in x-direction and in y-direction it is slightly higher at ± 33 µm for a slide-nozzle distance of 500 µm. The maximum directionality angle error is then in x-direction ± 3.3 deg and in y-direction ± 3.7 deg. The maximum misplacements are small compared to the droplet spacing of 500 µm and no overlying of droplets is observed. By reducing the nozzle-substrate distance from 500 µm to 250 µm, the misplacement can be divided by a factor of 2.

5.7.6 Dispensing with or without well plate

It is foreseen that the dispenser stays together with the well plate for dispensing. While biological samples are expensive, it may be appropriate to split the well plate from the dispenser after filling. Then, the well plate could be stored or used for other applications.

For dispensing without well plate, a backpressure must be applied during dispensing. The pressure pushes the liquid into the channel and guaranteed the refilling the chamber.

5.7.7 Outlook: Scalability of format and nozzle spacing

More and more, higher densities of µ-titer plate are used today. A standard format next to the 384-well plate is a 1536-well plate. This plate has a well-to-well spacing of 2.25 mm and the same outer dimension as a 384-well plate. The 384-channel dispenser is scalable to 1536 channels in 32x48 format at a nozzle spacing of 500 µm. Any other formats can be also achieved. Moreover, also other nozzle spacing is possible within a certain range, as for instance 450 µm in x-direction and 550-µm in y-direction. The same fabrication process can be used as developed for the 384-channel dispenser.

5.8 Conclusion

All characterizations have been done by a common driving signal using one power supply. The velocity of the droplets varies for a 24-channel dispenser of about ±10 % because of fabrication and assembling tolerances of the first prototype. The fabrication has been mainly done by hand. Further optimization of the fabrication process is planned. It is believed, that the CV value of 20 % could be reduced to 10 % by refining the electronic driving circuit. The presented 384-channel dispenser is scalable up to a 1536-channel dispenser or any other format with the same technology processes developed within this project.

6 CONCLUSION

To date, conventional pipetting and aspirating solenoid valve techniques are commonly employed for aspirating and dispensing samples in automated analysis systems. These methods can no longer be used for microarray technology as the dimensions are dramatically reduced. New efficient techniques that handle volumes in the picoliter domain are therefore needed. Not only the improved analytical performance, obtained by microscaling of chemical analysis systems is a driving force towards reduced sample volume, but also high-throughput screening (HTS), a method for rapid analysis, benefits greatly from new sample handling techniques, that offer an increased speed and smaller sample volumes.

The advantages of the 384-channel dispenser compared to commercially available spotting systems are: First, the highly parallel spotting of 384 samples at once onto a microarray. All actuators are powered by an identical driving signal, generated by one power supply. The small aspirated volume of only 2 µL, compared to the one of classical devices of 20-50 µL, reduces the amount of sample and therefore process cost. Second, the standalone configuration minimizes the used lab space and avoids complex robotics for positioning the biochip. The biochip is simply placed on top of the print head onto pillars at a fixed substrate nozzle distance. The biochip can also be positioned by means of stoppers.

Today, most of the biological applications are standardized to the 384 µ-titre plate, which has a well-pitch of 4.5 mm. The dispenser can be easily scaled to any other spacing at inlet side and also to

any other format. The 16x24 format has been chosen for the demonstration of the feasibility. The scale can be changed by a simple redesign of the channel layout. The developed technology can be used without any further optimization.

The nozzle spacing of 500 µm was set to this first prototype. However, other nozzle-to-nozzle spacings within a certain range are also possible according to a specified application.

Two aspects reach a high stability of dispensing. First, the piezoelectric actuators are not in contact with the dispensing liquid. Second, the hydrophobicity of the nozzle-outer surface, given by the material properties of the polyimide, results in a stable directionality of the droplet trajectory.

The development of the fabrication steps for the dispenser is well advanced, thus the industrialization phase is started. Most of the fabrication steps have already been optimized and a high yield has been achieved for the key processes.

The technology of flexible µ-channels can be used for many other applications, where handling of small liquid volumes is needed. Using laser technology, almost any channel layout can be ablated into a 150*150 mm² polyimide sheet. The outer shape of the sealed channel system can be tailored by the same laser technology within a short time.

REF. 1

A high insulating thin film ZnO piezoelectric actuator on a Polyimide substrate.

Proceedings of Eurosensors XVI, Prague, 228-231, 2002.

Pages 111-114

EUROSENSORS XVI The 16th European Conference on Solid-State Transducers | September 15-18, 2002, Prague, Czech Republic MP43

A high insulating thin film ZnO piezoelectric actuator on a Polyimide substrate

Andreas Kuoni[1], Christophe Quinche[3], Marc Boillat[2], Herbert Keppner[3], Nico de Rooij[1]
[1]Institute of Microtechnology, University of Neuchâtel, P.O. Box 3, CH-2007 Neuchâtel, Switzerland, andreas.kuoni@unine.ch
[2]Seyonic SA, CH-2000 Neuchâtel, Switzerland
[3]University of Applied Science, CH-2400 Le Locle, Switzerland

SUMMARY

Fabrication and characterization of a thin film ZnO piezoelectric actuator on a Polyimide substrate is presented in this paper. A major problem of ZnO thin film is the relatively low resistivity, which makes the use at low frequency unfavorable because of high leakage current. An innovative ambient temperature process has been developed for the deposition of an amorphous SiO_2 insulating layer on both side of the active piezoelectric layer. The deposited sandwich has a resistivity of at least 10 GΩcm for a surface of 8*2.5 mm², which is higher than in other publications [1,2]. A blocking force of 2.4 mN/10V has been measured. A static analysis results in a piezoelectric coefficient of d_{31}=-0.7 pC/N for a 0.65 µm thin insulated ZnO actuator on a Polyimide substrate.

Keywords: Piezoelectric, Thin film ZnO, Polyimide substrate

Subject category: Innovative processing methods, micromaching

Introduction

The research goal is to develop a piezoelectric thin film actuator at low frequency (quasistatic) on a Polyimide substrate. The use of Polyimide substrates demands that all process temperatures must not exceed approximate 100-130°C. Sputtered zinc oxide (ZnO) piezoelectric thin film is deposited at ambient temperature and has a self-poling effect in contrast to piezoelectric thin film materials such as AlN, PVDF, PZT which require high temperature processes for deposition or for poling [3,4,5]. Although, ZnO has a major problem of a relatively low resistivity as reported in [1,2]. This difficulty has been solved by introducing amorphous PECVD SiO_2 insulation layers at ambient process temperature [1,6]. The developed ambient temperature deposition processes can be used for a wide variety of materials. Piezoelectric ZnO thin films are widely used as sensing material but not as actuator because of a relatively low piezoelectric coefficient compared to PZT. This effect is compensated by using much less stiffer Polyimide than silicon substrates. Such a device shows a high efficiency of the ZnO piezoelectric actuator. The used substrate is commercially available Polyimide sheet, which can be processed by standard MEMS technologies. The Polyimide sheet has high mechanical properties and good chemical resistance compared to other plastics such as Polyethylentherephthalat PET or Polycarbonat PC. A cantilever device is used to characterize the piezoelectric properties of the insulated ZnO thin film actuator. The operation principle, fabrication and characterization of a cantilever actuator is presented.

Design and film deposition

For the characterization of the piezoelectric thin film a beam actuator has been chosen as test device. The different layers have been deposited directly onto a Polyimide sheet with a uniform thickness of 50 µm. The size of the cantilevers is 8*2.5 mm².

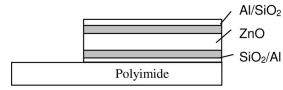

Fig. 1: *Schematic representation*

A schematic representation of the fabricated device is presented in Fig. 1. The thickness of the amorphous SiO_2 insulation layer is about 0.18 µm. The ZnO piezoelectric layer is about 0.65 µm thick. The bottom metal layer is 3000 Å thin and the top electrode is 1000 Å thin. Both electrodes are evaporated Aluminum.

Thin-film <i> ZnO actuators have been prepared using conventional RF-magnetron sputtering from a sintered ZnO target of a density higher than 70%. The ZnO layers grow in a hexagonal Wurzite structure showing the so-called fibre texture that leads to

piezoelectricity without post thermal treatments as poling [3]. The ZnO layers were sputtered using a partial pressure of 7 x 10^{-3} Pa O_2 in 0.5 Pa Argon atmospheres and 110 W RF power. In order to reduce the fast particle impact on the growing surface of the thin film and by that lattice damage, the pressure time distance product (p·d) of typical $1.75 \cdot 10^{-2}$ Pa·m has been increased to $4 \cdot 10^{-2}$ Pa·m. The deposition time for a 1 µm thin ZnO film is about 180 minutes. The columnar structure of ZnO favours inter-diffusion of the contact material that leads to a fast degradation of the film resistance. This drawback has been solved by introducing insulation layers. The ZnO piezoelectric layer is sandwiched between two anti-diffusion layers of amorphous SiO_2. The SiO_2 layer is deposited using a plasma-enhanced chemical vapour deposition PECVD process at ambient temperature. The silicon carrier gas is Hexamethyldisilazane, HMDS, at a partial pressure of 5 Pa. It was found that a partial O_2 pressure of 10 Pa helps to correct the stoichiometry. The deposition of a 0.2 µm thin insulation layer takes about 5 minutes at 94 W. Note, in order to assure best reproducibility all layers (except the metallic contacts) were carried out subsequently in the same chamber, hence "in-situ". Using this method high quality insulation layers are obtained. Furthermore, water vapour exposure of the interfaces before and after the ZnO deposition can effectively be avoided. We assume, high device resistance can be achieved by that. The patterning of the actuator has been done by only two standard lift-off processes. The Polyimide is very resistant to the photolithography's developer and to the stripper solvent (Acetone). The lift-off technique have the advantages of avoiding under cutting of the layers and no etch process step had to be developed for the etching of the insulation layers. Some prototypes have been patterned by shadow masking depending on the actuator size.

Piezoelectric Model

Fundamentals piezoelectric equations are described in [8]. A piezoelectric actuator induces stress or strain in the bender surface. This in-plane stress results in a deflection of the cantilever. The intensive piezoelectric relation is defined by equation (1).

$$S = s^E \cdot T + d \cdot E \qquad (1)$$

where S stands for strain, T for stress, E for electric field, d for piezoelectric charge coefficient and s^E for elastic compliance at constant electric field. In the case of a free actuator there is no external stress applied, but an electric field in 3rd direction. The strain $S_{1,2}$ is then expressed by equation (2).

$$S_{1,2} = d_{31} \cdot E_3 \qquad (2)$$

By using the relationship between the various piezoelectric coefficients, the transverse piezoelectric coefficient e_{31} is equal to (3) for a piezoelectric layer, which is free to expand or contract in the plane [8].

$$e_{31} = c_{11}^E d_{31} \qquad (3)$$

where c^E_{11} is the elastic stiffness (Young's modulus) at constant electric field. By introducing equation (3) into (2), the in-plane stress $T_{1,2}$ induced by the actuator can be expressed as (4).

$$T_{1,2} = e_{31} \cdot E_3 \qquad (4)$$

Equations (2) and (4) describe the bender behavior of strain and stress. By analyzing the bender surface strain and stress in function of the deflection, the deflection of a bender in function of the electric field can be calculated.

Smits et al. developed a piezoelectric heterogeneous bimorph deflection equation by considering an actuator device with two layers: one elastic and one piezoelectric [7]. The author derived the constituent equations of the bender by calculating the internal energy assuming thermodynamic equilibrium. The beam tip deflection *y* is expressed in function of the driving voltage V in equation (5).

$$y = \frac{3 \cdot d_{31} \cdot s_{11}^{PI} \cdot s_{11}^{ZnO} \cdot h_{PI} \cdot (h_{PI} + h_{ZnO}) \cdot L^2}{K} \cdot V \qquad (5)$$

$$K = (s_{11}^{PI})^2 \cdot (h_{ZnO})^4 + 4 \cdot s_{11}^{PI} \cdot s_{11}^{ZnO} \cdot h_{PI} (h_{ZnO})^3 + 6 \cdot s_{11}^{PI} \cdot s_{11}^{ZnO} \cdot (h_{PI})^2 \cdot (h_{ZnO})^2 + 4 \cdot s_{11}^{PI} \cdot s_{11}^{ZnO} \cdot h_{ZnO} \cdot (h_{PI})^3 + (s_{11}^{ZnO})^2 \cdot (h_{PI})^4$$

The subscript PI and ZnO in equation (5) refer to the elastic and piezoelectric layers, respectively. L stands for cantilever length, s for elastic compliance and h for layer thickness.

Results

Piezoelectric cantilevers have been fabricated and tested. An optical photograph of a ZnO thin film

piezoelectric actuator on a 50µm thick Polyimide substrate is shown in Fig. 2.

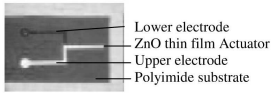

Fig. 2: *Optical Photograph of a prototype*

For a low frequency application of the actuator a high resistivity of the ZnO thin film is needed. Otherwise the actuator heats up and burns due to leakage current power dissipation. After introducing the amorphous SiO_2 insulation layer we measured an across film resistance of about 20-80 MΩ for a surface of 8*2.5mm². The resistivity is then calculated and is at least 10 GΩcm for a 0.65 µm thin film. Such a high resistivity can only be achieved with an excellent quality of insulation layers. These actuators can be even used in a DC mode, quasistatic respectively.

For finding the piezoelectric charge coefficient d_{31} of the deposited ZnO thin film, the actuator has been fixed at one end and has been left free at the other end. The free end is then placed under a contactless profilometer UBM. The measurements were performed at a square wave of 10 Volts with a pulse width of 0.1 sec. The actuation frequency is 2 Hz.

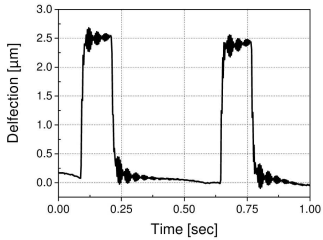

Fig. 3: *Deflection versus time at 2 Hz*

The cantilever deflection is shown in Fig. 3. We measured for an 8 mm long beam an amplitude of 2.63 µm at 10 Volts. The active ZnO layer has a thickness of 0.65 µm. The square shape of the displacement curves indicates that thermal effects of the leakage current has been deactivated by the insulation layers and the actuator can be used at low frequencies, quasistatic respectively. The piezoelectric coefficient has been calculated using equation (5). We obtain an average piezoelectric coefficient of d_{31}=-0.7 pC/N for an insulated ZnO thin film actuator. This value is smaller than reported in [2,6,8]. The values reported in the literature do normally not include insulation layers. There are certain effects of the insulation layers in the deflection/voltage behavior of the beam, which has been neglected such as thickness, internal stress, and distribution of the electric field. Blom et al [6] have done a demonstration of the insulation layer effects using a standard semiconductor theory.

In a next step the deflection in function of the voltage has been investigated. As shown in equation (2) the developed strain in the layer is linear to the applied electric field, to the voltage, respectively. The results of measurements of 8 mm long beam are shown in Fig. 4.

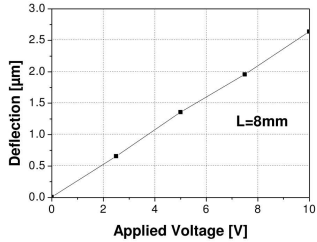

Fig. 4: *Deflection vs. voltage at low frequency*

The deflection of the beam is linear to the applied voltage. The amplitude has been stable over a measuring time of some minutes.

For piezoelectric materials, which have to be poled such as ceramic PZT, care must be taken to ensure that the ceramics are not depolarized. The depolarization may be electrically, mechanically or thermally. Electrically depolarization occurs when a strong electric field of opposite polarity to the poling field is applied. A ZnO thin film material has a self poling effect given by the crystal structure, which allows applying electric field in both polarities. By changing the polarity of the external voltage, the beam bends in the opposite direction at the same deflection. For the ZnO thin film cantilever, we applied voltages in both polarities without having any depolarizing effects for lower electric field than 30-50 V/µm. A depolarization has been observed for higher electric fields. However the actuators gained back the piezoelectric effect at lower electric field without reducing the performance.

The strain in the layers has been investigated by finite element simulation. The strain in the piezoelectric layer is given by equation (2) and has a

value of $7 \cdot 10^{-6}$ m/m at a voltage of 10 Volts. The strain at the bottom of the Polyimide beam is about $-1.41 \cdot 10^{-6}$ m/m per 10 Volts or for a tip deflection of 2.63 µm. The low strain attests, that the beam is clearly in the linear range of the material properties of the Polyimide.

Another important parameter for a cantilever design is the blocking force F. If a voltage is applied to an actuator there will be a displacement. When this displacement is blocked, a force is developed, the so-called blocking force, which is, in fact, a measure of the stiffness of the actuator. This blocking force has been measured and simulated with finite element program ANSYS and is presented in Fig. 5.

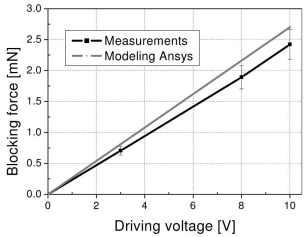

Fig. 5: *Blocking force*

The blocking force for a 8mm long ZnO cantilever has a measured value of 2.4 mN/10V compared to the slightly bigger simulated value of 2.7 mN/10V. The measurements have been carried out by varying the driving voltage at a constant force till the deflection was zero respectively smaller than the accuracy of the profilometer UBM for deflection measurements. We observed that the blocking force is linear to the driving voltage. The Polyimide beam has been compared to a silicon beam at the same thickness of 50 µm by a finite element simulation. The simulated blocking force of a Silicon beam is slightly higher at 3.3 mN/10V. The simulated deflection of a Silicon beam is only about 0.341 µm/10V, which is about 7 times lower than for a Polyimide beam. The merit of using a Polyimide sheet as substrate is that the beam deflection is much higher than for a Silicon beam at a constant blocking force and for a given substrate thickness.

Conclusion

The fabrication of a low frequency ZnO thin film piezoelectric actuator on Polyimide substrate has been demonstrated. Standard MEMS technologies can be used to pattern the different layers. The PECVD deposition of an amorphous SiO_2 insulation layer has been developed at ambient temperature. A very high resistivity is obtained and allows driving the actuator at low frequencies. A blocking force for 8 mm long beam actuator has been measured and is 2.4 mN/10V. The piezoelectric charge coefficient calculated with formula (5) is d_{31}=–0.7 pC/N for an insulated ZnO piezoelectric thin film actuator on a Polyimide substrate.

Acknowledgments

The authors would like to thank the following persons and institutions for the good cooperation and help: Daniel Gigon (HESSO), Fabian Thiébaud (HESSO), Gianni Mondin, Sylvain Jeanneret, all technicians at IMT, University of Neuchâtel and at HESSO, University of Applied Science, Le Locle. Their contributions are gratefully acknowledged.

References

[1] D. L. DeVoe, A. P. Pisano: Surface micromachined piezoelectric accelerometers, Journal of Microelectromechanical Systems, 10 (2001), 180-185.

[2] W. Tjhen, T. Tamagawa, C.-P. Ye, C.-C. Hsueh, P. Schiller, D.L. Polla: Properties of piezoelectric thin films for micromechanical devices and systems, IEEE Microelectromechanical Systems Workshop Japan, (1991), 114-118.

[3] L. Sagalowicz, G. R. Fox, M.-A. Dubois, C. A. P. Muller, P. Muralt, N. Setter: Microstructure and defects of Wurtzite structure thin films, Journal of the European Ceramic Society, 19 (1999), 1427-1430.

[4] Z. Zheng, I. Guy, T. Tansley: Piezoelectric coefficients of thin polymer film measured by interferometry, Journal of Intelligent Material Systems and Structures, 9 (1998), 69-73.

[5] M.-A. Dubois, P. Muralt: Measurements of the effective transverse piezoelectric coefficient $e_{31,f}$ of AlN and PB(Zr,Ti)O thin films, Sensors and Actuators, A 77 (1999), 106-112.

[6] F. R. Blom, D. J. Yntema, F. C. M. van de Pol, M. Elewenspoek, J. H. J. Fluitman, Th. J. A. Popma: Thin film ZnO as micromechanical actuator at low frequencies, Sensors and Actuators, A 21 (1990), 226-228.

[7] J. G. Smits, W.-S. Choi: The constituent equations of piezoelectric heterogeneous bimorphs, IEEE Transactions on Ultrasonics, Ferroelectrics, and Frequency Control, 38 (1991), 256-270.

[8] T. Ikeda, Fundamentals of piezoelectricity, New York, Oxford Science Publications, (1990), 16-18.

REF. 2

Polyimide Membrane with ZnO Piezoelectric Thin Film Pressure Transducers as a Differential Pressure Liquid Flow Sensor.

Journal of Micromechanics and Micro-engineering, Vol. 13, 4, 103-107, 2003.

Pages 117-121

INSTITUTE OF PHYSICS PUBLISHING JOURNAL OF MICROMECHANICS AND MICROENGINEERING
J. Micromech. Microeng. **13** (2003) S103–S107 PII: S0960-1317(03)59923-5

Polyimide membrane with ZnO piezoelectric thin film pressure transducers as a differential pressure liquid flow sensor

Andreas Kuoni[1], **Raphaël Holzherr**[1], **Marc Boillat**[2] **and Nico F de Rooij**[1]

[1] Institute of Microtechnology, University of Neuchâtel, PO Box 3, CH-2007 Neuchâtel, Switzerland
[2] Seyonic SA, CH-2000 Neuchâtel, Switzerland

E-mail: andreas.kuoni@unine.ch and marc.boillat@seyonic.com

Received 24 February 2003, in final form 25 April 2003
Published 13 June 2003
Online at stacks.iop.org/JMM/13/S103

Abstract
Fabrication and characterization of ZnO thin film piezoelectric sensors on a polyimide membrane is presented in this paper. As a test device a differential pressure liquid flow sensor has been fabricated. We discuss new material combinations for the fabrication of the test devices. The pressure sensor membrane is a thin polyimide sheet bonded to a silicon wafer and the sensing material is sputtered ZnO piezoelectric thin film. The fabricated liquid flow sensor has been tested with a piezoelectric micropump for flow rates from 30 μl h^{-1} to 300 μl h^{-1}. Stroke volumes of 1 to 10 nl have been measured. The strain in the sensing layer has been modeled and a transverse piezoelectric coefficient of $e_{31,f} = -0.294$ C m^{-2} has been extracted.

1. Introduction

The new aspect of this research work is that thin polyimide sheets are thermally bonded to silicon without using an adhesive to seal microchannels in combination with piezoelectric thin film pressure transducers.

For the piezoelectric sensing layer zinc oxide (ZnO) has been chosen because it can be deposited with no external heating by sputtering onto the bonded polyimide membrane. ZnO does not require a subsequent electric-thermal poling such as PZT, PVDF because of its self-poling capability [1]. Another advantage is that a seed layer, as for instance for AlN, is not necessary [2]. A seed layer is usually deposited at a higher temperature than the glass transition temperature T_g of the polyimide. The relative high surface roughness of the bonded polyimide membrane compared to polished silicon has a minor influence on the piezoelectric efficiency when using ZnO. The different films of the sensor can be patterned by lift-off, which avoids exposing the bonded polyimide membrane to strong bases and acids for etching.

On the other hand, zinc oxide thin film usually presents a low resistivity, preventing low frequency operation. As a way to increase it, a PECVD co-deposition of two amorphous SiO_2 insulation layers has been added, which allows increasing the film resistance as reported by the same author in [3]. The piezoelectric constitutive equation has been solved for strain in the sensing layer. The geometry has been modeled by finite element simulation ANSYS to analyze the piezoelectric transducer.

For the characterization of the transducers a liquid flow sensor has been built as a test device. The flow sensor is based on the measurement of the pressure across a fluidic restriction. The merit of this flow sensor is that the sensing material is not in contact with the liquid [4].

2. Design and fabrication

The devices have been fabricated by using standard MEMS technologies. Two pressure sensors with piezoelectric readout are connected to a hydraulic restriction. The key processes

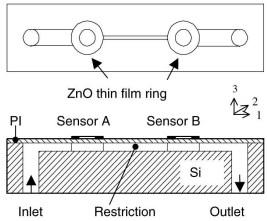

Figure 1. Schematic view of the device.

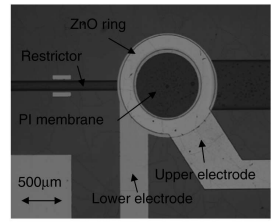

Figure 2. Top view of a pressure sensor.

of the device are a thermal bonding of a polyimide sheet to an already micromachined silicon wafer and the deposition of transducers onto the polyimide membrane. A schematic cross section is depicted in figure 1.

The piezoelectric constitutive equation describes the relation between the transverse piezoelectric coefficient e_{31} and the electrical charge Q_3. The constitutive equation can be written as [5]

$$D_3 = \varepsilon_0 \varepsilon_{33} E_3 + d_{31}(T_1 + T_2) + d_{33} T_3 \tag{1}$$

$$S_1 = s_{11}^E T_1 + s_{12}^E T_2 + s_{13}^E T_3 + d_{31} E_3 \tag{2}$$

$$S_2 = s_{12}^E T_1 + s_{11}^E T_2 + s_{13}^E T_3 + d_{32} E_3, \tag{3}$$

where D_3, E_3, T_i, S_i stand for electric displacement, electric field, stress components and strain components. The coefficients s_{ij}^E, ε_{33} and d_{31} describe elastic compliance at constant electrical field, relative dielectric constant and piezoelectric charge coefficient. Since the thin film is free to move in the third direction, the stress coefficient T_3 must be zero. In the sensor mode no electric field is applied, thus the field E_3 is zero. The stress T_i can be expressed as a function of strains S_i by adding equations (2) and (3):

$$T_1 + T_2 = \frac{S_1 + S_2}{s_{11}^E + s_{12}^E}. \tag{4}$$

The combination of equations (4) and (1) gives the relation between displacement D_3 and strain $S_1 + S_2$ and where the transverse piezoelectric coefficient for a thin film $e_{31,\mathrm{f}}$ is introduced [2]:

$$D_3 = \frac{d_{31}}{s_{11}^E + s_{12}^E}(S_1 + S_2) = e_{31,\mathrm{f}}(S_1 + S_2). \tag{5}$$

The electric displacement D_3 describes the charge density per unit surface $D_3 = Q_3/A_{\mathrm{el}}$ where Q_3 is the charge developed and A_{el} the area of the electrode surface. The strain $S_1 + S_2$ can be expressed as the total strain S_{tot} in the ZnO piezoelectric thin film layer:

$$Q_3 = A_{\mathrm{el}} e_{31,\mathrm{f}} S_{\mathrm{tot}}. \tag{6}$$

Charge is proportional to strain and increases linearly with the sensor surface. Equation (6) allows calculating the transverse piezoelectric coefficients $e_{31,\mathrm{f}}$ for the device presented in figure 2.

The ZnO sensing layout is a ring on the top of a circular pressure membrane. The size of the ring is designed in such a manner that the piezoelectric ZnO layer is only under compressive strain. Highest sensitivity is reached by the ring arrangement because the compressive strain at the edge of the membrane is high and the electrode surface is large compared to other configurations. The top view of a fabricated ZnO piezoelectric transducer is shown in figure 2. The diameter of the pressure sensing membrane is 1 mm with a thickness of 25 μm.

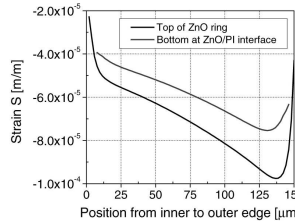

Figure 3. Strain distribution in the ZnO layer at a pressure of 100 mbar.

The total strain S_{tot} in the sensor ring on the circular polyimide membrane has been analyzed by finite element simulation with ANSYS. The curves in figure 3 are simulated values for the strain distribution in the ZnO ring with a width of 150 μm, from the inner to the outer edge (built-in side) and from top to bottom of the ZnO layer.

The strain distribution is not uniform and an integration for an average strain has been done. The average compressive strain is then 6.8×10^{-5} m/m for a pressure of 100 mbar.

The stress in the polyimide membrane has also been investigated with finite element simulation. A compressive stress of 3.8 MPa at the bottom and a tensile stress of 5.3 MPa at the top of the built-in edge for a channel pressure of 100 mbar have been found. These stresses are very low compared to the ultimate tensile strength of 570 MPa of the polyimide material. The low stresses result in a good linear behavior and in a high mechanical stability of the pressure membrane.

The devices have been designed to measure flow rates from 30 μl h^{-1} to 300 μl h^{-1} created by a piezoelectric membrane pump [6]. The restrictor has a hydraulic resistance

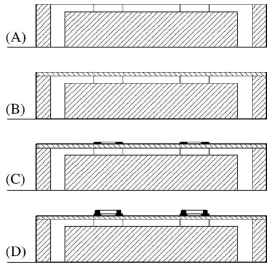

Figure 4. Schematic process flow of a cross section view, top view is depicted in figures 1 and 2. A: DRIE dry etching in silicon and Ultrasonic drilling of interconnection holes. B: Bonding of a polyimide sheet to silicon at 300 °C. C: Deposition and lift-off of lower ring electrode. D: Deposition and lift-off of SiO_2/ZnO/SiO_2 layers and upper ring electrode.

of $R_h = 60$ mbar/(ml h^{-1}) with a channel length of 10 mm and a hydraulic diameter of 67 μm [7]. The testing liquid is degassed water at 20 °C.

The test device is fabricated starting from a silicon wafer as shown in figure 4. First, 50 μm deep channels have been etched by deep reactive ion etching (DRIE) into the wafer. Fluidic interconnection holes are drilled by Ultrasonic through the wafer. Next, a commercially available heat bonding type polyimide sheet UPILEX® VT with a thickness of 25 μm has been bonded to the etched silicon wafer to seal the channels without using adhesive. The thermal bonding process of a polyimide sheet to a prefabricated silicon wafer is carried out with a mechanical press. The press is equipped with a bottom and top heating chuck. A bond pressure of 50–100 bars and a temperature of about 300 °C are applied for 30–60 min. On the prefabricated sealed wafer a gold electrode is evaporated and patterned on the planar polyimide membrane, followed by a SiO_2 insulation layer deposited by PECVD. A 1 μm thick ZnO film is then sputtered and finally a second 0.2 μm thin insulation layer is added. Note that in order to assure best reproducibility SiO_2 and ZnO layers were carried out subsequently in the same chamber, hence *in situ*. Thin film $\langle i \rangle$ ZnO layers have been deposited using conventional rf-magnetron sputtering from a sintered ZnO target. The ZnO and SiO_2 thin films have been deposited with no external heating of the substrate. Finally, an aluminum electrode is evaporated on the top of the sandwich completing the sensor. The sensors are patterned by two lift-off processes. The prefabricated wafers have been temporarily bonded to a blank silicon wafer for lithography. Before applying the adhesive temporarily, the interconnection holes of the devices have been sealed with a blue tape. This method allows holding the wafer with a backside vacuum for alignment and exposure. The lithography has been carried out in a hard contact mode.

The electronic circuit consists of charge amplifier with an offset and drift compensation followed by a voltage amplifier. The pressure sensor overall sensitivity K_p is adjustable by the electronic circuit and has been set for the characterization of

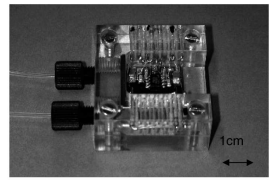

Figure 5. Assembled flow sensor with electronics.

the device at $K_p = S_i S_a = 8$ mV mbar^{-1}, where S_i is the internal sensor sensitivity of 0.08 pC mbar^{-1} and S_a the transducer and amplifier sensitivity of 0.1 V pC^{-1}. The offset and the drift of the charge amplifier have been compensated by an RC feedback loop at a time constant of about 1.5 s.

3. Results

The fabricated flow sensor has been mounted in a Plexiglas holder that provides fluidic interconnections. The charge converter circuit is directly assembled onto the chip with connections to an external circuit as shown in figure 5.

The piezoelectric coefficient has been extracted by measuring the membrane deflection and electrical charge at a pressure of 100 mbar. We measured a charge of 8 pC. The active electrode surface of the device is $A_{el} = 4 \times 10^{-7}$ m^2 and the average strain is $S_{tot} = 6.8 \times 10^{-5}$ m/m at 100 mbar. By rewriting equation (6) the coefficient $e_{31,f}$ can be calculated as

$$e_{31,f} = \frac{Q_3}{A_{el} S_{tot}}. \tag{7}$$

The transverse piezoelectric coefficient is $e_{31,f} = -0.294$ C m^{-2} for the insulated ZnO thin film layer, which is close those reported in [8, 9].

The stability of the polyimide membrane has been investigated by measuring the deflection as a function of time by profilometer UBM. We did not observe any changes in the behavior of the membrane deflection for tens of thousands of pressure cycles at 200 mbar. The membrane deformation has been 500 nm, measured on the ZnO ring opposite to the built-in side. No delamination has been observed at the interface of polyimide and silicon up to a pressure of 400 mbar.

The piezoelectric pressure sensors have been characterized at low frequency. Quasistatic pressure pulses of nitrogen have been applied by a solenoid valve. The output voltage of the sensor is monitored by a digital oscilloscope.

Both sensors show a high linearity, which is important for accurate measurements. For the device presented, we measured an average pressure sensor overall sensitivity of $K_p = 8$ mV mbar^{-1} as shown in figure 6.

For the characterization of the liquid flow sensor, the sensor has been connected to a silicon piezoelectric membrane micropump [6]. This micropump supplies a pulsed flow rate. The differential pressure sensor response is given in figure 7 (curve A-B) for a pump frequency of 10 Hz.

The positive part of the curve corresponds to the forward pumping mode and the negative part corresponds to a back flow

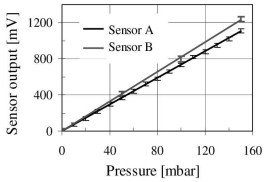

Figure 6. Pressure–sensor characterization.

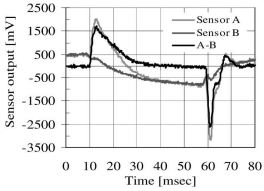

Figure 7. Flow sensor response of a micropump stroke.

due to the closing time and the compliance of the microvalves. The volumetric flow rate Q_v can be calculated by

$$Q_v = S_s f A, \qquad S_s = \frac{1}{R_h K_P}, \tag{8}$$

where S_s is the flow sensor sensitivity, f the pump frequency, A the integrated surface of the differential output signal for a cycle, respectively, for a pump stroke as shown in figure 7, R_h the hydraulic resistance and K_p the pressure sensor overall sensitivity. The flow sensor sensitivity according to equation (8) is $S_s = 2.08\ \mu$ l/h/mV. The stroke volume of the micropump in forward and backward directions has also been analyzed. The stroke volume can be calculated by

$$V_{\text{stroke}} = \frac{Q_v}{f} = S_s A, \tag{9}$$

where V_{stroke} is the pump stroke volume. The instantaneous stroke volume can be calculated simply by the integration of the surface of the flow sensor output signal (figure 7) multiplied by the flow sensor sensitivity. Stroke volumes in the range from 1 to 10 nl have been measured.

The minimal detectable stroke volume is given by the output noise of the electronic circuit. The noise has been measured at the output after amplification by an oscilloscope. A peak-to-peak noise level of 75 mV has been measured for this configuration. Sub-nl stroke volume pulses created by a micropump usually have a duration of about 10 ms, similar to that shown in figure 7. By using equation (9), the minimal detectable stroke volume for a pulse length of 10 ms is 0.43 nl. The flow sensor is able to detect sub-nl stroke volumes for pulse lengths shorter than 10–20 ms, as generated by piezoelectric membrane micropumps.

The calculated flow rates have been compared to a fast and convenient measurement with a high precision volumetric

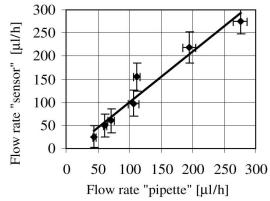

Figure 8. Comparison of flow rates.

pipette as a function of time and are shown in figure 8. The measurement errors are mostly done at the pipette level. The flow sensor shows a stable signal for every pump stroke.

A high resistivity of 1.2 GΩ cm has been measured for the insulated ZnO piezoelectric transducers. The frequency at which resistive and capacitive terms produce equal output noise occurs at $\omega = 1/(\varepsilon\varepsilon_0\rho)$, resulting in a frequency of 118 Hz. Below this frequency the finite resistance of the ZnO has an important effect on noise as reported in [10].

In the quasistatic mode piezoelectric sensors have a limit in precise detection for integration time constants higher than 0.5–1 s as known, for instance for force sensors. The accurate quasistatic measurements are influenced on the one hand by the internal resistance of the sensor and on the other hand by the time constant of the drift and offset compensation feedback loop. An optimum between quasistatic measurements and drift and offset compensation has been found at a feedback loop time constant of 1.5 s. We have measured an amplitude diminution of 10% of the initial signal after a time of 200 ms. The amplitude diminution is created by the offset and drift compensation loop. At an integration time constant of 200 ms in the quasistatic mode the sensor output signal (flow rate) shows an error of about 5%. More precise measurements at longer integration times would be possible by increasing the feedback loop time constant, but then the internal resistance of the sensor and electronic circuit becomes important.

4. Conclusion

We demonstrated the successful use of heat bonding type polyimide sheets in MEMS applications. Insulated ZnO thin film piezoelectric transducers have been deposited with no external heating of the substrate onto polyimide membranes. The high resistivity of 1.2 GΩ cm allows sensing at low frequencies. A transverse piezoelectric coefficient of $e_{31,f} = -0.294$ C m^{-2} for the ZnO thin film has been extracted for the insulated ZnO layer. The polyimide material UPILEX® VT has good mechanical and chemical properties, which is useful for microfluidic devices.

Flow rates generated by a micropump have been measured in the range from 30 to 300 μl h^{-1} at stroke volumes of 1 to 10 nl. The fabricated liquid flow sensors are capable of accurately measuring nl and sub-nl stroke volumes, which make them suitable for small dosing applications.

Acknowledgments

The authors would like to thank the following persons and institutions for the good cooperation and help: Herbert Keppner (HESSO) for ZnO deposition, Mario Dellea (HESSO) for advices on electronic circuit design, Raphaël Holzherr for his diploma work, Pierre-André Clerc, Sylvain Jeanneret, Sylviane Pochon, all technicians at IMT, University of Neuchâtel and at HESSO, University of Applied Science, Le Locle. Their contributions are gratefully acknowledged. This work has been supported by the commission for technology and innovation CTI.

References

[1] Zheng Z *et al* 1998 Piezoelectric coefficients of thin polymer film measured by interferometry *J. Intell. Mater. Syst. Struct.* **9** 69–73

[2] Dubois M A *et al* 1999 Measurements of the effective transverse piezoelectric coefficient $e_{31,f}$ of AlN and $Pb(Zr_x,Ti_{1-x})O_3$ thin films *Sensors Actuators* A **77** 106–12

[3] Kuoni A *et al* 2002 A high insulating thin film ZnO piezoelectric actuator on a polyimide substrate *Proc. Eurosensors XVI (Prague)* pp 228–31

[4] Boillat M *et al* 1995 A differential pressure liquid flow sensor for flow regulation and dosing systems *Proc. IEEE Microelectromech. Syst.* pp 350–2

[5] Moulson A J 1990 *Electroceramics* (London: Chapman and Hall)

[6] van Lintel H *et al* 1988 A piezoelectric micropump based on micromachining of silicon *Sensors Actuators* A **15** 153–67

[7] Gravesen P *et al* 1993 Microfluidics—a review *Micro Mechanics Europe MME'93, Workshop Digest* pp 143–64

[8] Tanaka K *et al* 1995 Measurements of piezoelectric constant of ZnO thin film on Si microstructure *Japan. J. Appl. Phys.* **34** 5230–2

[9] Ikeda T 1990 *Fundamentals of Piezoelectricity* (New York: Oxford Science Publications) pp 222

[10] DeVoe D L *et al* 2001 Surface micromachined piezoelectric accelerometers *J. Microelectromech. Syst.* **10** 180–5

REF. 3

Two-Dimensional Parallel Dispenser for Micro-array Printing.

Journal of Labautomation JALA, 8(5), 24-28, 2003.

Pages 125-129

Scientific Brief

Two-Dimensional Parallel Dispenser for Microarray Printing

Andreas Kuoni,[1,*] *Marc Boillat,*[2] *and Nico F. de Rooij*[2]
[1]*Institute of Microtechnology, University of Neuchâtel, Switzerland;*
[2]*Seyonic SA, Neuchâtel, Switzerland*

Keywords:
dispenser,
droplets,
microarray printing,
piezoelectric
actuator,
polyimide substrate

Parallel printing in a microarray format is becoming increasingly important. This paper presents a 2-D multi-channel dispenser with a spotting spacing of 500 μm. The dispenser is continuously loaded from a 384-well plate format and shoots upward. New technologies using polyimide substrate was developed, and the flexibility of the polyimide sheets allows scaling the dispenser up to an array format of 24 × 16. Drop formation is analyzed by stroboscopic illumination and by spotting onto glass slides. Droplets of 65 pL are dispensed in parallel up to 5 kHz at a droplet speed of 2 m/s. (JALA 2003;8:24–8)

Introduction

Microarrays of bioactive substances are becoming increasingly important for medical diagnostics and drug research. The ability to carry out assays in parallel in a microarray format is required for high-throughput analysis systems. This paper presents a new type of dispenser that dispenses 65 pL droplets in parallel on a 2-dimensional array plate (biochip) at a spacing of 500 μm. The dispenser is continuously loaded from a standard well plate with a well spacing of 4.5 mm during dispensing.

An innovative technology using polyimide sheets was developed for the construction of a 2-D microarray printing device. Polyimide is an established material for biological applications and is compatible with integrated circuit (IC) technology. It has excellent chemical and mechanical properties. The developed technology comprises microlithographic polymer structuring, polyimide–polyimide bonding and integrated piezoelectric actuators.

The advantages of the polyimide dispenser are that it does not require connecting tubes or interface change in the fluidic path, there is minimal dead volume, and most importantly, there is flexibility of the μ-channels compared to other inkjet-based piezoelectric dispensers.[1,2] This flexibility allows the formation of different sizes of dispensing arrays in a modular way by stacking dispenser lines (e.g., 24 × 16, 12 × 8).

Prototypes are characterized for different subjects. Droplet formation under stroboscope illumination is observed, and the directionality of droplet jet is analyzed, and it is explained why the dispenser does not show satellite droplets. Dispensing stability is investigated and demonstrated for different driving signals. Finally, droplets are spotted onto a glass slide in a 1-D array format and in a 2-D array format.

Design and Fabrication

Several prototypes were fabricated and assembled. Figure 1 depicts a schematic cross section of a dispenser array. At the bottom of the figure is the reservoir that corresponds to a 384-well plate. The lower end of the flexible polyimide channel is immersed into the well for filling the μ-channels. The filling is done by applying backpressure of some tens of millibars. When the liquid is forced into the

*Correspondence: Andreas Kuoni, Institute of Microtechnology, University of Neuchâtel, Rue Jaquet-Droz 1, 2007 Neuchâtel, Switzerland; Phone: +41.32.720.55.74; Fax: +41.32.720.57.11; E-mail: andreas.kuoni@unine.ch

1535-5535/2003/$30.00 + 0
doi:10.1016/S1535-5535(03)00007-8

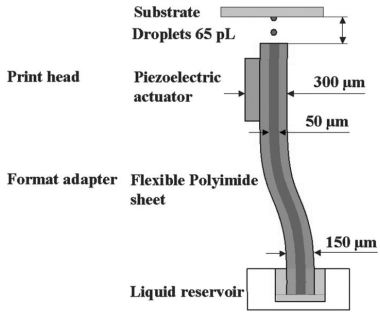

Figure 1. Schematic channel cross section of a 1-dimensional dispenser array.

channel, it flows up to the nozzle where it is stopped by surface tension. Once filled, an electrical signal is applied to the actuator, and droplets are ejected upward to a substrate at distance of 0.25 to 1 mm.

The dispensing mechanism relies on piezoelectric actuation. We use thin ceramic plate actuators made of lead zirconate titanate (PZT). The actuator squeezes the µ-channel and creates a stroke volume. The actuator has to be able to create the required stroke volume in some tens of microseconds in order to eject droplets at a sufficient speed. One part of the volume change is absorbed within the supply channel, and the other part is ejected through the nozzle. The relation between the two volume parts depends on the channel geometry, fluidic resistance, and on the physical properties of the testing liquid.

The device was fabricated with standard microelectromechanical systems (MEMS) technologies and microlithographies.[3] Starting material is commercially available heat-sealable polyimide sheets UPILEX® VT. Onto these 50-µm-thick polyimide sheets, thin film metal of aluminum (3000 Å) is evaporated and patterned by lithography. The aluminum is etched by standard al-etch solution at a temperature of 42 °C. The metal layer is used as masking material for the reactive ion etching (RIE) of the polyimide. The µ-channels are anisotropically dry etched, which allows tight dimension control of the µ-channel sizes. The minimal structure size is about 30 µm. The etched polyimide sheet is then sealed with a blank polyimide sheet of the same material grade. The sealing is done by a thermal bonding process and is carried out with a mechanical press (Type 465: Erichsen; Hemer, Germany). The press is equipped with a bottom and top heating chuck. A bond pressure of 50 to 100 bars and a temperature of about 300 °C are applied for 30 to 60 min. On the prefabricated, sealed µ-channels, lithography is carried out and a gold electrode is evaporated. The electrodes are patterned by lift-off technology for not exposing the bonded polyimide to strong etch solutions. Next, the polyimide sheets are tailored by a deep UV-Excimer Laser. This process defines the outer surface of the nozzles and also defines the shape of the inlet side. Finally, piezoelectric actuators are attached with a nonconducting adhesive onto individual metal electrodes. The top electrode is contacted by a silver epoxy trace to the nearby thin film electrode. Then, the fabricated polyimide sheets are stacked together to form a 2-D printing array.

The inlet side of the dispenser has a fingered shape as shown in Figure 2. The inlet channel spacing of 4.5 mm fits to a 384-well plate. For aspirating, these fingers are immersed into the dispensing liquid positioned by mechanical alignment to the well plate. Next, the dispenser is clamped to the well plate. The dispenser to the well plate is sealed with a gasket, which allows pressurizing the wells and pushes the liquid into the µ-channels and up to the nozzle where it is stopped by surface tension. A back pressure of 10 mbar is applied to fill the µ-channel. A pressure of about 20 mbar would be required to push the liquid out of the nozzle and wet the nozzle's outer surface. The etched channels do not have any sharp edges or corners where air bubbles could be trapped during filling of the µ-channels. Bubble-free filling results in stable shooting. Once the filling of the channels is complete, the dispenser is ready to dispense. For convenience, the dispenser stays together with the well plate during the spotting; thus the dispenser shoots upward. The upward shooting has no influence on the drop formation because the kinetic energy is more significant than the force of gravity. The kinetic energy is about 50 to 100 times higher than gravity at a droplet speed of 2 m/s. The upward shooting avoids complex robotics for positioning and displacing, and

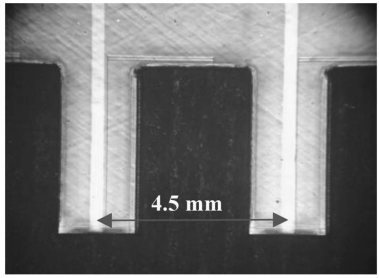

Figure 2. Fingered shape of the inlet side of the dispenser at a spacing of 4.5 mm. The polyimide outer shape was cut with an Excimer Laser at a wavelength of 193 nm.

the system becomes easy to handle and can be displaced manually. It is believed that the device could be used more than once. After dispensing, the dispenser is placed onto a well plate filled with a defined volume of cleaning solution. Applying a back pressure of 0.5 to 1 bar, the cleaning solution is flushed through the channels and out the nozzle, where the cleaning solution is collected by an absorbing tissue. The internal volume per channel of a full-size dispenser is only 2 µL, and a 384-well plate has a volume of 100 to 120 µL. After the cleaning solution is flushed through the channels, nitrogen from the pressure source dries the µ-channels. The cleaning procedure takes some time, but once the channels are dried, the device can be refilled from another well plate.

The format transfer from 4.5 mm to 500 µm is done in both x- and y-directions. In the x- direction, the channels are etched into a polyimide sheet in such a manner that all channels come together to form a 1-D nozzle array at a spacing of 500 µm as shown in Figure 3. In the y-direction, the polyimide sheets are assembled in a modular way by using the flexibility of the thin sheets. A bonded sheet is 150 µm thick and reaches a total thickness of 300 µm with the piezoelectric actuators. Single sheets are stacked together to form a 2-D printing array. Spacers have been used to respect a spacing of 500 µm. A top view of an assembled 2 × 3 nozzle array is shown in Figure 4. The smaller picture in Figure 4 shows a close-up of a single nozzle. The sidewall angle of the nozzle is defined by the anisotropical plasma etching process and has a slightly trapezoidal shape of about 50 µm. The trapezoidal nozzle shape has not shown any negative aspects in the experimental phase.

Drop formation is analyzed by video observation under stroboscope illumination. The test liquid is degassed water. The dispenser assembled to the well plate is shooting upward as shown in Figures 6 and 7. A microscope with a variable zoom is installed horizontally at the height of the nozzle to observe the drop formation. Opposite of the microscope, a red light-emitting diode (LED) for the stroboscopic illumination is positioned. The driving signal for the LED is a square wave with an amplitude of 5 volts and pulse length of 2 µs. During the 2- µs pulse, length the droplet only moves about 4 µm for an ejection speed of 2 m/s, which still results in a fairly sharp image. The LED driving signal is synchronized with the driving signal of the actuator with a variable delay time from zero to 500 µs. Installed on top of the microscope is a black-and-white charge-coupled device (CCD) camera with video output (CCD-IRIS: Hi Resolution; Sony, Japan). The video is recorded onto a Mini DV cassette for further treatment. The dispenser is able to dispense up to 5 kHz, but the dispensing frequency has been set to 500 Hz for video recording.

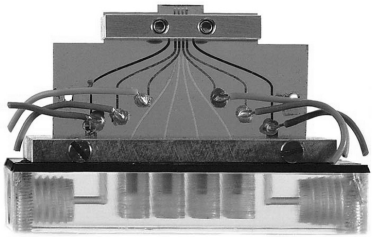

Figure 3. Front view of an assembled 1-D dispenser array. The channels come together to form a nozzle array at a spacing of 500 µm. On the right and left of the channels, thin-film electrodes connect the piezoelectric actuators. At the bottom is a homemade well plate with the same spacing as a 384 plate. The bores on the side are used to pressurize the wells for filling the dispenser.

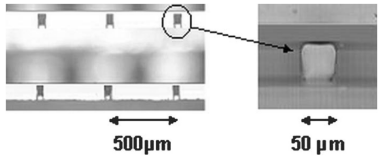

Figure 4. An assembled 2 × 3 nozzle array in microarray format is shown on the left (top view). On the right-hand side is a close-up of a single nozzle. The nozzle has a slightly trapezoidal shape with a dimension of (60/40) × 50 μm^2.

Results

A prototype of two assembled 1-dimensional printing arrays was built to form a 2-dimensional array as shown in Figure 5. The bottom plate represents the well plate. The bore in the middle part is used to pressurize the reservoirs for filling. On the flexible polyimide sheets, there are integrated thin film electrodes to connect the piezoelectric actuators. Electric wires are simply glued onto the lower end of electrodes to connect an external driving circuit. The clamps fixing the dispenser to the well plate have been omitted for better illustration.

Figure 6 presents a close-up of two channels during dispensing at 500 Hz and at a delay time of 150 µs. The image corresponds to a superposition of some tens of droplets. No wetting of the nozzle outer surface is observed. Ink-jet-based dispensers often show small secondary droplets called satellite droplets next to the main droplets.[2] Satellite droplets are undesirable because of cross contamination between spotting sides. Satellite droplets are avoided by using polyimide substrates and by optimizing the driving signal. Polyimide substrate tends to damp any secondary waves, which might provoke satellite droplets. No satellite droplets were observed for a rise and fall time of 5 µs for the driving signal of the

Figure 5. Side view of an assembled 2-D dispenser array. The flexibility of the polyimide sheets allows stacking of single sheets to form any desired format up to 24 × 16.

piezoelectric actuator.[4] The sharpness of the image is a good indication of stable droplet shooting as demonstrated in Figure 6. The droplet ejection speed is about 2 m/s. At this speed, no splashing occurs when the droplet arrives on the surface. A slight speed difference between the channels was observed, but it does not influence the spotting quality. The droplet volume is calculated by measuring the droplet diameter with a microscope. This method is a rough estimation for the first prototype. Droplets have a nominal diameter of 50 µm and the dispensed volume is then about 65 pL ± 15%.

An important parameter for multichannel dispensing in microarray format is the directionality of the droplets. A good directionality avoids cross contamination between spotting sides. The cutting quality and the non-wetting properties of the nozzle outer surface appear to be key factors. High cutting quality is reached by photoablation with a deep UV-Laser Excimer at a wavelength of 193 nm. A hydrophobic surface quality is given without a surface treatment by the property of polyimide. After cutting, no wetting on the nozzle's outer surface is observed. Because both factors are fulfilled, the droplet deviation is smaller than ±5° and results in maximum misplacement of 44 µm for a substrate distance of 500 µm.

The stability of multichannel parallel dispensing was also investigated. A square-shaped pulse of about 150 volts was applied to the piezoelectric actuators to create different pulse

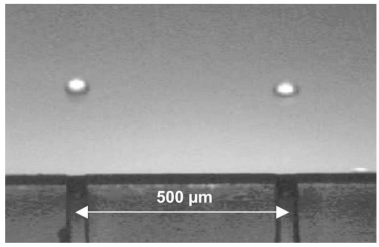

Figure 6. Parallel dispensing of 65 pL droplets at a spacing of 500 µm. This photo was taken with a stroboscopic illumination at a delay time of 150 µs. The dispensing frequency was 500 Hz. A good directionality and satellite-free droplets are achieved within this prototype.

widths. For pulse widths ranging from 20 to 70 µs, droplets are ejected. However, the stroboscope image indicates a droplet volume change in function of the pulse width. This effect is demonstrated in Figure 7. At a larger pulse width, the actuator creates a larger stroke volume, which explains the volume change. The wide range of the pulse width allows driving all channels at one common driving signal and makes it nonsensitive to small signal change. This is an important advantage for a full-size dispenser (e.g., 24 × 16) where only one power supply may be used.

After analyzing the droplet formation, parallel spotting onto a glass slide was explored. The dispenser is fixed to the well plate and stands on a table. On the top of the nozzle array a glass slide is placed at a distance of about 0.5 mm. A

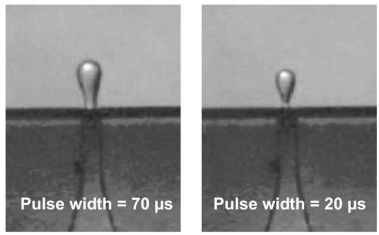

Figure 7. Drop formation for different pulse width. A controlled volume change can be seen between the left and right image. These pictures are taken under stroboscopic illumination at a delay time of 60 µs.

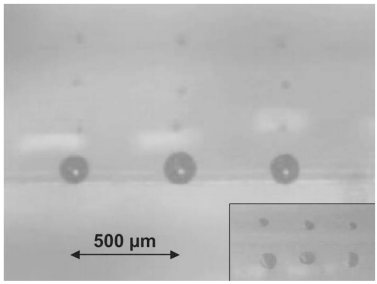

Figure 8. Parallel spotting onto a glass slide. The larger image shows a close-up of three nozzles at printing. The 1-D dispenser is manually displaced at 200 µm. The smaller image presents a close-up of 2-D parallel spotting of 2 × 3 array at a spacing of 500 µm in x- and y-direction (bottom right).

microscope with a video camera is installed above the glass slide. The droplets are observed through the glass slide during dispensing. In Figure 8, droplets are dispensed in parallel at 1 Hz. All three channels have the same electrical driving signal. By adding another sheet to the 1-dimensional dispenser array, a 2-dimensional microarray is formed. The parallel spotting of 2 × 3 array is shown in the smaller portion of Figure 8. A slight difference in the dispensed volume between the two sheets is observed because of different nozzle sizes from the etch time in the plasma reactor. When the dry-etching process is optimized, this aspect is reduced. All channels have the same driving signal and are connected to a single power supply. Parallel spotting in a microarray format significantly increases the throughput, which is required for HTS applications.

Outlook

There are future plans to fabricate a 24-channel, 1-dimensional array dispenser. The polyimide sheets will then be 6 inches square. After successfully dispensing with the 24-channel dispenser, a 2-dimensional array will be built and characterized, and then a 24 × 16 array will be assembled and tested.

Conclusion

A multichannel parallel dispenser for a 2-dimensional microarray format has been built and characterized. The flexibility of the polyimide substrate allows forming arrays by stacking of single sheets. The dispenser is scalable to any desired format up to an array of 24 × 16. Drop formation is analyzed with stroboscope illumination for different driving signals. A good directionality of less than 5° deviation of the droplets is reached without satellite droplets. The continuous filling from a 384-well plate makes the device easy to handle and minimizes the waste of samples and reagents. After filling, thousands of droplets of 65 pL can be dispensed in parallel onto different microarrays.

Acknowledgments

The authors would like to thank the following people and institutions for their cooperation and assistance: Prof. Herbert Keppner (HESSO) and Daniel Gigon (HESSO) for dry etching of polyimide sheets; technicians Nicole Hegelbach, Gianni Mondin, Sylviane Pochon, and Sylvain Jeanneret at IMT, University of Neuchâtel and at HESSO; and the University of Applied Science, Le Locle. Their contributions are gratefully acknowledged. This work has been supported by the Swiss Commission for Technology and Innovation CTI.

References

1. Wallace, D.; Trost, H.-J.; Eichenlaub, U. Multi-fluid Ink-jet Array for Manufacturing of Chip-based Micro-array Systems. Proceedings of Second International Conference on Microreaction Technology, March 1998, pp 1–5.
2. Laurell, T.; Wallman, L.; Nilsson, J. Design and development of a silicon microfabricated flow-through dispenser for on-line picolitre sample handling. *J. Micromech. Microeng.* **1999**, *9*, 369–376.
3. Kuoni, A.; Holzherr, R.; Boillat, M.; de Rooij, N.F. A polyimide membrane with ZnO piezoelectric thin film pressure transducers as a differential pressure liquid flow sensor. Proceedings Micromechanics Europe MME'02, Sinaia, Sept. 2002, pp 267–270.
4. Kuoni, A.; Boillat, M.; de Rooij, N.F. A modular high density multi-channel dispenser for micro-array printing. Digest of the 12th International Conference on Solid-State Sensors, Actuators and Microsystems. Transducers'03, Boston, June 2003, 1, pp 372–376.

REF. 4

A Modular High Density Multi-channel Dispenser for Micro-array Printing.

Digest of the 12th International Conference on Solid-State Sensors, Actuators and Microsystems, Transducers'03, Boston, 1, 372-376, 2003.

Pages 133-136

2C3.3

A MODULAR HIGH DENSITY MULTI-CHANNEL DISPENSER FOR MICRO-ARRAY PRINTING

Andreas Kuoni*, Marc Boillat and Nico F. de Rooij***

*Institute of Microtechnology, University of Neuchâtel, P.O. Box 3, CH-2007 Neuchâtel, Switzerland
Tel.: 00 41 32 720 55 74, e-mail: andreas.kuoni@unine.ch
**Seyonic SA, CH-2000 Neuchâtel, Switzerland

ABSTRACT

A multi-channel dispenser for micro-array printing has been developed and characterized. We report the fabrication of the dispenser using flexible Polyimide substrate. Polyimide sheets have been dry etched to form µ-channels. These sheets are sealed with virgin Polyimide sheets by a thermal bonding process. Piezoelectric actuators have been glued onto the channels. 1-dimensional dispenser array has been stacked together to form a 2-dimensional printing array at a nozzle spacing of 500 µm. The actuator displacement has been investigated by finite element analysis and by measurements during dispensing for different electrical pulse shapes. The drop formation is recorded with a standard video camera with stroboscope illumination. Droplets of 65 pL have been ejected in parallel at a speed of 2-3 m/s and up to a frequency of 5 KHz.

INTRODUCTION

Micro-arrays of bioactive substances are becoming more and more important for medical diagnostics and drug research. The ability to carry out assays in parallel in a micro-array format is essential for the success of high-throughput analysis systems. We report a new type of dispenser which dispenses 65 pL droplets in parallel on a 2-dimensional array plate (biochip) at a spacing of 500 µm. While the dispenser is continuously loaded from a standard well plate with a well spacing of 4.5 mm.

An innovative technology using Polyimide sheets has been developed for the construction of a 2-dimensional micro-array printing device. The developed technology comprises microlithographic polymer structuring, Polyimide-Polyimide bonding and integrated piezoelectric actuators. The flexibility of the Polyimide sheet allows forming different sizes of dispensing arrays in a modular way by stacking dispenser sheets.

The actuator displacement has been investigated by finite element modeling (Ansys) and measurements during dispensing, followed by the calculation of the effective stroke volume.

Furthermore, the speed of the actuator displacement has been measured for different pulse shapes. These measurements demonstrate that the stability of shooting can be improved by varying the rise and fall time of the electrical driving signal.

DESIGN AND FABRICATION

Several prototypes have been fabricated and assembled. Figure 1 depictes a schematic cross section of a dispenser array. At the bottom of the figure is the reservoir which corresponds to a well of 384-well plate. The lower end of the flexible Polyimide channel is immersed into the well for filling the µ-channels. The filling is done by applying a back pressure of some tens of millibars. The liquid is forced into the channel and flows up to the nozzle where the liquid stops by surface tension effect. Once filled, an electrical signal is applied to the actuator and droplet are ejected upwards to a substrate at distance of 0.25 to 1 mm.

The dispensing mechanism relies on piezoelectric actuation. We use thin ceramic plate actuators made of

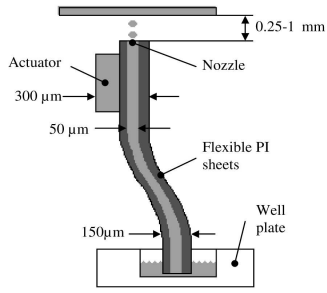

Figure 1. A schematic channel cross section of a 1-dimensional dispenser array.

0-7803-7731-1/03/$17.00 ©2003 IEEE

Lead Zirconate Titanate (PZT). The actuator squeezes the µ-channel and creates a stroke volume. The actuator has to be able to create the required stroke volume in some tens of micro-seconds in order to eject droplet at sufficient speed. One part of the volume change is absorbed within the supply channel and the other part is ejected through the nozzle. The relation between the two volume parts depend of the channel geometry, fluidic resistance and also of the physical properties of the testing liquid.

The device has been fabricated by using standard MEMS technologies and microlithographies [1]. Starting material is a commercially available heat sealable Polyimide sheets. Onto these 50 µm thick Polyimide sheets thin film metal of Aluminum (3000 Å) is evaporated and patterned by lithography. The Aluminum is etched by standard Al-etch solution at a temperature of 42°C. The metal layer is used as masking material for the reactive ion etching (RIE) of the Polyimide. The µ-channels are anisotropically dry etched which allows a tight dimension control of the µ-channel sizes. The minimal structure size is about 30 µm. The etched Polyimide sheet is then sealed with blamk Polyimide sheet of the same material grade. The sealing is done by a thermal bonding process and is carried out in a mechanical press. The press is equipped with a bottom and top heating chuck. A bond pressure of 50-100 bars and a temperature of about 300°C are applied during 30-60 min. On the prefabricated sealed µ-channels a lithography is carried out and a Gold electrode is evaporated. The electrodes have been patterned by lift-off technology for not exposing the bonded Polyimide to strong etch solutions. Next, the Polyimide sheets are tailored by Excimer Laser. This process defines the outer surface of the nozzles and also defines the shape of the inlet side. Eventually, piezoelectric actuators are glued with a non-conducting glue onto the single metal electrodes. The top electrode is contacted by a silver glue trace to the nearby thin film electrode.

The mechanical key part of the dispenser is the piezoelectric actuator. As mention in the introduction the dispenser has to be scalable to different formats at a nozzle center-to-center spacing of 500 µm in two directions. These factors limit the size of the actuator's width and thickness. The length of the actuator is free and may be in a range of 5-20 mm. A finite element analysis of the static membrane deflection of the actuator has been done using ANSYS. We investigated the PZT plate thickness in function of the deflection and analyzed the pressure dependency of the displacement. We found that the thickness of the piezoelectric plate should be as thin as possible for high stroke volume as shown in Figure 2. Also the driving voltage can be reduced by using thinner PZT plate. On the other hand the PZT ceramics plate should be commercially available and the handling of the single actuator plates should not be too critical. For the reason of commercial availability we had to choose a

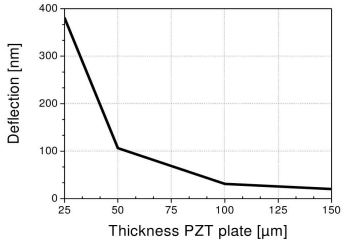

Figure 2. FEM analysis of actuator displacement in function of thickness at a driving voltage of 100 Volts.

130 µm thick PZT plate. The PZT plates have been diced in-house to the required size with a diamond blade saw as used for glas-silicon wafers.

We investigated the pressure dependence of the membrane displacement. For this simulation we chose a 25 µm thin plate because this plate shows a higher dependency than a 130 µm thin plate and applied a static pressure in the fluidic channel next to 100 Volts. By increasing the pressure in the channel the

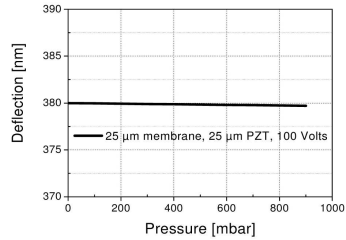

Figure 3. Pressure dependency of a 25 µm thick PZT plate at 100 Volts.

displacement of the actuator/membrane reduces slight. The pressure dependency is less than 1% up to 1 bar channel pressure at a driving voltage of 100 Volts. We conclude that the high stiffness is given by the PZT ceramic actuator.

Piezoelectric dispensers are used for different applications as for instance for ink-jet printing [2, 3]. A challenge of the piezoelectric principle is the relatively small actuator displacement which requires

an air bubble free filling of the device. The presented Polyimide technology improves the filling because of minimal dead volume and seamless transition from the

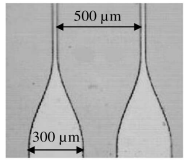

Figure 4. A close-up of the fluidic path of two independent channels at a spacing of 500 µm.

reservoir to the nozzle. The smoothless of the µ-channel is shown in Figure 4. The design of the µ-channels has been designed in such a manner that any sharp corners or discontinuity in the fluidic path has been avoided.

RESULTS

A prototype of two assembled 1-dimensional printing arrays has been built to form a 2-dimensional array. The fabricated 1-dimensional array has a total thickness of 280 µm where 130 µm is given by the PZT plate and 150 µm by the bonded µ-channels. Spacers of 220 µm have been introduced to form the nozzle array at a spacing of 500 µm. Single sheets are then mechanically fixed together to form the print head. Each channel is individual addressable. The inlet side spacing is 4.5 mm which corresponds to standard 384 well plate.

The device is scalable in x and y direction. In one direction by etching more channels into the Polyimide sheets and in the other direction by stacking Polyimide sheets. The flexible Polyimide sheets allow bringing all nozzles together to form a 2-dimensional printing array.

The drop formation has been analyzed by video observation under stroboscope illumination. The used test liquid is degassed water. The dispenser assembled to the well plate is shooting upwards as shown in Figure 5. A microscope with a variable zoom has been installed horizontally at the height of the nozzle to observe the drop formation. Opposite of the microscope a red light emitting diode (LED) for the illumination has been fixed. The driving signal for the LED is a square wave with an amplitude of 5 Volts and pulse length of 2 µs. During the 2 µs pulse length the droplet only moves about 4 µm for an ejection speed of 2 m/s, which still results in a fairly sharp image. The LED driving signal is synchronized with the driving signal of the actuator with a variable delay time from zero to 500 µs. On top of the microscope a black and white CCD camera with a video output has been installed. The video is then recorded onto a Mini

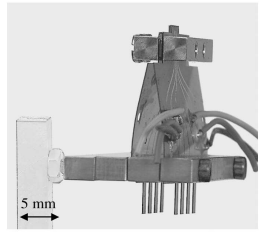

Figure 5. Assembled dispenser of two 1-d printing arrays of four channels each. The device is shown without well plate.

DV cassette for further treatment. The dispenser is able to dispense up to 5 KHz, but the dispensing frequency has been set to 500 Hz for video recording.

The sharpness of the image is a good indication for a stable droplet shooting. The droplet ejection speed is about 2 m/s. A slight speed difference between the channels has been observed, but it does not influence the printing quality. The droplet volume has been calculated by measuring the droplet diameter. The

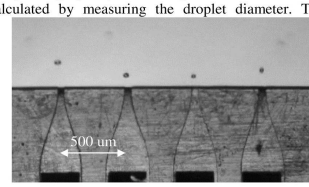

Figure 6. Parallel dispensing of four channels at 500 Hz. Stroboscope illumination at a delay time of 80 µs after the driving signal.

droplets have a diameter of about 50 µm resulting in a volume of about 65 pL.

The piezoelectric actuator has been analyzed in detail for different driving signals. We are interested in the deformation and displacement speed of the actuator. For this purpose, a single Polyimide sheet has been fixed under an optical microfocus measurement system (UBM). The working principle of the microfocus measurement system is that changing the distance between object surface and object lens the image focus point is shifted and the illumination of the photodiodes becomes unequal. This unequal illumination generates a focus error signal by means of

a differential amplifier. The focus error signal is then used to extract the membrane deformation. The 2 µm diameter Laser spot has been focused on the center part of the actuator surface.

In Figure 7 the membrane center deflection speed is given for different rise and fall times of the actuator driving signal. At a rise and fall time of t_r=2 ns ripples are created in the speed profile of the membrane displacement. These ripples tend to create small secondary droplets called satellite droplets. By increasing the rise and/or fall time these ripples disappear without influencing the dispensing behavior as demonstrated in Figure 7. Ripples also tend to push the liquid column forward and backward and may create turbulences in the µ-channels. The dispensing stability can be improved by increasing the rise and fall time.

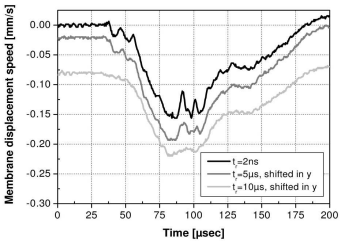

Figure 7. Membrane displacement speed for different rise and fall times t_r at 150 Volts for 50 µs. These profiles have been measured during dispensing.

Furthermore, we are interested in the membrane deformation of the dispenser during dispensing. By integration of the speed curve in Figure 7 over the time, the membrane deflection can be extracted. Then the stroke volume of the actuator can be calculated by the integration over the width $V_{trans}=\int a_{trans} \cdot l \cdot dw$, where a_{trans} is the transversal membrane deflection, w the width of the channel and l the length of the channel. The center membrane deflection is obtained by integration of the speed curve in Figure 7 and a_{trans} at the center is about 15-20 nm in the transversal direction. The calculated stroke volume in the transversal direction is then about V_{trans}=76–102 pL. There is also a longitudinal deformation in the width direction of the channel. This deformation can not be easily measured but has been found by a finite element simulation. The longitudinal stroke volume can be calculated by integration over the height $V_{long}=\int a_{long} \cdot l \cdot dh$, where a_{long} is the channel deformation in the width direction, h the channel height and l the channel length. The longitudinal stroke volume has been only simulated is about 14-18 pL. The total stroke volume is $V_{stroke}=V_{trans}+V_{long}$ The summation results in an estimated stroke volume between 90 and 120 pL which is created during short pulses. We conclude that the required stroke volume for droplet ejection is in the range of about 1.5 to 2 times of the droplet volume itself for the given device.

CONCLUSION

The fabrication and characterization of a multi-channel dispenser has been demonstrated. Novel technology of using Polyimide sheets as substrate has been used for building dispenser arrays. Droplets of 65 pL have been ejected parallel in a micro-array format of 500 µm. The membrane displacement during dispensing has been investigated for different driving signals of the piezoelectric actuator. The presented dispenser can be used for a large variety of array printing.

ACKNOWLEDGEMENTS

The authors would like to thank the following persons and institutions for the good cooperation and help: Prof. Herbert Keppner (HESSO) and Daniel Gigon (HESSO) for dry etching of Polyimide sheets, Nicole Hegelbach, Gianni Mondin, Sylviane Pochon, Sylvain Jeanneret, all technicians at IMT, University of Neuchâtel and at HESSO, University of Applied Science, Le Locle. Their contributions are gratefully acknowledged. This work has been supported by the commission for technology and innovation CTI.

REFERENCES

[1] A. Kuoni, R. Holzherr, M. Boillat and N. F. de Rooij, “A Polyimide membrane with ZnO piezoelectric thin film pressure transducers as a differential pressure liquid flow sensor,” Proceedings Micromechanics Europe MME’02, Sinaia, 267-270 (Sept. 2002).

[2] D. Wallace, H.-J. Trost, U. Eichenlaub, “Multi-fluid Ink-jet array for manufacturing of Chip-based microarray systems,” Proceedings of Second International Conference on Microreaction Technology, 1-5 (March 1998).

[3] T. Laurell, L. Wallman and J. Nilsson, “Design and development of a silicon microfabricated flow-through dispenser for on-line picolitre sample handling,” J. Micromech. Microeng., 9, 369-376 (1999).

REF. 5

A Highly Parallel Piezoelectric Printing Device for Micro-Array Technology.

Technical Digest, 17th IEEE International Conference on Micro Electro Mechanical Systems, MEMS 2004, 466-469, 2004.

Pages 139-142

A HIGHLY PARALLEL PIEZOELECTRIC PRINTING DEVICE FOR MICRO-ARRAY TECHNOLOGY

Andreas Kuoni[(1)], *Marc Boillat*[(2)] *and Nico F. de Rooij*[(1)]

[(1)] Institute of Microtechnology, University of Neuchâtel, CH-2007 Neuchâtel, Switzerland
[(2)] Seyonic SA, CH-2000 Neuchâtel, Switzerland

ABSTRACT

A 16x24 dispenser that prints in a micro-array format at a 500 µm spacing is presented. The dispenser is built from laminated flexible Polyimide sheets to form a 2-d printing array. The dispenser is continuously loaded from a 384-well plate format and shoots upward. This makes the device very easy to handle without any robotics. Droplets of 65 pL are dispensed parallel at a speed of 1.78 m/s at 180 Volts. A single channel has a CV value of 8.6 % and a 24-channel dispenser has a CV value of 20 % for a common driving signal.

1. INTRODUCTION

Micro-arrays of bioactive substances are becoming more and more important for medical diagnostics and drug research. The ability to carry out assays in parallel in a micro-array format is required for high-throughput analysis systems. This paper presents a new type of dispenser that dispenses in parallel 384 droplets over a volume of 65 pL on a 2-dimensional array at a spot spacing of 500 µm. The sample is continuously loaded from a standard well plate at a well spacing of 4.5 mm during dispensing.
An innovative technology using polyimide sheets has been developed for the construction of a 2-D micro-array printing device. Polyimide is an established material for biological applications and is compatible with integrated circuit technology (IC). It has excellent chemical and mechanical properties. The developed technology comprises microlithographic polymer structuring, polyimide-polyimide bonding and integrated piezoelectric actuators.
The advantages of using Polyimide sheets are, that it does not require connecting tubes or interface change in the fluidic path, minimal dead volume, and most importantly, flexibility of the µ-channels compared to other inkjet-based piezoelectric dispensers [1,2]. The flexibility allows building different sizes of dispensing arrays in a modular way by stacking dispenser sheets (e.g. **16x24**, 32x48, 8x12).
A 16x24 dispenser has been built and characterized. Two different channel geometries have been designed to analyze the effect of drop dispense versus driving voltage. The drop formation is observed under stroboscope illumination. A water/Methylene blue mixture has been used as test liquid for printing a micro-array onto paper for the characterization of droplet size and trajectory.

2. DESIGN AND FABRICATION

A schematic cross section of a dispenser showing one channel is depicted in Fig. 1. At the bottom of the figure is the reservoir that corresponds to a 384-well plate. The lower end of the flexible polyimide channel is immersed into the well for filling the µ-channels with the samples. Applying a backpressure of some tens of millibars is sufficient to force the liquid into the channels and to flow up to the nozzle where it is stopped by surface tension. Once filled, an electrical signal is applied to the piezoelectric actuator and droplets are ejected upward to a micro-array substrate, located at a distance of 0.25 to 1 mm of the nozzle.

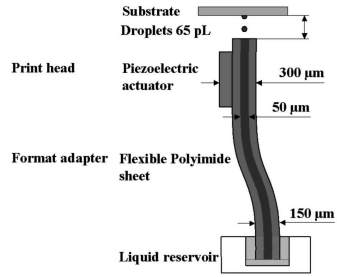

Figure 1: Schematic channel cross section of a single channel.

The device is fabricated with standard microelectromechanical systems (MEMS) technologies and microlithographies [3,4]. Starting material is commercially available heat sealable polyimide sheets UPILEX® VT, 50 µm thick. Onto these Polyimide sheets, thin film metal of copper (5000 Å) is evaporated and patterned by lithography. The copper is etched in a mixture of water and Sodium peroxodisulfate $Na_2S_2O_8$ at a temperature of 42°C. The metal layer is used as masking material for the reactive ion etching (RIE) of the polyimide. The µ-channels are anisotropically dry etched, which allows tight dimension control of the µ-channel sizes. The minimal structure size is about 30 µm. The etched polyimide sheet is then sealed with a blank

polyimide sheet of the same material grade. The sealing is done by a thermal bonding process and is carried out with a custom made mechanical press. The press is equipped with a bottom and top heating chuck. A bond pressure of 50-100 bars and a temperature of about 300°C are applied during 30-60 min. On the prefabricated sealed µ-channels, gold electrodes are evaporated and patterned by shadow masking. Next, the polyimide sheets are tailored by a deep UV-Excimer Laser at a wavelength of 193 nm. This process defines the outer surface of the nozzles and also defines the shape of the inlet side.

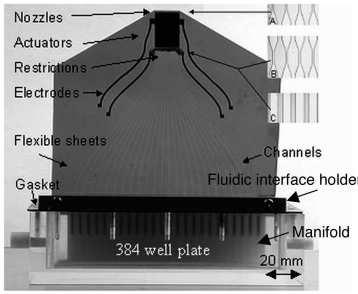

Figure 2: Front view of a 24-channel dispenser sheet mounted onto a 384 well plate. Picture B and C show the two different designs. Picture A discloses the nozzle shape.

The dispensing mechanism relies on piezoelectric actuation. We use thin ceramic plate actuators, which are commercially available, made of Lead Zirconate Titanate (PZT). The custom-sized plates are attached with a non-conducting adhesive onto individual metal electrodes. The top electrode is contacted by a silver epoxy trace to the nearby thin film electrode as shown Fig. 2. Two different designs have been characterized with and without a restriction as shown in Fig. 2 picture B, with restriction, and picture C, without restriction at the end of the actuator opposite of the nozzle.

Filling and handling of the dispenser

The dispenser is easy to handle and use. As usually, a 384 well plate has to be prepared with samples in a regular way. Once the well plate is ready, it is placed into the manifold. Then the dispenser is placed over the well plate by mechanical alignment and is slowly lowered to the well plate and the inlets of the channels are immersed into the wells. A gasket seals to surroundings between manifold and fluidic interface holder. Then, the dispenser is held tight to the manifold. By applying a back pressure of some tens of millibars, all channels are filled simultaneously.

3. RESULTS

A first dispenser with 384 nozzles assembled as a 16x24 printing array with 500 µm spacing has been built and characterized. The device is constructed by assembling of 16 dispenser sheets containing each 24 channels. Spacers are used in between the Polyimide sheets to respect the 4.5 mm spacing of the inlet side at the 384 well plate and thinner spacers are used the built the 500 µm spacing at the nozzle side at the other end. Each dispenser sheet has two electrodes for common contacting of the 24 single piezoelectric actuators. The 24 actuators are driven with the same driving signal. In Fig. 3 a side view of a 16x24 dispenser is shown. In the manifold at the bottom of Fig. 3 is a standard 384 well plate placed. The well plate can be pressurized through a connecting tube, which allows filling the µ-channels.

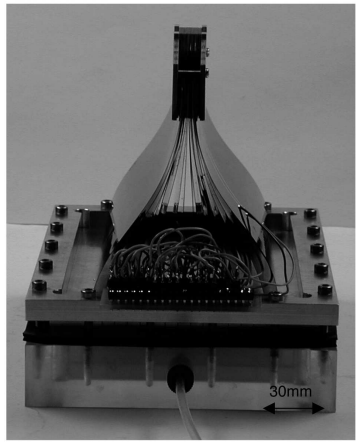

Figure 3: Side view of a 16x24 dispenser including the well plate, which functions as reservoir, the electrical connections and, on the top, print head where the substrate is placed for parallel printing.

The flexibility of the laminated polyimide sheets allows building a print head as shown in Fig. 4. 16 dispenser sheets are hold mechanical together by clamping two Aluminum plates. The sheets are separated around the actuator with spacers to respect the 500 µm spacing. The actuators itself are free to displace because their thickness is only about 475 µm. The substrate (biochip) is just placed onto the Aluminum plates for printing. The air gap between the substrate and the nozzle has been set to 500 µm. No critical alignment or displacement of the substrate is required since the whole array is spotted at once.

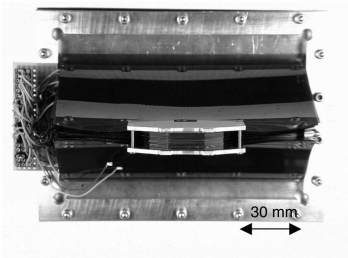

Figure 4: Top view of a 16x24 dispenser, which shows the flexibility of the Polyimide sheets and the nozzle array where the substrate is placed for printing.

The nozzle array is assembled by stacking of Polyimide sheets as mentioned above. The stacking requires a tight dimensional control of the nozzle positioning for minimizing droplets misplacement given by the nozzle misplacement. The single sheets are aligned through bores, which have been fabricated within the same process step as the channels, and pins at the Aluminum plate.

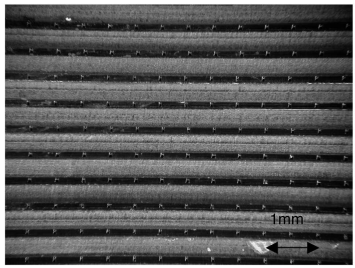

Figure 5: Close up of Fig. 4 top view, showing a section of the 16x24 nozzle array. The dark lines corresponds to the Polyimide sheets with nozzles and the white lines are spacers cut out of a Mylar sheet.

To complete the illustration of the prototype a bottom view of the fluidic interface holder is added in Fig. 6. The holder is made of Aluminum and clamps 16 dispenser sheets together. The sheets are aligned by pins. The Polyimide sheet has a fingered shape and each finger fits into the well of a standard 384 µ-titre plate. For dispensing, the fluidic interface holder is placed over the manifold where the well plate is placed and sealed with a gasket for pressurizing the wells and filling the channels simultaneously.

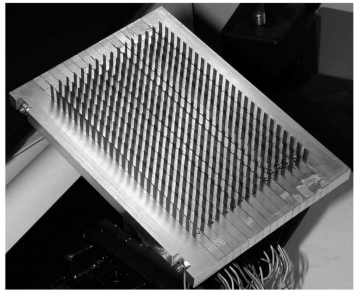

Figure 6: Bottom view of the 16x24 dispenser. Each channel is independent and is spaced at 4.5 mm. Other spacing would be also possible.

Once the device is filled it is ready for dispensing. For the characterization the dispensing liquid was water. It is also possible to dispense liquid with lower surface tension such as Ethanol, for instance. The drop formation has been observed under stroboscope illumination at a frequency of 250 Hz. All characterizations were done by a common driving signal for all actuators. In Fig. 7, a close up of 8 channels out of 24 is shown. We observed no wetting of the outer nozzle surface during dispensing and have also achieved Satellite-free dispensing. The velocity of droplets varies slightly from channel to channel at a common driving signal. The droplet velocity has been characterized by measuring the travel distance between two stroboscope delay time of 200 and 300 µsec. The average velocity is v=1.79 m/s ± 0.2 m/s at a driving voltage of 180 volts.

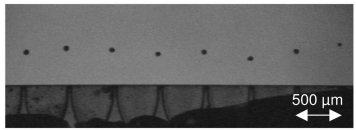

Figure 7: Drop formation of 8 channels out of 24 under stroboscope illumination at a delay time of 300 µsec for nozzle spacing of 500 µm.

In the fabrication we mentioned two different designs with and without a restriction in the channel at the end of the actuator opposite of the nozzle. The restriction has the effect of adding a fluidic resistance to the supply channel. Both designs have been fabricated and characterized for droplet velocity versus driving voltage as shown in Fig. 8. In both case the droplet velocity is linear to the driving voltage. In the case with a restriction the driving voltage is about 50 Volts lower. The drop formation was similar for both case with and without a restriction but without restriction the

dispenser tends to have some satellite droplets. In order to avoid satellite droplets and to have a stable shooting without restrictions, each channel has to be driven by an individual driving signal. Since only one power supply is required we use for further characterization channels with restrictions.

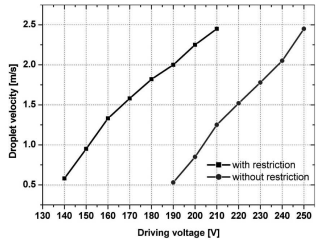

Figure 8: Droplets velocity versus driving voltage for two different designs with and without a restriction in the supply channel.

The variation of the droplets volume has been characterized. For that, the dispenser dispensed droplets upward to glass slide at 0.5 Hz. From the top through the glass slide the droplet has been observed by a microscope equipped with a video camera. The dispensed droplet has a nominal volume of 65 pL, calculated from the droplet diameter. The variation of dispensed volume between spotting has been compared first by calculating the evaporation rate and then applying this to the droplet evaporation time. The average evaporation time for a single channel measuring 30 successive droplets is t=1.40 sec ± 0.12 sec results in a CV value of 8.6 %.

For the characterization of the spot size and spot misplacement of droplets the dispenser has been filled with a mixture of water and colorant Methylene blue. Then, droplets were dispensed onto paper. After drying, the spotted array has been characterized. We used a regular bright white paper as substrate. A close-up of a spotted array out of a 16x24 is shown in Fig. 9.

The spot size has been measured for a 1-d dispenser sheet with 24 channels. The spot size has an average diameter of 110 µm and CV value of 20 % for a common driving signal for all actuators. By applying to every channel the same driving signal, the advantage is that only one power supply is required. However, the CV value could be easily reduced by integration of resistors onto the Polyimide sheets for each actuator. This would allow to control the driving signal for each channel and so also the droplet volume. This has been foreseen but has not been realized so far. We expect that the CV value of spot size is then around 5-10 % for a 16x24 array.

The misplacement of droplets has also been measured. In x-direction the misplacing is ± 29 µm and in the y-direction it is slightly higher at ± 33 µm for a slide-nozzle distance of 500 µm. The directionality angle error is then in x-direction is ± 3.3° and in y-direction ± 3.7°.

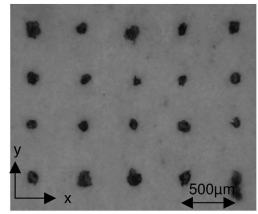

Figure 9: A close-up of a 16x24 spotted array. A mixture of water/Methylene blue has been dispensed onto a bright white paper for characterization.

4. Conclusion

A 16x24 parallel dispenser for a 2-dimensional micro-array format has been built and characterized. The flexibility of the polyimide substrate allows forming arrays by stacking of single sheets. The dispenser is scalable to any desired format up to an array of 1536. Drop formation is analyzed with stroboscope illumination for different channel geometry. The continuous filling from a 384-well plate makes the device easy to handle and minimizes the waste of samples and reagents. After filling, thousands of droplets of 65 pL can be dispensed in parallel onto different micro-arrays.

Acknowledgments

The authors would like to thank Prof Herbert Keppner, Daniel Gigon, Francisco Dias, Fabian Thiebaud from EIAJ Le Locle and all technicians at IMT, Neuchâtel for their work. This work has been supported by the Swiss Commission for Technology and Innovation CTI.

References

1. D. Wallace, H.-J. Trost, U. Eichenlaub, "Multi-fluid Ink-jet Array for Manufacturing of Chip-based Micro-array Systems," Proceedings of Second International Conference on Microreaction Technology, 1-5 (March 1998).
2. T. Laurell, L. Wallman and J. Nilsson, "Design and Development of a Silicon Microfabricated Flow-through Dispenser for On-line Picolitre Sample Handling," J. Micromech. Microeng., 9, 369-376 (1999).
3. A. Kuoni, R. Holzherr, M. Boillat and N. F. de Rooij, "A Polyimide Membrane with ZnO Piezoelectric Thin Film Pressure Transducers as a Differential Pressure Liquid Flow Sensor," Proceedings Micromechanics Europe MME'02, Sinaia, 267-270 (Sept. 2002).
4. A. Kuoni, M. Boillat and N. F. de Rooij, "A Modular High Density Multi-channel Dispenser for Micro-array Printing," Digest of the 12th International Conference on Solid-State Sensors, Actuators and Microsystems, Transducers'03, Boston, 1, 372-376, (June 2003).

REFERENCES

Blalock E., A beginner's guide to microarrays, Kluwer academic publishers, 2003.

Bogy D.B., Talke F.E., Experimental and theoretical study of wave propagation phenomena in drop-on-demand inkjet devices, IBM Journal of research and development, 28(3), 314-321, 1984.

Brown H.R., Yang C.M., Russe T.P., Volksen W., Diffusion and self-adhesion of the polyimide PMDA-ODA, Polymer, 29, 1807-1811, 1988.

CFDRC, www.cfdrc.com, Version 2002.

Chen U.A., Basaran O.A., A new method for significantly reducing drop radius without reducing nozzle radius in drop-on-demand drop production, Physics of fluids, 14(1), L1-L4, 2002.

De Heij B., Steinert C., Sandmaier H., Zengerle R., A tunable and highly parallel picoliter dispenser based on direct liquid displacement, Proceedings of MEMS conference, 706-709, 2002.

De Heij B., Steinert C., Sandmaier H., Zengerle R., A tunable and highly parallel picoliter dispenser based on direct liquid displacement, Sensors and Actuators, A 103, 88-92, 2003.

Dijksman J.F., Hydrodynamics of small tubular pumps, Journal of fluid mechanics, 139, 173-191, 1984.

Dubois M.A. et al, Measurements of the effective transverse piezoelectric coefficient e31,f of AlN and Pb(Zrx,Ti1-x)O3 thin films, Sensors and Actuators, A 77, 106-112, 1999.

Eggers J., Theory of drop formation, Phys. Fluids, 7(5), 941-953, 1995.

Frohn A., Roth N., Dynamics of droplets, Springer publishing group, 2000.

Ghosh K.M., Mittal K.L., Polyimides, fundamentals and applications, Published by Marcel Dekker Inc., 1996.

Gongora-Rubio M.R., Espinoza P., Sola-Laguna L., Santiago-Avilés J.J., Overview of low temperature co-fired ceramics tape technology for meso-system technology (MsST), Sensors and Actuators, A89, 222-241, 2001.

Hirt C.W., Nichols B.D., Volume of fluid (VOF) method for the dynamics of free boundaries, Journal of computational physics, 39, 201-225, 1981.

Ikeda T., Fundamentals of piezoelectricity, New York, Oxford Science Publications, 16-18, 1990.

Kamisuki S., Hagata T., Tezuka C., Nose Y., Fujii M., Atobe M., A low power, small, electrostatically-driven commercial inkjet head, IEEE, 0-7803-4412-X, 63-68, 1998.

Lankard J.R., Wolbold G., Excimer laser ablation of polyimide in a manufacturing facility, Appl. Phys., A54, 335-359, 1992.

Laurell T., Wallmann L., Nilsson J., Design and development of a silicon microfabricated flow-through dispenser for on-line picolitre

sample handling, Journal of Micromech. Microeng., 9, 369-376, 1999.

MacBeath G., Schreiber S.L., Printing protein as microarrays for high-throughput function determination, Science, 289 (5458), 1760-1763, 2000.

Morgan, Electro Ceramics, Technical publication TP-226, Properties of the piezoelectrical ceramics, www.morgan-electroceramics.com, 1999.

Mutz M., Harris D., Kannegard E., Pringle J., Stearns R., and Ellson R., Array production by acoustic ejection of single and multilayer fluids and cell suspensions, SmallTalk in San Diego, July 30, 2002.

Notz P.K., Chen A.U., Basaran O.A., Satellite drops: Unexpected dynamics and change of scaling during pinch-off, Physics of fluids, 13(3), 549-552, 2001.

Oh T.S., Buchwalter L.P., Kim J., Adhesion of polyimides to ceramic substrates: role of acid-base interactions, Journal of Adhesion Sci. Technol., 4(4), 303-317, 1990.

Okamoto T., Suzuki T., Yamamoto N., Microarrays fabrication with covalent attachment of DNA using bubble jet technology, Nature Biotechnology, 18, 438-441, 2000.

Papageorgiou D.T., Analytical description of the break-up of liquid jets, Journal of fluid mech., 301, 109-132, 1995.

Ramsay G., DNA chips-states-of-the-art, Nature Biotechnology, 16(1), 40-44, 1989.

Schena M., Shalon D., Davis R.W., and Brown P.O., Quantitative monitoring of gene expression patterns with a complementary DNA microarray, Science 270, 467-470, 1995.

Schena M., Heller R.A., Theriault T.P., Konrad K., Lachenmeier E., Davis R.W., Microarrays: biotechology's discovery platform for functional genomics, Trends Biotechnology, 16, 301-306, 1996.

Schena M., Microarray biochip technology, Eaton publishing, 2000.

Selby J.C., Shannon M.A., Xu K., Economy J., sub-micrometer solid-state adhesive bonding with aromatic thermosetting copolyester for the assembly of polyimide membranes in silicon-based devices, Journal of Micromech. and Microeng., 11, 672-685, 2001.

Srinivasan R., Braren B., Ultraviolet laser ablation of organic polymers, Chem. Rev., 89, 1303-1316, 1989.

Tyers M., Mann M., From genomics to proteomics an insight overview, Nature, 422, 193-197, 2003.

Wallace D., Trost H.-J., Eichenlaub U., Multi-fluid ink-jet array for manufacturing of chip-based microarray systems, Proceedings Second International Conference on Microreaction Technology, 1-5, 1998.

White F.M., Fluid mechanics, McGraw-Hill international editions, fourth edition, 215-258, 1999.

Wilkes E.D., Scott D.P., Basaran O.A., Computational and experimental analysis of dynamics of drop formation, Physics of fluids, 11(12), 3577-3598, 1999.

Yeh J.-T., A VOF-FEM and coupled inkjet simulation, Proceedings of ASME FEDSM'01 Fluids Engineering, 1-5, 2001

Zheng Z. et al, Piezoelectric coefficients of thin polymer film measured by interferometry, J. of Intelligent Material Systems and Structures, 9, 69-73, 1998.

ACKNOWLEDGEMENTS

First of all I would like to thank Prof. Nico F. de Rooij for giving me the opportunity to work in his research group. I had the change to develop a new polyimide technology, which leads to the presented device. I appreciate very much his enthusiastic support during the thesis.

Special thanks to my experts Marc Boillat, Herbert Keppner and Urs Staufer for kindly agreeing to be examiners of this thesis.

Excimer laser cutting was done at the Laser Zentrum in Münster, Germany. Many thanks to Jens Hildenhagen and Marco Lentjes for the excellent work with the Excimer laser.

A thank you goes to the group of Prof. Herbert Keppner of the University of Applied Sciences, Le Locle, Switzerland. His group was involved in the project for the deposition of piezo thin film and for YAG laser cutting. Francisco Dias, Daniel Gigon, Christophe Quinche, and Fabian Thiébaud, for their excellent work and effort of fulfilling all requirements. Thanks for spending all the hours together in the Lab and for finding smart solutions.

The realization of the work was not possible without the support of the members of SAMLAB including all technicians. I could add at least 50 names here because almost everybody was involved somehow. But the most important was the good teamwork, which made it possible to finish this research work on time. Thanks a lot for your contribution to this work.

I would also like to thank Marc Boillat and Bart van der Schoot, Seyonic SA, for guiding me through the project and for the motivation. I appreciate very much their fore looking in the project and their confidence.

I address my acknowledgements to Mr. Kumura from UBE, Germany, for supplying the polyimide sheets free of charge and also to Heinrich Zimmermann, Blösch AG, Grenchen, for the copper deposition onto polyimide sheets.

The work was financially supported by the Swiss Commission for Technology and Innovation. Thanks to Heinz Rüegg for good contact.

LIST OF PUBLICATIONS, PROCEEDINGS, WORKSHOPS AND PATENTS

Related to this thesis

Kuoni A., Quinche C., Boillat M., Keppner H., and de Rooij N.F., A high insulating thin film ZnO piezoelectric actuator on a Polyimide substrate, Proceedings of Eurosensors XVI, Prague, 228-231, 2002.

Kuoni A., Holzherr R., Boillat M., and de Rooij N.F., A Polyimide membrane with ZnO piezoelectric thin film pressure transducers as a differential pressure liquid flow sensor, Proceedings Micro-mechanics Europe MME'02, Sinaia, 267-270, 2002.

Kuoni A., Holzherr R., Boillat M., and de Rooij N.F., Polyimide Membrane with ZnO Piezoelectric Thin Film Pressure Transducers as a Differential Pressure Liquid Flow Sensor, Journal of Micromechanics and Microengineering, Vol. 13, 4, 103-107, 2003.

Kuoni A., Boillat M., de Rooij N.F., A Modular High Density Multi-Channel Dispenser for Micro-Array Printing, Digest of the 12th International Conference on Solid-State Sensors, Actuators and Microsystems, Transducers'03, Boston, 1, 372-376, 2003.

Kuoni A., Boillat M., and de Rooij N.F., 2-Dimensional Parallel Dispenser for Micro-array Printing, Journal of Labautomation JALA, 8(5), 24-28, 2003.

Kuoni A., Boillat M., and de Rooij N.F., Modeling of Drop Formation for a Piezoelectric Actuated Dispenser, CFDRC Workshop, Mainz, June 25, 2003.

Kuoni A., Boillat M., and de Rooij N.F., Multi-channel dispenser for microarray printing, Labautomation 2003, Palm Springs, 161-162, 2003.

Kuoni A., Boillat M., and de Rooij N.F., Multi-channel dispenser for microarray printing, Labautomation 2004, San José, 173, 2004.

Kuoni A., Boillat M., and de Rooij N.F., A Highly Parallel Piezoelectric Printing Device for Micro-Array Technology, Technical Digest, 17th IEEE International Conference on Micro Electro Mechanical Systems, MEMS 2004, Maastricht, 466-469, 2004.

Patent

Boillat M., van der Schoot B., Kuoni A., Papen R., de Rooij N.F., Dispensateur de fluide multi-canal, Seyonic SA, Application No. 01810661.7, European Patent Office, 2001.

Other Patents

Maier F., Jeanneret S., Kuoni A., Virole d'horlogerie, Patek Philippe SA, Application No. 03019944.2, European Patent Office, 2004.

Musy J.-P., Maier F., Jeanneret S., Kuoni A., Spiral d'horlogerie, Patek Philippe SA, Application No. 03020347.7, European Patent Office, 2004.

In other areas

Obi S., Gale M. T., Kuoni A., and de Rooij N.F., Replication of Optical MEMS Structures in Sol-Gel Materials, Proceedings MNE 2003 Micro and Nano Engineering, Cambridge, UK, 482-483, 2003.

Obi S., Gale M. T., Kuoni A., Noell W., and de Rooij N.F., Fabrication of Optical MEMS in Sol-Gel Materials, Proceedings IEEE/LEOS International Conference on Optical MEMS, Lugano, Switzerland, 39-40, 2002.

Obi S., Gale M. T., Kuoni A., and de Rooij N.F., Replication of optical MEMS structures in Sol-Gel materials, Microelectronic Engineering, Volumes 73-74, 157-160, 2004.

BIOGRAPHY

Andreas Kuoni, born on January 25, 1969, in Aarau, Switzerland. After regular school, Andreas made an apprenticeship as mechanic on farming machines from 1985 to 1989. He received his diploma in mechanical engineering at the University of Applied Sciences of Muttenz in 1992. In 1997 he graduated in physical electronics at the University of Neuchâtel, Switzerland. After a sabbatical period, he joined the Institute of Microtechnology at the University of Neuchâtel, where he worked towards his PhD in the micro-fluidic field on a multi-channel dispenser.